DEVELOPMENT OF RELATIONSHIPS BETWEEN SHRP ASPHALT TEST PARAMETERS AND STRUCTURAL MIXTURES FOR MECHANISTIC ANALYSIS AND REHABILITATION DESIGN OF FLEXIBLE PAVEMENTS

By

MING-GIN LEE

A DISSERTATION PRESENTED TO THE GRADUATE SCHOOL
OF THE UNIVERSITY OF FLORIDA IN PARTIAL FULFILLMENT
OF THE REQUIREMENTS FOR THE DEGREE OF
DOCTOR OF PHILOSOPHY

UNIVERSITY OF FLORIDA

1996

ACKNOWLEDGMENTS

The author wishes to express his sincere thanks to his advisor and supervisory committee chair, Dr. Mang Tia, for his technical and personal help throughout his graduate school career. To the author, he is everything a teacher should be. Without his support and guidance this dissertation would not have been possible.

Special appreciation is expressed to Dr. Byron Ruth, who has kindly served as the cochairman of his supervisory committee, for his technical and good-nature advice during his entire stay at the university. The author is also deeply indebted to Dr. Reynaldo Roque for his detailed and painstaking guidance through the challenging stages of this study. Thanks are given to Dr. Mark C. K. Yang and Dr. David Bloomquist for serving on the author's supervisory committee and having given of their expertise and time.

Thanks are extended to the Florida Department of Transportation (FDOT) for providing financial support, and to the FDOT Materials Office personnel, particularly Toby Dillow, George Lopp, Glen Schiller, Aaron Turner, Patrick Upshaw, David Webb, and Randy West. The author would like to thank Ed Dobson, Daniel Richardson, and Bill Studstill, and to all the other graduate students, W. Buttlar, C. Chiu, J. Chou, S. Dickson, S. Huang, T. Leung, D. Lu, C. Shih, and X. Wang for their help.

Finally, The author wishes to thank the Lord Jesus, his family, and his wife, Mi-Mi, for their love, confidence and motivation in his studies.

TABLE OF CONTENTS

Page

ACKNOWLEDGMENTS ii

LIST OF TABLES vi

LIST OF FIGURES ix

ABSTRACT xv

CHAPTERS

1 INTRODUCTION 1

1.1 Background 1
1.2 Study Objectives 2

2 LITERATURE REVIEW 3

2.1 Conventional Characterization and Evaluation of Asphalt Binder . 3
2.1.1 Consistency of Asphalt Cements 5
2.1.2 Temperature Susceptibility of Asphalt Binders 7
2.1.3 Shear Susceptibility of Asphalt Binders 10
2.1.4 Nomographs for Determining Asphalt Stiffness 13
2.1.5 Characterization of Asphalt Aging Potential 13
2.2 SHRP Pavement Performance-Based Asphalt Specification 14
2.3 Master Curves for Asphalt Binders and Mixtures 20
2.4 Overview of Rehabilitation Design of Asphalt Pavement Systems (REDAPS) 22

3 RESEARCH PROGRAM AND INSTRUMENTATION 27

3.1 Introduction 27
3.2 Laboratory Testing Program Using Conventional Binder Tests . . . 27
3.2.1 Rolling Thin Film Oven Test 28

3.2.2 Pressure Aging Vessel 32
3.2.3 Cannon Schweyer Constant Stress Rheometer 32
3.2.4 Brookfield Rheometer 36
3.2.5 Fraass Breaking Point Tester 39
3.3 Laboratory Testing Program Using SHRP Binder Tests 39
3.3.1Standard SHRP Binder Tests for Performance Grading 39
3.3.1.1 Dynamic Shear Rheometer 41
3.3.1.2 Bending Beam Rheometer 44
3.3.1.3 Direct Tension Test 46
3.3.2 Additional SHRP Binder Tests for Characterization 47
3.4 Laboratory Testing Program on Asphalt Mixtures 49
3.4.1 GTM Compaction and Tests 51
3.4.2 Diametral Resilient Modulus Test 54
3.4.3 Indirect Tensile Creep Test 61
3.4.4 Indirect Tensile Strength Test 64
3.4.5 Asphalt Extraction and Recovery Methods 65

4 RESULTS OF CONVENTIONAL AND SHRP BINDER TESTS . . . 67

4.1 Results of Conventional Binder Tests 67
4.1.1 Statistical Model 67
4.1.2 Weight Change 69
4.1.3 Penetration 69
4.1.4 Absolute Viscosity and Brookfield Viscosity 73
4.1.5 Constant Power Viscosity 79
4.1.6 Fraass Breaking Test 83
4.2 Results of SHRP Binder Tests 88
4.2.1 Dynamic Shear Rheometer Test 88
4.2.2 Bending Beam Rheometer Test 107
4.2.3 Direct Tension Test 115
4.2.4 SHRP Binder Performance Grading 115
4.2.5 Comparison of PG Grade and Bitumen Test Data Chart . . . 117
4.3 Summary of Findings 118

5 RESULTS OF MIXTURE STRENGTH TESTS 124

5.1 Introduction 124
5.2 Statistical Model 124
5.3 Results of Diametral Resilient Modulus test 125
5.4 Results of Indirect Tensile Creep Tests 126
5.5 Results of Indirect Tensile Strength Tests 135
5.6 Fracture Energy 144
5.7 Summary of Findings 144

6 RESULTS OF RHEOLOGICAL TESTS ON RECOVERED ASPHALT RESIDUES 149

6.1 Results of Conventional and SHRP Binder Tests 149
6.1.1 Penetration 150
6.1.2 Brookfield Viscosity 150
6.1.3 Bending Beam Rheometer (BBR) 150
6.1.4 Dynamic Shear Rheometer (DSR) 153
6.2 Comparison Between the SHRP Aging Processes for Asphalt Mixtures and Those for Asphalt Binders 158
6.3 Summary of Findings 165

7 RELATIONSHIPS BETWEEN BINDER AND MIXTURE PROPERTIES 169

7.1 Comparison of Results of SHRP and Conventional Binder Tests on Florida Asphalt Cements 169
7.1.1 Binder Rheological Properties at High Service Temperature 169
7.1.2 Binder Rheological Properties at Intermediate Service Temperature 170
7.1.3 Binder Rheological Properties at low service temperature . 172
7.2 Relationships Between SHRP Binder and Mixture Properties at Low Temperatures 178
7.3 Summary of Findings 187

8 CONCLUSIONS AND RECOMMENDATIONS 190

8.1 Conclusions 190
8.2 Recommendations 194

APPENDICES

A RESULTS OF BINDER TESTS 196

B RESULTS OF MIXTURE TESTS 212

REFERENCES 223

BIOGRAPHICAL SKETCH 228

LIST OF TABLES

Tables Page

2.1 Time Required for Pure Viscous Flow for Typical Paving Grade Asphalt Binder 6

2.2 Performance Graded Asphalt Binder Specification 17

3.1 Asphalt Binders Used in This Study 30

3.2 Gradation of Aggregates and Job Mix Formula for Asphalt Mixture 52

3.3 GTM Settings Used for Simulation of Initial Compaction and Densification . 53

4.1 Results of ANOVA and Duncan's Grouping on the Percent Retained Penetration in the comparison of RTFOT and PAV on Asphalt Binders 72

4.2 Results of ANOVA and Duncan's grouping on the Logarithm of Absolute Viscosity and Brookfield Viscosity in the comparison of RTFOT and PAV on Asphalt Binders 75

4.3 Summary of Results of Regression Analyses for the Viscosity-Temperature Relationship (Constant Power Viscosity) 84

4.4 Results of ANOVA and Duncan's Multiple Range Test on the Aging Index in the comparison of RTFOT and PAV on Asphalt binders 85

4.5 Results of ANOVA and Duncan's Grouping on the Fraass Breaking Point in the comparison of RTFOT and PAV on Asphalt binders 89

4.6 Summary of Results of Regression Analyses for the Viscosity-Temperature Relationship (Dynamic Viscosity) 106

4.7 Results of Bending Beam Rheometer Test on PAV+RTFOT-aged Asphalt Binders 114

4.8 Results of Direct Tension Test on PAV+RTFOT-aged Asphalt Binders 116

5.1 Results of Analysis Creep Compliance Data for Samples of Initial Compaction 133

5.2 Results of Analysis Creep Compliance Data for Samples of Ultimate Compaction 134

5.3 Results of Indirect Tensile Strength Test for Samples of Initial Compaction . 139

5.4 Results of Indirect Tensile Strength Test for Samples of Ultimate Compaction 140

5.5 Results of ANOVA and Duncan's Grouping on Indirect Tensile Strength . . . 141

5.6 Results of ANOVA and Duncan's Grouping on Failure Strains 143

5.7 Results of ANOVA and Duncan's Grouping on Fracture Energy 146

6.1 Results of Tests on Recovered Binder 151

6.2 Conventional Binder Test Results by Different Aging Processes 160

6.3 Results of BBR Test on Binders Aged by Different Processes 161

7.1 Results of Direct Tension Test on PAV+RTFOT-aged Asphalt Binders 179

A.1 Penetration of Asphalt at 25°C Before and After the RTFOT and PAV Processes. 196

A.2 Absolute Viscosity of Asphalts at 60°C Before and After the RTFOT and PAV Processes 197

A.3 Brookfield Viscosity of Asphalts at 60°C Before and After the RTFOT and PAV Processes 198

A.4 Results of Fraass Breaking Point Test 199

A.5 Results of Schweyer Constant Stress Rheometer Test 200

A.6 Weight Changes of Asphalts after the RTFOT and PAV processes 203

A.7 Results of Dynamic Shear Rheometer Test 204

A.8 Results of Classification Testing of Asphalt Binders 207

A.9 Height, %Air Voids, Gyratory Shear, %VMA, and Bulk Density of the GTM Specimens 209

B.1 Results of Instantaneous and Total Resilient Modulus 212

B.2 Results of Indirect Tensile Creep and Strength Test 214

LIST OF FIGURES

Figure		Page
2.1	Idealized Time-of-Loading Dependence of the Stiffness Characteristics of an Asphalt Materials Subjected to an Axial Tensile Stress	4
2.2	Temperature Susceptibility of Three Viscosity or Penetration Graded Asphalt	9
2.3	Temperature Dependency of Typical Asphalt Cement at Two Loading Times	11
2.4	Schematic Illustration of Changes in Mastercurve During Aging	15
2.5	Flow Chart for Testing Required to Grade an Asphalt Cement Using SHRP Binder Specification	19
2.6	Binder and Mixture Complex Modulus and Phase Angle as a Function of Frequency	21
2.7	Flow Chart of the REDAPS Program	24
3.1	Flow Chart of the Testing Program Using Conventional Binder Tests	29
3.2	Rolling Thin Film Oven	31
3.3	Schematic of Pressure Aging Vessel	33
3.4	Canon Schweyer Rheometer System	34
3.5	Schematic of Canon Schweyer Rheometer	35
3.6	Brookfield Rotational Viscometer	37
3.7	The Comparison of Brookfield Viscosity at Shear Rate of 1 sec^{-1} with Capillary Tube Viscosity at 60°C	38
3.8	Fraass Breaking Point Tester	40

3.9 Bohlin Dynamic Shear Rheometer Test System 42

3.10 Dynamic Shear Rheometer Principles 43

3.11 Schematic of the Beading Beam Rheometer 45

3.12 Flow Chart of Additional SHRP Binder Tests for Characterization 48

3.13 Flow Chart of Testing Program on Asphalt Mixtures 50

3.14 Indirect Tensile Testing Device 55

3.15 Mounting and Centering LVDTs for Indirect Tensile Test 57

3.16 Typical Load, Deformation versus Time Relationships in a Repeated-Load Indirect Tension Test 59

4.1 Weight Change of Nine Asphalts Aged by the RTFOT and PAV 70

4.2 Percent retained Penetration of Nine Asphalts Aged by the RTFOT and PAV 71

4.3 The Comparison of Aging Indices by Absolute and Brookfield Viscosity at 60°C 78

4.4 The Comparison of Aging Indices of Nine Asphalts Aged by the RTFOT and PAV Processes 80

4.5 Constant Power Viscosity at 5°C of Nine Asphalts Aged by the RTFOT and PAV Processes 81

4.6 Relationship Between Viscosity and Temperature for the Coastal AC-30 Asphalt 82

4.7 Fraass Breaking Point Temperature of Nine Asphalts Aged by the RTFOT and PAV 87

4.8 Isochronal Plots of Complex Modulus of Original Asphalt at w=10 rad/sec 92

4.9 Isochronal Plots of Complex Modulus of RTFOT-aged Asphalt at w=10 rad/sec 93

4.10 Isochronal Plots of Complex Modulus of PAV+RTFOT-aged Asphalt Binders at w=10 rad/sec 94

4.11 Plot of Complex Modulus at 76°C as a Function of Frequency for Unaged Asphalt Binders 95

4.12 Plot of Dynamic Viscosity at 76°C as a Function of Frequency for Unaged Asphalt Binders 96

4.13 Plot of Phase Angle at 76°C as a Function of Frequency for Unaged Asphalt Binders 97

4.14 Plot of Complex Modulus at 76°C as a Function of Frequency for RTFOT-aged Asphalt Binders 99

4.15 Plot of Dynamic Viscosity at 76°C as a Function of Frequency for RTFOT-aged Asphalt Binders 100

4.16 Plot of Phase Angle at 76°C as a Function of Frequency for RTFOT-aged Asphalt Binders 101

4.17 Plot of Complex Modulus at 3°C as a Function of Frequency for PAV +RTFOT-aged Asphalt Binders 102

4.18 Plot of Phase Angle at 3°C as a Function of Frequency for PAV +RTFOT-aged Asphalt Binders 103

4.19 Relationship Between Dynamic Viscosity and Temperature for the Coastal AC-30 Asphalt 105

4.20 Relationship Between Dynamic Viscosity at 1 Hz and Constant Power Viscosity at 25°C 108

4.21 Plot of Creep Stiffness at -12°C Versus Loading Time for PAV +RTFOT-aged Asphalt Binders 109

4.22 Plot of Creep Stiffness at -18°C Versus Loading Time for PAV +RTFOT-aged Asphalt Binders 110

4.23 Plot of Creep Stiffness at -24°C Versus Loading Time for PAV +RTFOT-aged Asphalt Binders 111

4.24 Isochronal Plot of Creep Stiffness at 60 sec Loading Time for PAV +RTFOT-aged Asphalt Binders 113

4.25 Bitumen Test Data Charts for Unaged Asphalt Binders 119

4.26 Bitumen Test Data Charts for RTFOT-aged Asphalt Binders 120

4.27 Bitumen Test Data Charts for PAV+RTFOT-aged Asphalt Binders 121

5.1 Comparison of Instantaneous Resilient Moduli of Mixtures 127

5.2 Comparison of Total Resilient Moduli of Mixtures 128

5.3 Response of a Burgers Model Subjected to a Unit Load 129

5.4 Comparison of Creep compliance of Mixtures at Different Temperatures . . . 131

5.5 Comparison of Creep compliance of Mixtures at Different Aged Conditions . 132

5.6 Comparison of the Creep Compliance Slopes for Different Asphalt Mixes . . 136

5.7 Comparison of the Creep Compliance Intercepts for Different Asphalt Mixes 137

5.8 Comparison of Indirect Tensile Strengths of Mixtures 142

5.9 Comparison of Fracture Energies of Mixtures at Initial Compaction 145

5.10 Comparison of Fracture Energies of Mixtures at Ultimate Compaction 145

6.1 Percent Retained Penetration of three Asphalts Aged by the STOA and LTOA Processes 152

6.2 The Comparison of Aging Indices of three Asphalts Aged by the STOA and LTOA Processes 152

6.3 Isochronal Plot of Creep Stiffness at 60 sec Loading Time of STOA Residues 154

6.4 Isochronal Plot of Creep Stiffness at 60 sec Loading Time of LTOA Residues 154

6.5 Isochronal Plot of m-value at 60 sec Loading Time of STOA Residues 155

6.6 Isochronal Plot of m-value at 60 sec Loading Time of LTOA Residues 155

6.7 Isochronal Plot of Complex Modulus of STOA Residues at w=0.01 Hz ... 156

6.8 Isochronal Plot of Phase Angle of STOA Residues at w=0.01 Hz 156

6.9 Isochronal Plot of Complex Modulus of LTOA Residues at w=30 Hz 157

6.10 Isochronal Plot of Complex Modulus of LTOA Residues at w=30 Hz 157

6.11 Percent Retained Penetration of three Asphalts Aged by the RTFOT, STOA, PAV and LTOA Processes 162

6.12 The Comparison of Aging Indices of three Asphalts Aged by the RTFOT, STOA, PAV and LTOA Processes 162

6.13 The Comparison of Creep Stiffness at 8, 60 and 240 seconds Loading Time at -10°C of Binders aged by RTFOT, STOA, PAV, and LTOA Processes .. 163

6.14 The Comparison of Creep Stiffness at 8, 60 and 240 seconds Loading Time at -24°C of Binders aged by RTFOT, STOA, PAV, and LTOA Processes .. 164

6.15 The Comparison of m-value at 60 sec Loading Time at -10°C of Binders aged by RTFOT, STOA, PAV, and LTOA Processes 166

6.16 The Comparison of m-value at 60 sec Loading Time at -24°C of Binders aged by RTFOT, STOA, PAV, and LTOA Processes 166

6.17 The Comparison of G*/sinδ of RTFOT and STOA Residues at w=10 rad/sec at High Service Temperatures 167

6.18 The Comparison of G*×sinδ of PAV and LTOA Residues at w=10 rad/sec at Intermediate Service Temperatures 167

7.1 Relationship Between Brookfield Viscosity at 60°C and G*/sinδ at 64°C .. 171

7.2 Relationship Between Penetration and G*sinδ before and after RTFOT and PAV at 25°C 171

7.3 Verification of Results Between Penetration and G* at 25°C 173

7.4 Relationship Between Constant Power Viscosity and G*sinδ before and after RTFOT and PAV at 25°C 174

7.5 Relationship Between Constant Power Viscosity at 5°C and Fraass Temperature before and after RTFOT and PAV 174

7.6 Relationship Between Fraass Temperature and Creep Stiffness at -12, -18, and -24°C after PAV 176

7.7 Relationship Between Fraass Temperature and Failure Strain at -12, -18, and -24°C after PAV 176

7.8 Relationship Between Creep Stiffness and Failure Strain at -12, -18, and -24°C after PAV 178

7.9 Relationship Between Mixture and Binder Stiffness at -10°C for samples at Initial Compaction 181

7.10 Relationship Between Mixture and Binder Stiffness at -10°C for samples at Ultimate Compaction 181

7.11 Relationships Between Mixture and Binder Stiffness for Initially Compacted Samples Aged by the STOA and LTOA Processes 182

7.12 Relationships Between Mixture and Binder Stiffness for Ultimately Compacted Samples Aged by the STOA and LTOA Processes 183

7.13 Relationships Between Mixture and Binder m-value for Initially Compacted Samples Aged by the STOA and LTOA Processes 184

7.14 Relationships Between Mixture and Binder m-value for Ultimately Compacted Samples Aged by the STOA and LTOA Processes 184

7.15 Relationships Between Mixture and Binder m-value for Initially Compacted Samples Aged by the STOA and LTOA Processes 185

7.16 Relationships Between Mixture and Binder m-value for Ultimately Compacted Samples Aged by the STOA and LTOA Processes 186

7.17 Plot of Mixture Resilient Modulus versus Binder Stiffness at -10°C 188

7.18 Plot of Mixture Failure Strain versus Binder Stiffness at -10°C 188

7.19 Plot of Mixture Tensile Strength versus Binder Stiffness at -10°C 189

7.20 Plot of Mixture Fracture Energy versus Binder Stiffness at -10°C 189

Abstract of Dissertation Presented to the Graduate School
of the University of Florida in Partial Fulfillment of the
Requirements for Degree of Doctor of Philosophy

DEVELOPMENT OF RELATIONSHIPS BETWEEN SHRP ASPHALT TEST PARAMETERS AND STRUCTURAL MIXTURES FOR MECHANISTIC ANALYSIS AND REHABILITATION DESIGN OF FLEXIBLE PAVEMENTS

By

Ming-Gin Lee

August 1996

Chairman: Mang Tia
Cochairman: Byron E. Ruth
Major Department: Civil Engineering

A laboratory investigation was conducted to evaluate the relationships between the results of the SHRP binder tests and the results of the conventional asphalt tests, and between the results of the SHRP binder tests and the cracking resistance of the asphalt mixtures under Florida conditions. Six different base asphalts from five different refinery sources were used in this study. The three types of modifiers used in this study were ground tire rubber (GTR), styrene-butadiene rubber (SBR) and styrene block copolymer. These modified and unmodified asphalts were subjected to the standard RTFOT process to simulate the short-term aging effect that occurs in the hot-mixing process and followed by the SHRP PAV process at 100°C to simulate the additional aging of the asphalt binder in the field. All these asphalts and asphalt blends were evaluated by the SHRP and

conventional binder tests. Asphalt mixtures (made of three different binders) were compacted by the gyratory testing machine (GTM) and aged according to the SHRP proposed short term oven aging (STOA) procedure and long term oven aging (LTOA) procedure. These aged and unaged asphalt mixtures were evaluated by resilient modulus, indirect tensile strength, and indirect tensile creep tests at 0, -10 and -20°C. Asphalt residues were recovered from the broken samples and evaluated by the binder tests.

The results show that the $G^*\sin\delta$ and G^* values as measured by the dynamic shear rheometer correlate well with results of conventional tests (penetration and viscosity) on the same binders at similar temperatures. The creep stiffness as measured by the bending beam rheometer at low temperatures correlates well with the Fraass breaking point temperature. However, the failure strain as measured by the direct tension tester at low temperatures correlates poorly to the Fraass breaking point temperature.

It was found that the creep compliance measured in the indirect tensile creep test reached a steady state at a time of 500 seconds and it was possible to predict the creep compliance at 1000 seconds or beyond from the test results up to 500 seconds. The mixture stiffness at -10°C was found to be linearly related to the creep stiffness of the binder. The tensile strength, failure strain and fracture energy of the mixtures at -10°C were found to be not related to the binder creep stiffness at the same temperature. The resilient modulus was found to be close to the stiffness of the mixture at 1 second as determined by the creep test.

The test results indicate that asphalt modification with SBR or GTR could improve both the high temperature and low temperature characteristics of the asphalt binders.

CHAPTER 1
INTRODUCTION

1.1 Background

A pavement engineer is concerned with the performance of pavements which is affected by the type, time of application, and quality of the maintenance it receives. Preventive timely maintenance will slow the rate of pavement deterioration. Delays in maintenance and deferred maintenance increase the quantity of defects and their severity so that, when corrected, the cost of repair is greater. Continued deferral of maintenance and rehabilitation shortens the time between overlays and reconstruction, and thus increases the life cycle costs of a pavement considerably. There is an increasing emphasis upon the development and use of mechanistic analysis and rehabilitation design. Prior research conducted for the FDOT (Florida Department of Transportation) established relationships between the constant power viscosity and asphalt concrete mixture parameters. This resulted in the development of a computer program for the Rehabilitation Evaluation and Design of Asphalt Pavement Systems (REDAPS) which has combined all key elements in the process of pavement evaluation and rehabilitation design.

The recent SHRP asphalt research program has resulted in the development of performance-based asphalt binder and asphalt-aggregate mixture specifications. The FDOT is in the process of evaluating and implementing these new tests and specifications.

While these new tests and specifications offer potential for improved pavement performance and management, there has been very little experience with them. There is a need to evaluate these new test methods with regard to their applicability for use as direct input for mechanistic pavement analysis and design. SHRP test methods and specifications have not addressed pavement rehabilitation nor mechanistic analysis. Consequently, there is a need to relate asphalt properties to mix behavior at the critical thermal-load conditions where pavement failures are most likely to occur.

1.2 Study Objectives

The main objectives of this study are as follows:

1. To develop and evaluate the relationships between the results of the SHRP binder tests and the results of the Schweyer rheometer test and other conventional asphalt tests that have been commonly used by the FDOT.
2. To develop and evaluate the relationships between the results of the SHRP binder tests and the cracking resistance of the asphalt mixtures under Florida conditions.
3. To evaluate and compare the SHRP aging processes for asphalt mixtures and those for asphalt binder under typical Florida conditions.
4. To study and evaluate the aging characteristics of selected modified asphalts and mixtures which are likely to be used in Florida.
5. To evaluate the SHRP Performance-related tests for asphalt binders and modified asphalt binders to be used in Florida.

CHAPTER 2
LITERATURE REVIEW

2.1 Conventional Characterization and Evaluation of Asphalt Binder

When asphalt is cold and brittle, it may behave as a nearly elastic solid material that exhibits stress in proportion to the strain, but not in proportion to the rate of strain. At elevated temperatures, most asphalts will approach perfectly viscous (Newtonian) fluids that exhibit stress in proportion to the rate of strain, but not in proportion to the amount of strain. A viscoelastic material, such as asphalt, exhibits both elastic and viscous behavior response and displays a time dependent relation between an applied stress and the resultant strain. Within the linear viscoelastic region of an asphalt, the interrelation of stress and strain is influenced by time alone, and not by the magnitude of the stress [1]. On the other hand, using stiffness (stiffness modulus) to describe asphalt behavior is appropriate. Stiffness is the relationship between stress and strain as a function of time of loading and temperature; this relationship between stress, strain and time is also referred to as the rheological behavior of asphalt cements or mixtures. Figure 2.1 shows a simplified diagram illustrating the time-of-loading dependence of the stiffness of asphalt materials for a particular temperature [2]. At very short loading times, it is noted that stiffness is essentially time independent; in this case, the stiffness approaches the elastic modulus. For an intermediate range on the time scale, the stiffness decreases with an

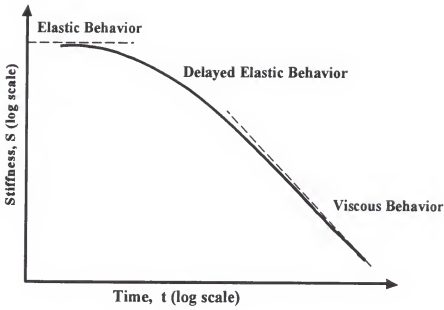

Figure 2.1 Idealized Time-of-Loading Dependence of the Stiffness (Stress/Strain) Characteristics of an Asphalt Materials Subjected to an Axial Tensile Stress

increase in time of loading. At very long loading times, the stiffness may still decrease, but at a uniform rate, and the behavior may be considered to be purely viscous [2].

This section reviews the conventional methods of characterizing the rheological properties of asphalt cements.

2.1.1 Consistency of Asphalt Cements

The current methods to characterize the consistency of asphalt cements are by penetration or viscosity tests. The penetration grading test (ASTM D 5) involves the measurement of penetration of a standard needle into a sample of asphalt cement under a standardized time of 5 seconds, temperature of 25°C and load of 100gs [3]. The second method of evaluating asphalt cements is by viscosity grading (ASTM D 3381) which is controlled by the absolute viscosity at 60°C.

These two sets of specifications, penetration-graded and viscosity-graded, are currently in use in the United States and Canada. The primary purpose of these specifications is to grade an asphalt cement according to its consistency.

Although viscosity is a fundamental property measuring flow, absolute viscosity at 60°C it only provides information about high temperature viscous behavior. Viscosity grading at 60°C (140°F) is deceptive for indicating performance at average or low pavement service temperatures. Creep tests have been conducted by a large number of researchers to attempt to calculate the viscosity (η) of asphalt cement at average or low pavement temperatures [4]. To make such a calculation, it is necessary to apply a constant shear stress (τ) to an asphalt cement until the shear strain (γ) versus time response becomes linear causing a constant slope or shear rate ($\dot{\gamma}$). At temperatures

below 25°C (77°F), long loading times at a constant stress are required before a linear response or steady-state flow occurs. The loading times required to achieve a constant shear rate for a typical paving grade asphalt binder are shown in Table 2.1 [4]:

Table 2.1 Time Required for Pure Viscous Flow for Typical Paving Grade Asphalt Binder

Temperature, °C	Time Required to Achieve Steady-State Flow
5	3 days
15	1½ hours
25	5 minutes
35	60 seconds

At loading times less than those given in the above table, asphalt cement displays a delayed elastic response where the shear rate ($\dot{\gamma}$) is not constant. If a long time period is allowed for the delayed elastic response to be completed, very large strains could result which cause the response to be nonlinear. When this occurs, these large strains in a short duration test are so large that the assumption of small strains, which is used in the analysis of the problem, is invalid [4]. Also, viscosity results do not provide information about low temperature elastic behavior which is needed to predict pavement performance at low temperatures and which may prevent low temperature cracking [5].

Penetration is an empirical test which indicates the consistency of an asphalt binder at an average pavement service temperature of 25°C (77°F). The applied shear rate is high during the test and could vary depending on the consistency of the asphalt. Penetration testing at 25°C (77°F) is a poor indicator of pavement performance at higher

or lower pavement service temperatures. In the penetration grading system, no viscosity value is available to establish mixing and compaction temperatures. Often, both grading systems have problems in predicting the performance of modified asphalt binders. The two grading systems do not address specific distress modes or ensure long-term field performance [4]. In summary, the current specifications and test methods are not performance-related because they [6]:

a. lack adequate low-temperature measurements

b. do not include fundamental binder properties that can be related to fundamental mixture properties or to pavement performance

c. are not appropriate (capillary viscometer) for measuring consistency at the upper service temperatures, and

d. do not consider long-term in-service aging.

Because of these deficiencies, as mentioned above, many agencies have made changes to these testing procedures and specifications in order to relate them to field performance and to accommodate local conditions. In many areas of the United States, these different tests and specifications have caused problems for asphalt producers wishing to market their products. Many times, states with similar performance conditions will specify very different asphalt binders. The lack of relationships between the specifications and pavement performance have made it impossible to develop performance-related specifications which relate to the performance of the material in the field [4].

2.1.2 Temperature Susceptibility of Asphalt Binders

Temperature susceptibility is defined as the change in consistency, stiffness, or

viscosity of an asphalt cement as a function of temperature. Temperature susceptibility is usually quantified through parameters calculated using consistency measurements made at two different temperatures [4,6]. Two parameters, viscosity and penetration, have been used to measure the temperature susceptibility of an asphalt cement. As illustrated in Figure 2.2, asphalt cements A, B and C all have the same viscosity and penetration grade because they are within the specification limits at 60°C (140°F) and 25°C (77°F). Asphalts A and B have the same temperature susceptibility, as indicated by the same slope of the consistency versus temperature plots, but they have a different consistency at all temperatures. Asphalts A and C have the same consistency at 25°C (77°F), but they have a different high temperature consistency. Asphalts B and C have the same consistency at 60°C (140°F) but a different consistency at other temperatures. Asphalt C is an example of a highly temperature susceptible asphalt which is undesirable because of its high viscosity at lower temperatures and a low viscosity at higher temperatures. Since all three of these asphalt cements share the same grade, they might be expected to have the same behavior during placement and during hot and cold weather conditions [7].

As shown in the previous example, many problems observed in asphalt pavements are a result of changes in consistency of an asphalt cement over a range of temperatures. It would appear that temperature susceptibility would be a good parameter to characterize asphalt cements. However, the rheological behavior of an asphalt cement under a specified loading or testing condition depends on the temperature and time of loading. The effect of temperature on the rheological response of asphalt binders is perhaps better considered in terms of temperature dependency which, as illustrated by the isochronal

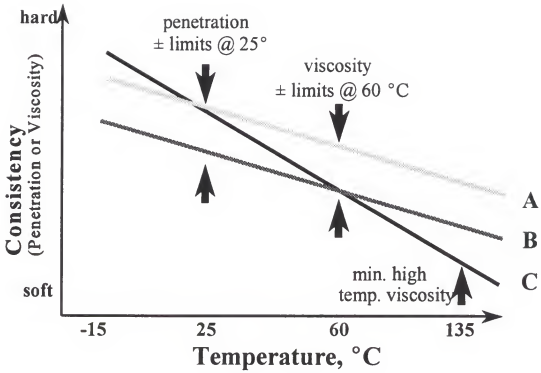

Figure 2.2 Temperature Susceptibility of Three Viscosity or Penetration Graded Asphalt Cements

curves shown in Figure 2.3, varies with both loading time and temperature [6]. Since these two parameters, temperature and time dependency are not simple linear functions, the temperature susceptibility of an asphalt will depend on the testing temperature of the material. Moreover, temperature susceptibility is not a parameter which is based on a single variable, but it depends on temperature range, time of measurement, and the physical property that is measured. Therefore, using parameters which are based on measurements at specific conditions, such as PI, PVN, or VTS as indicators of temperature susceptibility can not characterize fully the rheological behavior of asphalt cements [4,6].

2.1.3 Shear Susceptibility of Asphalt Binders

At high temperatures, asphalt cements behave as simple Newtonian fluids where the ratio of shear stress to shear rate is constant. However, at low temperatures or after aging, most asphalt cements exhibit a non-Newtonian or viscoelastic flow. For a non-Newtonian fluid, the measured viscosity is dependent on the applied shear rate. The effect of changes in shear rate on the measured viscosity is referred to as the "shear susceptibility". The shear susceptibility of an asphalt cement is determined by conducting viscosity tests at different shear rates. Roberts et. al. [2] stated that shear susceptibility is the tangent of the angle of log shear rate (x-axis) versus log viscosity (y-axis) plot, or the shear susceptibility is the slope of this plotted line.

In describing the applications of rheological concepts proposed by H.E. Schweyer, Tia and Ruth [7] defined shear susceptibility of an asphalt cement by the power law function using shear stress (τ) and shear rate ($\dot{\gamma}$) as follows:

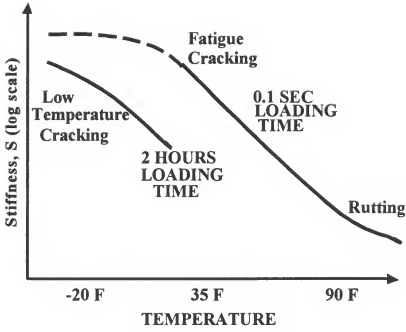

Figure 2.3 Temperature Dependency of Typical Asphalt Cement at Two Loading Times.

$$\tau = \eta_1 \dot{\gamma}^c$$

where:

τ = shear stress
η_1 = viscosity at a shear rate of 1 s^{-1}
$\dot{\gamma}$ = shear rate
c = shear susceptibility

Shear susceptibility, c, can be expressed as:

$$c = \frac{\log(\tau_2) - \log(\tau_1)}{\log(\dot{\gamma}_2) - \log(\dot{\gamma}_1)}$$

A C-value of one indicates a Newtonian fluid. Pseudoplastic fluids have a C-value less than 1, while have a C-value greater than 1.

The power law equation is used often for characterizing the flow behavior of non-Newtonian materials subjected to simple shear stresses with certain ranges [9]. As the shear stress or shear rate changes over a large range, the C value may also change. Therefore, C may not a constant, but its value may be shear-rate dependent, and is also dependent upon prior aging and stress history of the asphalt [8,9].

Kandhal P. S. [2] stated that the aging index - shear susceptibility relationship appears to determine the pavement performance. Control of gain in shear susceptibility and aging index seems to be a necessary specification requirement for paving asphalts. But, unfortunately, power law examples are not currently being used in the development of SHRP binder specifications. Anderson et. al. [4] stated that such nonlinear models are in practice very complex and difficult to apply and therefore are not suitable for specification purposes. The shear susceptibility, C, may be useful in

understanding the molecular actions which occur in asphalt cement in the non-Newtonian response region [4].

2.1.4 Nomographs for Determining Asphalt Stiffness

Various nomographs have been developed by different researchers for determining the stiffness of asphalt cement at various test temperatures and loading times. Vander Poel developed the first nomograph which can be used to determine the stiffness of asphalt cement at any temperature and at any rate of loading if the softing point (R&B) and the penetration index PI (Pen/R&B) of the asphalt cement are known. This nomograph was subsequently updated and revised by Mcleod to accommodate penetration and viscosity measurements [11]. Although these nomographs are quick and easy to use, they have the following limitations [2]:

a. The scale of nomographs requires that extreme care be used in interpolating the data and results. A dull pencil can lead to appreciable errors.

b. Determining stiffness of asphalt cement and mix by a series of transformations, starting from routine test data on the asphalt cement, appears to be somewhat "unscientific" to a number of engineers.

Despite the foregoing limitations, these nomographs provide reasonable estimates of asphalt stiffness at temperatures above room temperature. However, the estimates provided by these nomographs are in considerable error at lower temperatures and longer loading times [4].

2.1.5 Characterization of Asphalt Aging Potential

A decrease in penetration and increase in viscosity are the direct sign of aging of an asphalt binder. For most of the cracked pavements, the recovered asphalts have a penetration value of less than 20 [7]. McLeod and other researchers [12] suggested that when the viscosity of asphalt exceeds 1×10^{10} poises at the lowest service temperature, the pavement will undergo thermal cracking. As a rough prediction of thermal cracking, a limit viscosity of 2×10^{10} poises has been suggested by Davis [13]. Additionally, many researchers have used aging index to quantify long-term aging that occurs in service. Kandhal P. S. [14] stated that raveling was observed on the test pavements when this aging index exceeded 12. Although a single-point aging index can effectively describe the increase in stiffness when the response is essentially viscous, such single-point aging indices will not always accurately reflect changes in stiffness at low temperatures, where delay elasticity is a significant portion of the response. That means that a single-point measurement is insufficient to characterize the rheological changes that occurs with aging. This is illustrated in Figure 2.4 [4], which shows the changes of the master curve for an asphalt at different aging conditions.

2.2 SHRP Pavement Performance-based Asphalt Specification

The main goal of the SHRP research program was to develop pavement performance-based specifications for asphalt binders and mixtures. These specifications would let the engineer select an asphalt binder and mixture on the basis of the required pavement performance level under the present and predicted traffic and environmental conditions [15]. The performance-based specifications were to be established on a set of

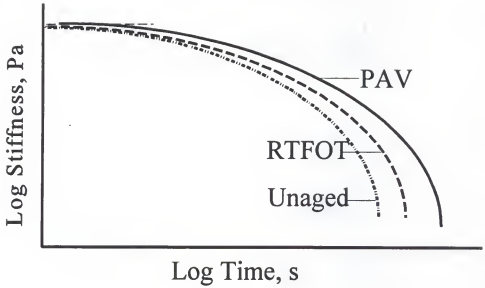

Figure 2.4 Schematic Illustration of Changes in Mastercurve during Aging.

validated relationships among asphalt binder properties, mixtures properties and pavement performance that establish acceptable response ranges to control low temperature cracking, fatigue cracking, permanent deformation (rutting), aging, adhesion, and water sensitivity. Accelerated laboratory tests and parameters that relate to field performance are used in the specification [6.15]. The procedures and properties consider the three basic modes of distress: permanent deformation (rutting), low temperature cracking, and fatigue cracking. The SHRP proposed asphalt binder specification as shown in Table 2.2 would allow the engineer to match materials to different levels of pavement service and to make the choice of asphalt binder to resist specific distress mechanisms [15]. The system was to be based upon rational performance indices established for both low temperature and high temperature pavement service. Performance grading is based upon the properties of the asphalt binder aged to simulate a specific pavement service life (5 years). Thus, a precise grade may be selected to fit the need to control low-temperature cracking, fatigue cracking and rutting, or any combination in a particular construction project [4,6].

The following requirements are specified in the SHRP specification [6]:

a. A minimum value (1 KPa) of $G^*/\sin\delta$ measured at the maximum pavement temperature ranging from 46 to 82°C are specified to control tenderness and rutting.

b. RTFOT residue should have a minimum value (2.2 KPa) of $G^*/\sin\delta$ measured at the maximum pavement temperature ranging from 46 to 82°C in order to control rutting.

c. PAV residue should have a maximum limit value (5000 KPa) of $G^* \times \sin\delta$

Table 2.1 Performance Graded Asphalt Binder Specification

Performance Grade	PG 52							PG 58					PG 64					PG 70			
	-10	-16	-22	-28	-34	-40	-46	-16	-22	-28	-34	-40	-16	-22	-28	-34	-40	-10	-16	-22	-28
Average 7-day Maximum Pavement Design Temperature, °C [a]	<52							<58					<64					<70			
Minimum Pavement Design Temperature, °C [a]	>-10	>-16	>-22	>-28	>-34	>-40	>-46	>-16	>-22	>-28	>-34	>-40	>-16	>-22	>-28	>-34	>-40	>-10	>-16	>-22	>-28
Original Binder																					
Flash Point Temp, T48: Minimum °C	230																				
Viscosity, ASTM D 4402: [b] Maximum, 3 Pa·s (3000 cP), Test Temp, °C	135																				
Dynamic Shear, TP5: [c] G*/sin δ, Minimum, 1.00 kPa Test Temperature @ 10 rad/s, °C	52							58					64					70			
Rolling Thin Film Oven (T240) or Thin Film Oven (T179) Residue																					
Mass Loss, Maximum, %	1.00																				
Dynamic Shear, TP5: G*/sin δ, Minimum, 2.20 kPa Test Temp @ 10 rad/sec, °C	52							58					64					70			
Pressure Aging Vessel Residue (PP1)																					
PAV Aging Temperature, °C[d]	90							100					100					100(110)			
Dynamic Shear, TP5: G*/sin δ, Maximum, 5000 kPa Test Temp @ 10 rad/sec, °C	25	22	19	16	13	10	7	25	22	19	16	13	28	25	22	19	16	34	31	28	25
Physical Hardening [e]	Report																				
Creep Stiffness, TP1: [f] S, Maximum, 300 MPa m-value, Minimum, 0.300 Test Temp, @ 60 sec, °C	0	-6	-12	-18	-24	-30	-36	-6	-12	-18	-24	-30	-6	-12	-18	-24	-30	0	-6	-12	-18
Direct Tension, TP3: [f] Failure Strain, Minimum, 1.0% Test Temp @ 1.0 mm/min, °C	0	-6	-12	-18	-24	-30	-36	-6	-12	-18	-24	-30	-6	-12	-18	-24	-30	0	-6	-12	-18

measured at the intermediate pavement temperature ranging from 4 to 40°C in order to reduce fatigue failure.

d. To minimize thermal cracking, PAV residue should have a maximum value (300MPa) of stiffness and a minimum value (0.3) of m (the slope of the log stiffness versus log time curve) measured at the minimum pavement design temperature plus 10°C. The stiffness requirements can be relaxed when enhanced strain to failure properties can be demonstrated.

A flow chart [6,7] for testing required to grade an asphalt cement in according to the SHRP PG grading system is shown in Figure 2.5. The specification also includes requirements related to the behavior of the asphalt binder during hot mix production and pavement construction. A minimum flash point (230°C) is specified for safety consideration. A maximum viscosity value (3Pa s) at 135°C is specified for all grades to assure that the binder is sufficiently fluid for hot mix production. However, it is unlikely that any binder with or without modifier will be specified which can as a complete panacea for inadequate pavement design or poor construction practice [4].

The SHRP mixtures specification, which is a complete part of the mixtures design system, includes both performance-based and performance-related criteria. Performance-based properties can be used to predict the response of an asphalt pavement under loads. However, performance-related properties are not directly related to pavement performance. Many empirical properties currently in common use are performance-related properties which affect performance but do not control performance [17]. The SHRP specification for mixtures is a three tiered mix design system which is also intended to

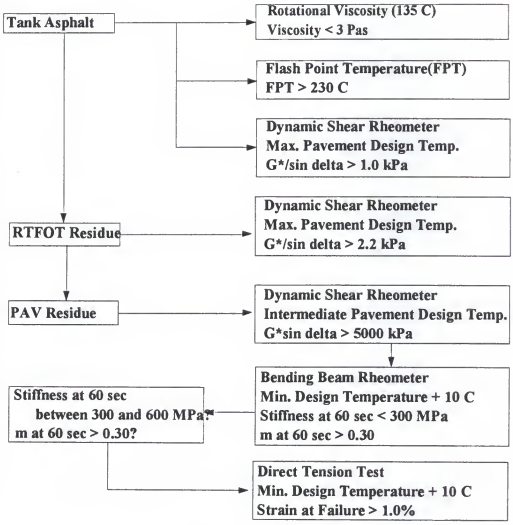

Figure 2.5 Flow Chart for Testing Required to Grade an Asphalt Cement using SHRP Binder Specification

address the three basic modes of distress : permanent deformation (rutting), low temperature cracking, and fatigue cracking. The final step of mix design is field mixture verification. The scope of the SHRP mix design procedure is broader than the current mixture design methods, in that the SHRP procedure included field control tests as a necessary part of the mix design [6,17].

2.3 Master Curves for Asphalt Binders and Mixtures

Asphalt and asphalt mixture are very complex both in their chemistry and rheology. The rheology of asphalt binders directly affects the performance and distress of asphalt pavements. Conventional measurements cannot provide information on how an asphalt's rheology changes as a result of loading, time, and temperature over its entire service life. The viscoelastic behavior of an asphalt binder or mixture can be characterized by dynamic rheometer tests over a sufficient range of frequencies and temperatures. By varying the frequency of the input strain or stress in a dynamic rheometer test, the time-dependent viscoelastic behavior of an asphalt binder or mixture could be easily measured. The balance between the viscous and the elastic response of an asphalt binder or mixture could be measured as a function of frequency or temperature. According to the principle of time-temperature superposition, the data obtained from dynamic testing at a higher or lower temperature can be equated simply and graphically with the data obtained at a lower or higher frequency, respectively. Conversely, data obtained at a higher or lower frequency can be transformed into the data at a lower or higher temperature, respectively [1]. A standard reference temperature must be selected in the transformation process. The data at all other temperatures are then shifted with respect to time or frequency, until

the curves merge into a single, smooth function known as the master curve [18]. Figure 2.6 shows the master curves of the dynamic complex modulus and phase angle (obtained from dynamic rheometer test) as a function of reduced frequency for an asphalt binder and an asphalt mixture [18,19]. A master curve for a typical asphalt binder shows the complex modulus approaches a limiting value of about 1 GPa at very high frequency. Plots of complex modulus and phase angle versus frequency for asphalt binder show that the complex modulus increases and phase angle decreases as the frequency increases. It means that at the high frequency (or the low temperature) asphalt behaves like an elastic material, gradually changes to a viscoelastic material, and continues to change into a viscous material as the frequency decreases (or the temperature increases). Mixture master curves show the complex modulus at high frequencies generally approaches a limiting value which has a trend similar to the binder master curves. Therefore, the thermal cracking behavior of a mixture could be explained by the modulus of the binder. The modulus of the mixture decreases as the frequency decreases. However, unlike the binder's modulus which continues to drop as the frequency decreases, the mixture's modulus reaches a limiting value as the frequency decreases to a low level. The limiting modulus of the mixture at high temperature is due to the aggregate interlocking action since the aggregates themselves do not creep. Therefore, the behavior of the mixtures at high temperature will not be only dependent upon the binder rheological properties but also upon the mix design itself such as binder content, air void content, aggregate shape and hardness, and compaction [20].

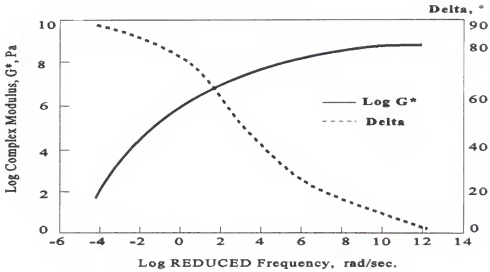

(a) Binder Master Curves [18]

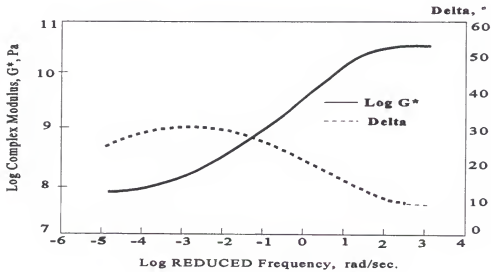

(b) Mixture Master Curves [19]

Figure 2.6 Binder and Mixture Complex Modulus and Phase Angle as a Function of Frequency

2.4 Overview of Rehabilitation Design of Asphalt Pavement Systems (REDAPS)

The REDAPS computer program was developed to provide a comprehensive mechanistic method for the analysis and rehabilitation design of flexible pavements. It is different from the current overlay design procedures which are generally based on fatigue failure criteria. The REDAPS program was formulated according to the critical condition concept proposed by Roque and Ruth [21]. Failure in an asphalt pavement occurs at the critical condition when the combination of thermal condition and the vehicular loading effects produce stress, strain, or energy sufficient to break the asphalt concrete. Thermal and load stressing conditions are major factors to produce pavement cracking [22].

The REDAPS program consists of eleven major sub-programs. They are TRSLATOR, SORT, MEAPS, CRACK3, PLOTQ, STRATEGY, OVLR and OVLR2, PROJ, PROJ2 and BISAR. The flow chart of the REDAPS program, as illustrated in Figure 2.7, identifies the key elements incorporated into this analysis and design system for flexible pavement [23]. Pavement evaluation (Dynaflect) data can be input into the program which will place the data into categories (segments of pavement) having different pavement response. Typical Dynaflect deflection basins for each category are analyzed using an elastic multi-layer subroutine (BISAR program) to determine their pavement layer moduli. Subsequently, the program provides two pavement evaluation options : the simplified analysis and the detailed analysis [22].

The simplified analysis (Path A) identifies the sequence required for utilization of NDT (nondestructive test) data to separate a length of pavement into segments, each having similar response characteristics, and to evaluate these segments using stress

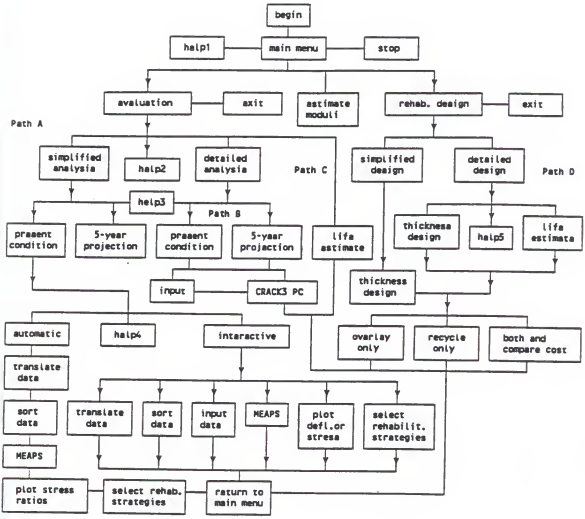

Figure 2.7 Flow Chart of the REDAPS Program

analysis. Each segment is analyzed using the Mechanistic Evaluation of Asphalt Pavement System (MEAPS) to a) determine layer moduli and verify deflections using an elastic layer program, and b) evaluate load-induced stresses at the typical low pavement temperature [21]. The stress ratio (SR) of the maximum load stress (tensile positive) to the maximum indirect tensile strength of the asphalt concrete at low temperature is used as a relative indicator of the structural adequacy of the pavement. For example, a $SR<0.30$, $0.30 \leq SR \leq 0.55$, and $SR>0.55$ indicates good, questionable, and poor structural capacity, respectively, for the state of Florida [23].

When the SR is between 0.30 and 0.55, it is necessary to perform the detailed (subroutine Crack3) analysis (Path B). The detailed analysis option evaluates the pavement cracking potential under combined effects of thermal and vehicular loadings under the specified cooling curves. This analysis uses three failure criteria : the accumulated energy ratio, the accumulated stress ratio and the incremental creep strain to evaluate the pavement cracking potential. If necessary, the life of the existing pavement can be estimated (Path C) using the concept that age hardening produces a parallel shift in the constant power viscosity-temperature relationship for all asphalt binders [24,25].

After completion of the structural analysis, the user may proceed to conduct a rehabilitation design using either the simplified (subroutine OVLR) or detailed (subroutine OVLR2) design procedures. In the detailed rehabilitation design procedure, the material properties are characterized in the same ways as used in the simplified design procedures except considering the age hardening of asphalt binders [22].

At the present condition, the new or aged asphalt viscosity is expressed as

$$\text{Log } \eta_{100} \text{ (Pas)} = B_0 + B_1 \times \text{Log (temperature in } ^\circ\text{K)}$$

Based on the parallel shift aging principle, the constant power viscosity after further age hardening at a future time is

$$\text{Log } \eta_{100} \text{ (Pas)} = DB + B_0 + B_1 \times \text{Log (temperature in } ^\circ\text{K)}$$

where DB = hardening rate ×Log (design life in days). The default binder hardening rate is 0.70 unless specified by the user.

The detailed design procedure is based on the applied energy ratio criterion or the maximum combined stress criterion (whichever is greater) to measure the cracking potential of the pavements as compared with the vehicular-induced stress ratio criterion used in the simplified design. The simplified design procedure iterates by computing stress ratios for different thickness of overlay or recycled pavement to achieve a design thickness corresponding to a stress ratio of 0.25, whereas the detailed procedure determines the required thickness by achieving an applied energy or combined stress ratio of 0.95 for a given design life and asphalt material under the default 24 kip truck load (with a default repetitions of 12 axles per hour) and a selected critical cooling condition [23]. Moreover, the simplified design procedure is developed using an empirical stress criterion which is applicable only to the climatic conditions in Florida. The detailed design procedure, on the other hand, considers the actual cooling condition, binder age hardening and vehicular loads for any type of material and climatic conditions.

CHAPTER 3
RESEARCH PROGRAM AND INSTRUMENTATION

3.1 Introduction

One of the major objectives of this study is to determine the relationships between the results of the SHRP binder tests and the results of the Schweyer rheometer test and other conventional asphalt tests that have been commonly used by the FDOT. Asphalt cements (conventional and modified) were aged by using the SHRP accelerated aging processes: the standard Rolling Thin Film Oven Test (RTFOT) and followed by the Pressure Aging Vessel (PAV) process. The effects of aging conditions will be obtained and their relationships will be established. Asphalt mixtures (made of three different binders) were aged according to the SHRP proposed short term oven aging (STOA) procedure and long term oven aging (LTOA) procedure, and the binders of the aged mixtures were recovered from a selected number of the broken asphalt mixture samples. The recovered binders will be evaluated by the binder tests. The test data of binders and mixtures were analyzed to establish relationships or as direct input for the Rehabilitation Evaluation and Design of Asphalt Pavement Systems (REDAPS). This chapter describes the detailed research program and instrumentation.

3.2 Laboratory Testing Program Using Conventional Binder Tests

Figure 3.1 shows the testing program on asphalt binders using conventional tests. Nine different asphalt binders, which had been acquired from five refinery sources for use in this study, were subjected to the standard RTFOT process (which simulates the age-hardening of the asphalt binder due to the hot-mixing process and construction) and followed by the SHRP PAV process at 100°C (which simulates the additional aging of the asphalt binder in the field). The nine binders and their abbreviations used in this study are listed in Table 3.1. The following tests were performed on the original unaged binders, and on the RTFOT and RTFOT+PAV residues:

(1) Penetration test at 25°C

(2) Absolute viscosity at 60°C

(3) Brookfield viscosity at 60°C

(4) Fraass breaking point test

(5) Schweyer rheometer tests at 5, 15, and 25°C

Two replicate tests were performed for each combination of conditions. The following section describes some special facilities for the conventional binder tests used in this study including a Rolling Thin Film Oven (RTFOT), a Pressure Aging Vessel (PAV), a Cannon Schweyer rheometer, a Brookfield rheometer and a Fraass breaking point tester.

3.2.1 Rolling Thin Film Oven Test

A Rolling Thin Film Oven (RTFOT, ASTM D2872) as shown in Figure 3.2 was used in this study. The bottle carriage assembly rotates at a rate of 15 ± 0.2 RPM. The air flow was set at a rate of 4000 ± 200 ml/min. The RTFOT bottles with 35 g samples

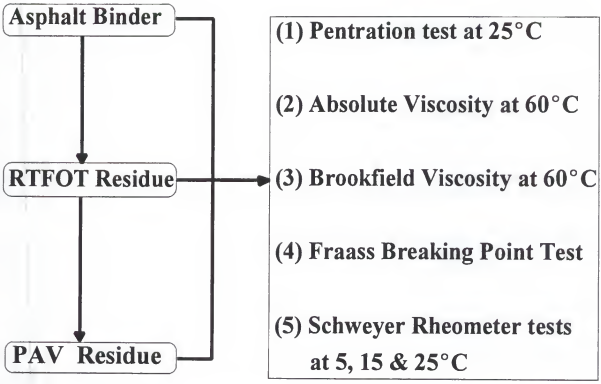

Figure 3.1 Flow Chart of the Testing Program Using Conventional Binder Tests

Table 3.1 Asphalt Binders Used in This Study

Asphalt Binder	Abbreviation
COASTAL AC-10	CT10
COASTAL AC-10 + 3% SBR (UP2879)	C1S2
COASTAL AC-10 + 3% SBR (UP70)	C1S7
ERGON PMAC-20	PM20
COASTAL AC-30 + 10% GTR	C3GT
COASTAL AC-30	CT30
KOCH AC-30	KH30
MARATHON AC-30	MT30
MARIANI AC-30	MA30

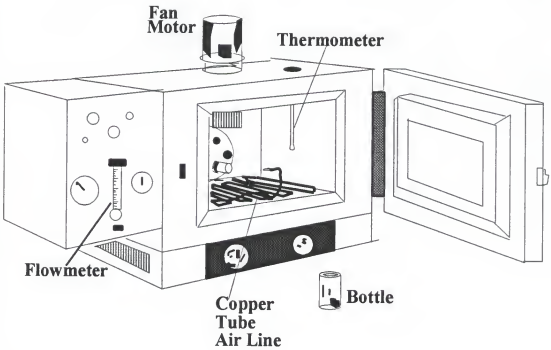

Figure 3-2 Rolling Thin Film Oven

were heated at the temperature of 163°C for 85 minutes. After the process, the RTFOT-aged residues are ready to pour out of the bottles.

3.2.2 Pressure Aging Vessel

The SHRP Pressure Aging Vessel which is the SHRP Product 1003 was used in this study. Figure 3.3 shows the schematics of the PAV test system consisting of a pressure vessel, pressure controlling devices, temperature controlling devices, pressure and temperature measuring devices, and a temperature readout device. The system was performed following SHRP procedure in according to AASHTO Designation PP1 [26] and under a pressure of 300 psi for 20 hours at a temperature of 100°C. In accordance to the SHRP recommended procedure, it was decided to perform the PAV test on RTFOT residues (35 g samples transferred directly from RTFOT oven), rather than on TFOT residues.

3.2.3 Cannon Schweyer Constant Stress Rheometer

A Cannon Schweyer Constant Stress Rheometer as shown in Figure 3.4 and 3.5 was used to characterize low temperature rheology of the binders in this study. A review on the theoretical background for the Schweyer constant stress rheometer and the application of rheological concepts proposed by H. E. Schweyer has been presented in a paper by Tia and Ruth [27]. The rheometer consists of a gas-operated pneumatic cylinder which applied a specified force to the plunger in the sample tube, as shown in Figure 3.5. A LVDT measured the movement of the plunger and the output voltage was digitized and acquired by a data acquisition and analysis system, which was operated on an IBM PC-compatible computer. The sample tube is inserted into an insulated aluminum

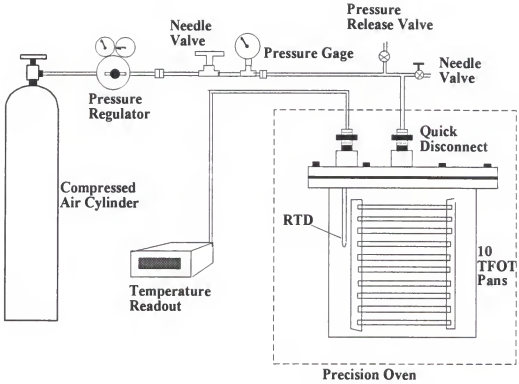

Figure 3-3 Schematic of PAV Test System

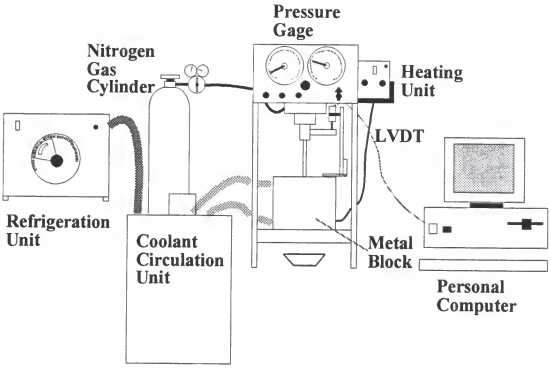

Figure 3-4 Canon Schweyer Rheometer System

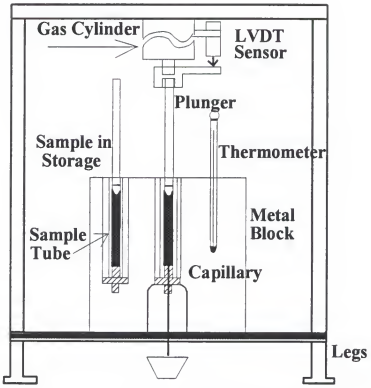

Figure 3-5 Schematic of Cannon Schweyer Rheometer

block which is maintained at the test temperature using coolant from a refrigeration unit in combination with an electrical wire heater, as shown in Figure 3.4.

Based on the assumption of a steady-state laminar flow of a power law fluid in a capillary tube, the shear stress and shear rate under an applied pressure can be calculated from the movement of the plunger and dimensions of the tube. Tests are usually conducted at a minimum of five stress levels. The shear susceptibility is computed and used to calculate the constant power viscosity ($\eta_{ij=100}$) at 100 W/m^3. This is the viscosity when the shear stress times the shear rate equals 100 W/m^3.

3.2.4 Brookfield Rheometer

The Brookfield Rheometer is a rotational viscometer. The torque required to rotate an immersed element (the spindle) in a fluid and the angular velocity of the spindle are measured and used to compute the shear stress and shear rate, respectively. A model HB DV-3 with thermoset system is to be used in this study.

The DV-3 model is designed to be connected to a personal computer to form a testing system as shown in Figure 3.6. Tests were performed at more than five rotation speeds (shear rates). A power law equation was used to analyze these data and the viscosity at a shear rate equal to 1 sec^{-1}, $\eta_{1.0}$ was selected to be the viscosity to be reported. A total of 54 samples, which cover different types of modified binders and different degrees of age hardening, were tested for absolute viscosity and Brookfield viscosity at 60 °C. It can be observed in Figure 3.7 that $\eta_{1.0}$ is larger than the absolute viscosity obtained from a capillary tube in the lower viscosity range ($\leq$ 10000 poises), while the reverse is true in the high viscosity range ($\geq$ 10000 poises). It is believed that

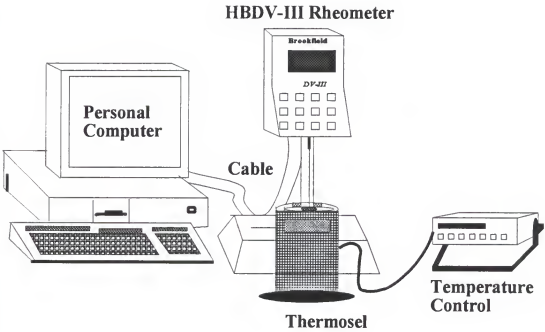

Figure 3-6 Brookfield HBDV-III Rheometer Reading and Controlling System

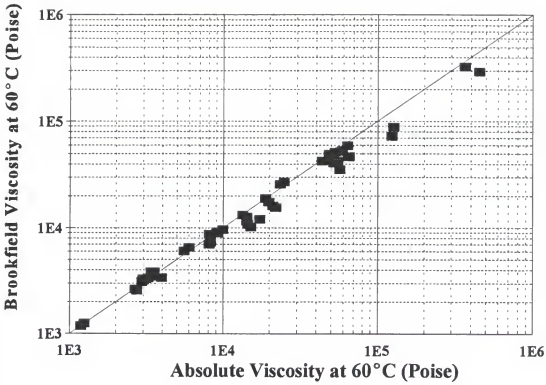

Figure 3.7 The Comparison of Brookfield Viscosity at Shear Rate of 1 sec^{-1} with Capillary Tube Viscosity at 60°C

$\eta_{1.0}$ can be used in place of the absolute viscosity [11]. The SHRP specifications require a maximum acceptable viscosity of 3 Pa-s at a test temperature of 135°C(274°F).

3.2.5 Fraass Breaking Point Tester

The Fraass breaking point test is one of the few standard tests which can be used to characterize the behavior of bitumens at very low temperatures (as low as -38°C). In this test, a film of asphalt is placed on a thin metal plate, and then is flexed it at increasing lower temperatures until the first crack is observed [28]. Figure 3.8 gives a general description of the component parts. The handle of the apparatus 'C' is turned at a rate of one revolution per second for 11 turns and then unwound at the same rate [29]. The controlled temperature of the plaque is lowered steadily at a rate of 1°C per minute by adding solid carbon dioxide (dry ice) to the acetone bath (G tube). Comparison of the Fraass temperature to the theoretical cracking temperature shows that the Fraass breaking point is usually 16-19°C above the cracking temperature. This is due to the much higher strain rate which is applied to the asphalt in Fraass Breaking Point test [28].

3.3 Laboratory Testing Program Using SHRP Binder Tests

3.3.1 Standard SHRP Binder Tests for Performance Grading

There are two forms of testing associated with the new SHRP binder specification: conformance testing and classification testing. The conformance testing is an accept/reject form of testing where the properties of a binder sample are compared to the required properties for a single grade. However, research and development laboratories usually perform classification testing. In classification testing, a coordinated series of tests must be performed to classify an unknown material according to the proposed SHRP binder

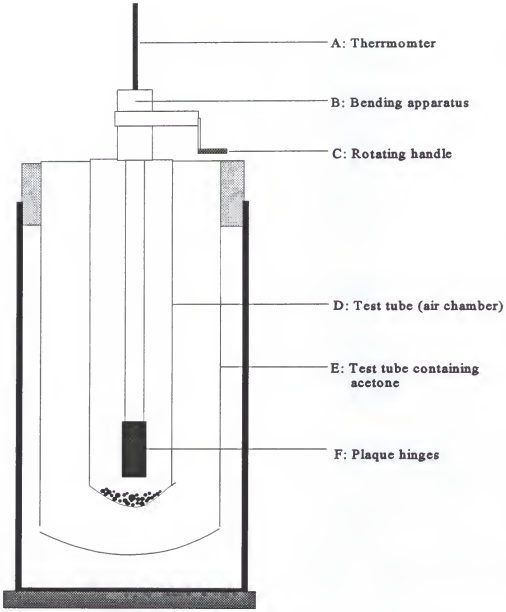

Figure 3.8 Schematic of Fraass Breaking Point Tester

specification. The classification testing was employed in this study to classify performance grade of asphalt binders according to AASHTO MP, "Standard Specification for Performance Graded Asphalt Binder," and AASHTO PP, "Standard Practice for Grading or Verifying the Performance Grade of an Asphalt Binder."

A flow chart illustrating the testing program to grade an asphalt cement in according to the SHRP PG grading system is shown in Figure 2.5. The low-temperature measurements are made at the minimum pavement design temperature plus 10°C. The following section describes some special facilities for the SHRP binder tests used in this study including a dynamic shear rheometer, a bending beam rheometer and a direct tension tester.

3.3.1.1 Dynamic Shear Rheometer

Dynamic shear rheometers (DSR) are used to measure the elastic and viscous properties and the time - temperature effects of asphalt cements at intermediate and high temperatures. A Bohlin Instruments Dynamic shear rheometer was used in this study and is illustrated in Figure 3.9. It is applicable to asphalt binders having dynamic shear modulus (G*) values in the range from 100 Pa to 100 MPa. This range of modulus is typically obtained between 5°C to 85°C. It is intended to determine the linear viscoelastic properties of asphalt binders as required for specification testing and is not intended as a comprehensive procedure for the full characterization of the viscoelastic properties of asphalt binder [30].

The principle of a dynamic shear rheometer test is simple (Figure 3.10) [3]. A sample of asphalt cement is placed between a fixed plate and a plate which oscillates

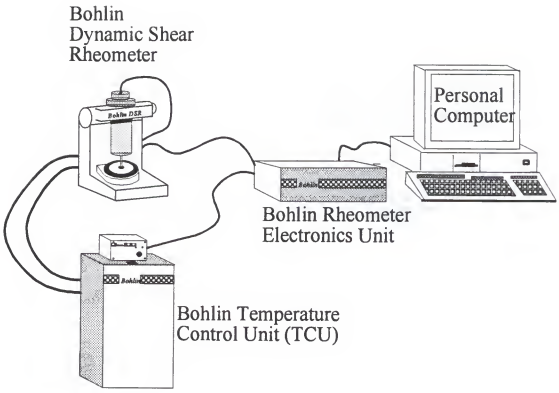

Figure 3.9 Bohlin Dynamic Shear Rheometer Test System

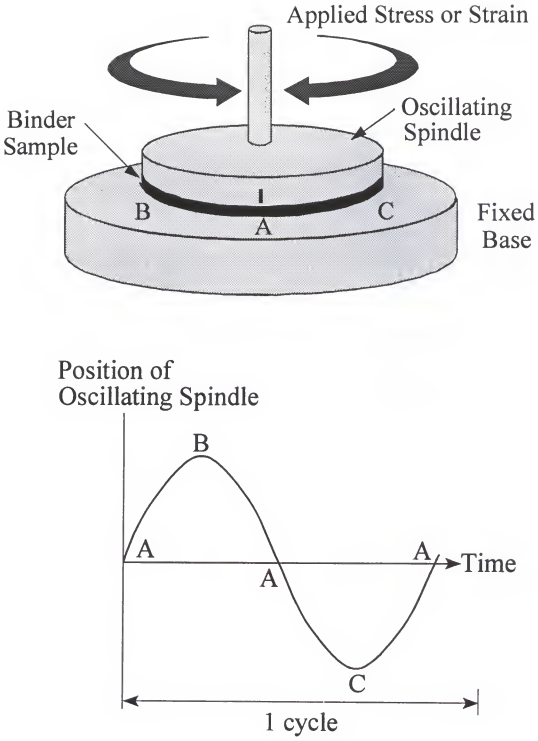

Figure 3.10 Dynamic Shear Rheometer Principles

back and forth. This oscillation movement, from point A to point B, back through point A to point C, and then back to point A, comprises one cycle of the dynamic shear rheometer. The frequency of this oscillation is simply the number of cycles of oscillation per unit time. The two expressions used to describe the frequency of oscillation are Hertz (Hz) and radians per second (rad/sec). All SHRP dynamic shear rheometer tests are performed at a frequency of 10 rad/sec or 1.59 Hz [30].

3.3.1.2 Bending Beam Rheometer

Since asphalt binders at low temperatures are very stiff, SHRP developed a new test which can accurately measure the low temperature properties of an asphalt binder. The new SHRP test which is the bending beam rheometer (BBR) as described in AASHTO TP1 [31], is a device which measures how much an asphalt binder will deflect or creep under a constant load. The asphalt binder is tested at its lowest pavement service temperature when the asphalt binder behaves like an elastic solid. The principle of operation for the bending beam rheometer is shown in Figure 3.11[3].

A Cannon Instruments Bending Beam Rheometer was used in this study and the schematic of the BBR is shown in Figure 3.11 [1]. It is applicable to material having flexural creep stiffness value from 30 MPa to 1 GPa and can be used within the temperature range from -40 to 25°C [30].

The bending beam rheometer test loads an asphalt beam for four minutes with a constant load and measures the deflection at the center of the beam continuously throughout the test. From the continuous deflection data, the time dependent flexural

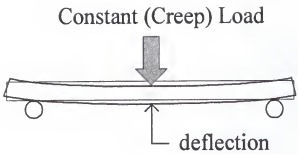

Bending Beam Rheometer Princip

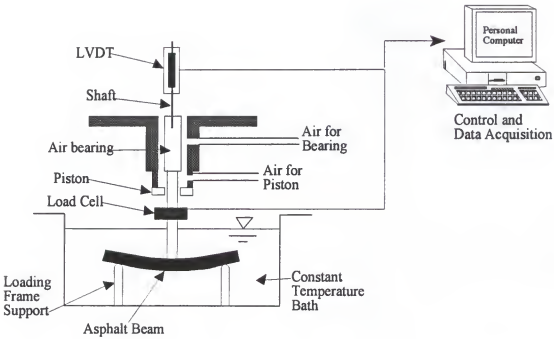

Figure 3.11 Schematic of the Bending Beam Rheometer

creep stiffness, "S(t)", and the slope, "m", of the logarithm of stiffness curve versus the logarithm of time are measured and calculated.

3.3.1.3 Direct Tension Test

Although creep stiffness can be used to estimate failure properties of asphalt binders, for some modified asphalt binders, the relationship between stiffness and failure strength is unknown. Moreover, the parameter creep stiffness as measured by the bending beam rheometer is not enough to characterize the ability of an asphalt binder to stretch before breaking. Some asphalt binders can have a high creep stiffness and are able to stretch far before failure or breaking. Recently, SHRP researchers devised a new device to measure the strength and the ability of an asphalt binder to stretch strain before failure at low temperatures. This device is called the direct tension test (DTT), which is described in AASHTO TP3 [32]. The direct tension test is used to identify the temperature region where an asphalt binder has limited ability to stretch without cracking . In the new SHRP asphalt binder specifications, a minimum allowable strain at failure of 1.0% for PAV+RTFOT residues is required at a specified temperature and rate of elongation. In SHRP specification testing, the elongation rate is 1.0 mm/min., and the test temperature is selected according to the performance grade of asphalt binder being tested.

In the direct tension test, an asphalt binder specimen is loaded at a slow constant rate until failure. The failure strain is calculated from the sample elongation at failure as follows:

$$\text{failure strain} = \frac{\text{elongation}}{\text{length before test}}$$

The failure strain gives an indication of the brittleness of a binder at low temperatures [3].

3.3.2 Additional Binder Characterization by SHRP Tests

In addition to specification testing, the binders used in this study are also to be characterized more extensively by the SHRP tests. A flow chart illustrating the testing program to be used to characterize the asphalt binders is shown in Figure 3.12. This testing program is to evaluate nine asphalt binders by a dynamic shear rheometer (DSR), a bending beam rheometer (BBR) and a direct tension tester (DTT) at different aging conditions. Both DSR and BBR can characterize the linear viscoelastic behavior of asphalt binders by using the time-temperature superposition method. These tests are performed at convenient temperatures using small strains within the linear viscoelastic region. The response of an asphalt at higher frequency is similar to its response at a lower temperature and lower frequency. Conversely, the response of an asphalt at lower frequency is similar to its response at a higher temperature and higher frequency. This phenomenon is according to the principle of superposition [33].

In the DSR test, the frequency sweep was performed from the highest frequency to the lowest frequency (30, 10, 2, 1.5, 1.0, 0.1, and 0.01Hz), beginning with the lowest temperature and proceeding to the warmer temperatures. The testing temperature includes two temperature ranges. One is the maximum pavement design temperature ranging from 52 to 76°C. The other is the intermediate pavement design temperature

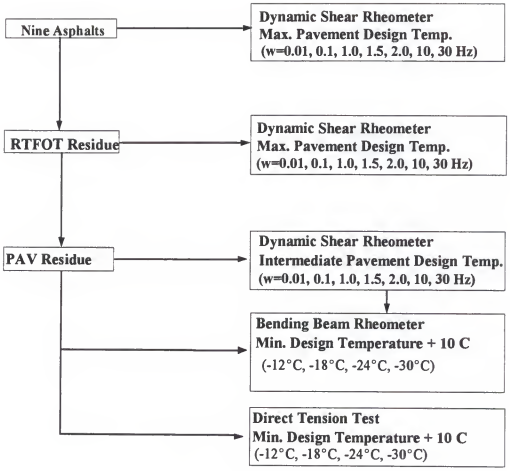

Figure 3.12 Flow Chart of Additional SHRP Binder Tests for Characterization

ranging from 3 to 34°C. In BBR and DTT tests, the testing temperature is at approximately the minimum design temperature ranging from -12 to -30°C.

3.4 Laboratory Testing Program on Asphalt Mixture

The testing program on asphalt mixtures is shown in Figure 3.13. Three different asphalts (conventional and modified) were blended with an aggregate with a fixed gradation and at a fixed asphalt content in the laboratory to produce mixtures complying with the Florida DOT S-I mix specification. The three binders used were (1) Coastal AC-30, (2) Coastal AC-30 + 10%GTR, and (3) Coastal AC-10 + 3%UP2879SBR. The control specimens were those made of unaged mixtures compacted by the gyratory testing machine (GTM). The other mixtures were subjected to the SHRP proposed short term oven aging (STOA) and long term oven aging (LTOA) processes. After the STOA or LTOA process, all mixtures were compacted by the gyratory testing machine at initial and ultimate compactions, 18 and 200 revolutions respectively, to reach air contents of 6 to 7 and 3 to 4 percents. Nine replicate samples were fabricated and tested for each condition. In addition, for each type of mixture, two extra samples were made in order to run the Rice specific gravity tests. This amounts to a total of ($9\times3\times3\times2+2\times3\times3=$) 180 samples were tested in this study. The compacted asphalt mixture samples were evaluated by the following tests:

(1) Diametral resilient modulus and indirect tensile creep tests at temperatures of 0, -10 and -20°C.

(2) Indirect tensile strength tests at a temperature of -10°C.

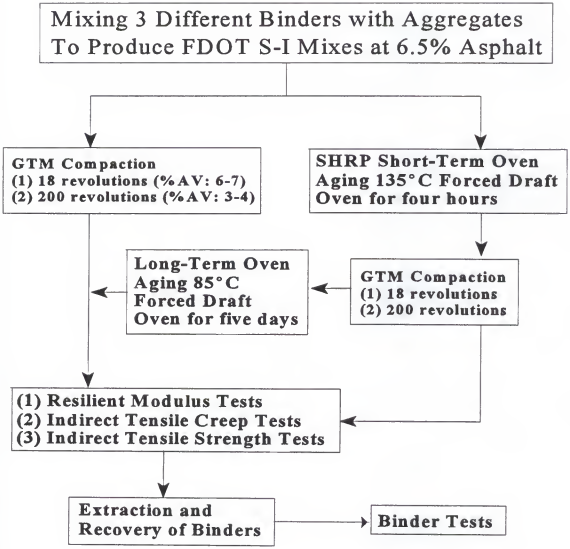

Figure 3.13 Flow Chart of Testing Program on Asphalt Mixtures

After the mixtures were evaluated and failed by the indirect tensile strength test at -10°C, asphalt binders were extracted and recovered by means of the reflux, centrifuge and rotavapor methods, which are presently used by the Florida Department of Transportation. All of the recovered STOA and LTOA residues were evaluated by (1) Penetration test at 25°C, (2) Brookfield viscosity test at 60°C, (3) Dynamic Shear Rheometer (DSR) test at high service temperatures from 52 to 70°C on STOA residues and at intermediate temperatures from 13 to 31°C on LTOA residues, (4) Bending Beam Rheometer (BBR) test at low service temperatures of -10 and -24°C.

3.4.1 GTM Compaction and Tests

The specimens for the mixture testing program were compacted in the Gyratory Testing Machine (GTM). The three asphalt binders were blended with a washed aggregate with a controlled gradation and at a fixed asphalt content (6.5%) in the laboratory to produce mixtures complying with the Florida DOT S-I (structural) mix specifications. The aggregate blend was obtained by blending a Florida Mining Materials #67 stone, S1-B, screening, a Canal Auth sand, and a mineral filler. Table 3.2 lists the gradations of the individual aggregates and the gradation of the aggregate blend used. The gradation of aggregate blend used also meets the SHRP specifications for a 19.0 mm mixture, which are also listed in Table 3.2. Marshall-size (4 inches in diameter and 2 inches in height) specimens were compacted in the GTM to two compaction levels which are to simulate (1) the initial field compaction and (2) the condition after five to ten years of traffic on the pavement. Table 3.3 displays the machine settings used for simulation of these two different compaction conditions. The initial compaction condition was achieved

Table 3.2 Gradation of Aggregates and Job Mix Formula for Asphalt Mixture

Aggregate Type	#67 stone	S-1B	Screening	Sand	Mineral Filler	Bulk Specific Gravity of Aggregates Retained
Sieve (Percentage Passing)						
3/4"	100	100	100	100	100	-
1/2"	72.2	100	100	100	100	2.375
3/8"	25.0	89.5	100	100	100	2.379
#4	4.7	14.7	97.3	100	100	2.345
#10	1.0	1.0	61.2	100	100	2.298
#40	0.5	0.4	16.0	72.8	100	2.333
#80	0.4	0.2	2.3	15.0	99.1	2.655
#200	0.0	0.0	0.0	0.0	85.8	2.784

Sieve (%passing)	S-I Mixture Specification	Job Mix Formula	Sieve (%passing)	SHRP Specification for 19.0 mm Mixture	Job Mix Formula
3/4"	100	100	1"	100	100
1/2"	88-100	94	3/4"	90-100	100
3/8"	75-93	84	#8	23-49 **(34.6)***	44.3
#4	47-75	57	#16	**(22.3-20.7)***	34.5
#10	31-53	42	#30	**(16.7-20.7)***	25.7
#40	19-35	22	#50	**(13.7)***	11.9
#80	7-21	8	#200	2-8	4.0
#200	2-6	4			

Note: ( )* means restricted zone which is outside of the specification limits.

Table 3.3 GTM Settings Used for Simulation of Initial Compaction and Densification

Testing Condition	Initial Compaction	Densification
Gyratory Angle (°)	3	3
Ram Pressure (psi)	100	100
Air Roller Pressure (psi)	9	9
Revolutions	18	200

by applying 18 GTM revolutions to the samples at 275 - 300°F. After initial compaction, specimens were cooled in the molds to room temperature for at least 6 hours, then reheated to 140°F for the ultimate compaction. The ultimate compaction condition was achieved by applying 200 GTM revolutions to the samples at 140°F. Specimens heights and air roller pressures were read at specified intervals during the GTM compaction process, and these data were used to compute the gyratory shear, bulk density, %Air Voids, %VMA and %MTD of the mixtures at these different compaction levels. These properties of the mixtures at various compactive levels as they were compacted to the initial and ultimate compaction conditions are listed in Table A.9 in the Appendix.

3.4.2 Diametral Resilient Modulus Test

Diametral resilient modulus test was run using the test set-up for the SHRP Indirect Tensile Test at Low Temperatures (ITLT), which is illustrated in Figure 3.14. The resilient modulus is defined as the ratio of the applied stress to the recoverable strain when a repeated dynamic load is applied. The resilient modulus test is run in a load-control mode and involves applying a repeated haversine waveform load to the specimen for a period (0.1 second). The load was selected to keep horizontal strains in the linear viscoelastic range (typically below a horizontal strain of 350 microstrains) during the resilient modulus test and is applied vertically in the vertical diametral plane of a cylindrical specimen of asphalt mixture. Poisson's ratio, which is essential for accurate determination of resilient modulus in this method, is determined using the measured horizontal and vertical deformations. Resilient modulus can be determined using this Poisson's ratio along with repeated load, specimen dimensions, and the time-dependent

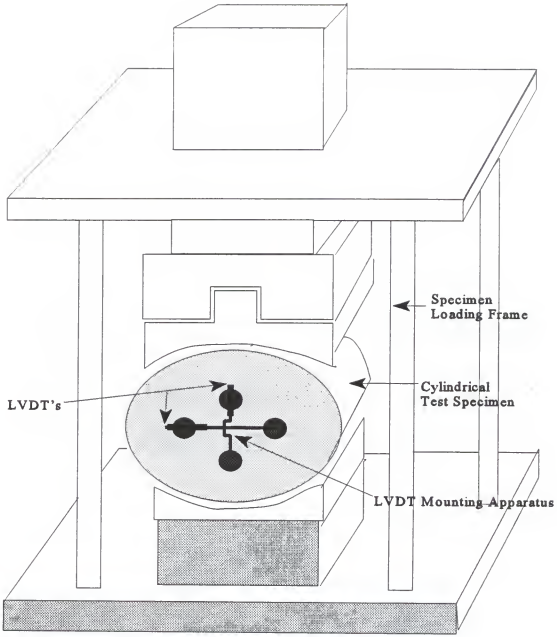

Figure 3.14 Indirect Tensile Testing Device

horizontal deflection, using equations which were developed based upon three-dimensional finite element analysis by Roque and Buttlar [34-36]. The procedure for resilient modulus test consists of the following steps:

1) The test specimens were cut parallel and close to the top and bottom faces using a water-cooled masonry saw to produce smooth and parallel faces. Four brass gage points (5/16-inch diameter by 1/8-inch thick) were affixed with epoxy to each specimen face. Specimens were stored in a cabinet at a constant relative humidity of 60 percent for 3 days prior to testing to ensure uniform moisture conditions. Specimens were cooled at least 3 hours before the test.

2) LVDTs are mounted and centered on the specimen. Horizontal and vertical deflections were measured on each side of the specimen using linear voltage differential transducers (LVDT) mounted to the gage points. The mounting apparatus and LVDT are showed in Figure 3.15. The required range and resolution of measurements were ±0.1-inch and $\pm 10\times10^{-6}$ inch, respectively.

3) The test specimen is placed into load frame. A seating load of 10 to 30 pounds was applied to the test specimens to ensure that proper contact of the upper loading head was achieved before test loads were applied.

4) The specimen is then loaded by applying a repeated haversine waveform load to obtain horizontal strains between 150 and 350 microstrains during a 5 second resilient modulus test. If the horizontal strains are higher than 350 microstrains, the load is immediately removed from specimen. Specimens should be allowed to recover for a minimum of 3 minutes before reloading at a different level.

Figure 3.15 Mounting and centering LVDT'S for Indirect Tensile Test

5) When the applied load is determined, the computer software (data acquisition program) will begin recording test data. The specimen is cycled (loaded and unloaded) five times at the load. Data aquisition system samples at 150 Hz.

In order to reduce the variability of the determined Poisson's ratio and resilient modulus, 3 replicate samples are used to generate one value of Poisson's ratio and one value of resilient modulus. The resilient modulus and Poisson's ratio are calculated by the following steps:

1) The average thickness, diameter and maximum load for each set of 3 samples are computed.

2) Find the instantaneous and total recoverable horizontal and vertical deformations (ΔH_I, ΔH_T, ΔV_I and ΔV_T). Interpretation of the data (ΔH_I, ΔH_T, ΔV_I and ΔV_T) is shown in Figure 3.16.

3) Compute normalized instantaneous and total recoverable horizontal and vertical deformations ($\Delta H_{I(NORM)}$, $\Delta H_{T(NORM)}$, $\Delta V_{I(NORM)}$ and $\Delta V_{T(NORM)}$) for each of the 6 specimen faces (3 specimens, 2 faces per specimen).

$$\Delta H_{I(NORM)} = \Delta H_I \times C_{NORM}; \qquad \Delta H_{T(NORM)} = \Delta H_T \times C_{NORM};$$

$$\Delta V_{I(NORM)} = \Delta V_I \times C_{NORM}; \qquad \Delta V_{T(NORM)} = \Delta V_T \times C_{NORM};$$

$$C_{NORM} = \frac{t_i \; D_i \; P_i}{t_{avg} \; D_{avg} \; P_{avg}}$$

where,

$\Delta H_{I(NORM)}$ = normalized instantaneous recoverable horizontal deformation

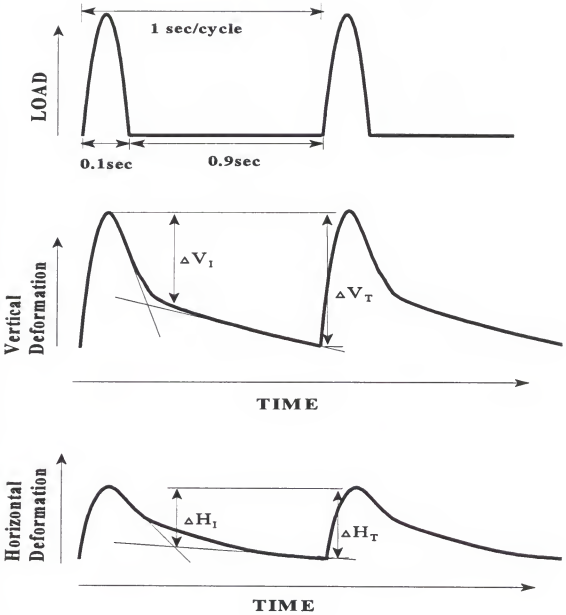

Note:

ΔH_I = Instantaneous recoverable horizontal deformation
ΔH_T = Total recoverable horizontal deformation
ΔV_I = Instantaneous recoverable vertical deformation
ΔV_T = Total recoverable vertical deformation

Figure 3.16 Typical Load, Deformation versus Time Relationships in a Repeated-Load Indirect Tension Test

$\Delta H_{T(NORM)}$ = normalized total recoverable horizontal deformation
$\Delta V_{I(NORM)}$ = normalized instantaneous recoverable vertical deformation
$\Delta V_{T(NORM)}$ = normalized total recoverable vertical deformation
C_{NORM} = normalized factor
t_i, D_i, P_i = thickness, diameter, and maximum load of specimen i (i=1 to 3)
t_{avg}, D_{avg}, P_{avg} = average thickness, diameter, and maximum load of three replicate specimens

4) Obtain the trimmed mean of the normalized instantaneous and total recoverable horizontal and vertical deformations by numerically ranking the 6 $\Delta H_{I(NORM)}$, $\Delta H_{T(NORM)}$, $\Delta V_{I(NORM)}$ and $\Delta V_{T(NORM)}$ values and averaging the 4 middle values. Thus, the highest and lowest values of the normalized instantaneous and total recoverable horizontal and vertical deformations are not included in the trimmed mean.

5) Obtain the ratio of horizontal to vertical deformations, X/Y, which is equal to the ratio of trimmed mean of the normalized horizontal to vertical deformations.

6) Compute resilient moduli and Poisson's ratio by the following equations:

$$MR_I = \frac{P_{avg}\ GL}{\Delta H_{I_{trimmean}}\ t_{avg}\ D_{avg}\ C_{cmpl}}$$

$$MR_T = \frac{P_{avg}\ GL}{\Delta H_{T_{trimmean}}\ t_{avg}\ D_{avg}\ C_{cmpl}}$$

$$v_I = -0.10 + 1.480\times(X/Y)_I^2 - 0.778\times(t_{avg}/D_{avg})^2\times(X/Y)_I^2$$

$$v_T = -0.10 + 1.480\times(X/Y)_T^2 - 0.778\times(t_{avg}/D_{avg})^2\times(X/Y)_T^2$$

where,

MR_I = instantaneous resilient modulus, GPa
MR_T = total resilient modulus, GPa
v_I = instantaneous resilient Poisson's ratio
v_T = total resilient Poisson's ratio
GL = gage length, inch
$\Delta H_{I\ trimmean}$ = trimmed mean of the instantaneous horizontal deformation
$\Delta H_{T\ trimmean}$ = trimmed mean of the total horizontal deformation
$(X/Y)_I$ = ratio of the instantaneous horizontal to vertical deformations
$(X/Y)_T$ = ratio of the total horizontal to vertical deformations
$C_{cmpl} = 0.6354 \times (X/Y)^{-1} - 0.332$

A computer program, which was written by R. Roque and X. Wang, was used to analyze these load and deflection data obtained by the data acquisition program to determine the instantaneous and total resilient moduli and Poisson's ratio. The instantaneous and total resilient moduli and Poisson's ratio obtained were tabulated in Table B.1 in the Appendix.

3.4.3 Indirect Tensile Creep Test

The SHRP Indirect Tensile Test at Low Temperatures (ITLT) was used to measure the creep properties of the mixtures. The test set-up is illustrated in Figure 3.14. The creep test is run in a load-control mode and involves applying a static load very quickly and then holding it constant throughout the duration of the test. The horizontal and vertical deformations measured near the center of the specimen are used to calculate a tensile creep compliance as a function of time. The load was selected to keep horizontal strains in the linear viscoelastic range (typically below a horizontal strain of 500 microstrains) during the creep test. Poisson's ratio, which is essential for accurate determination of creep compliance in this method, is determined using the measured

horizontal and vertical deformations. The development and evaluation of this test method and specific test procedures were presented in detail by Buttlar and Roque [35], and in the AASHTO Provisional Standard TP9 [37]. The procedure for tensile creep test consists of the following steps:

1) The preparation of test specimens are same as that for resilient modulus test as described in section 3.4.2.

2) The mounting and centering LVDT of test specimens are same as that for resilient modulus test.

3) The test specimen is placed into load frame. A seating load of 10 to 30 pounds was applied to the test specimens to ensure that proper contact of the upper loading head was achieved before test loads were applied.

4) A test specimen under an applied creep load should have horizontal strains between 40 and 120 microstrains at t= 30 seconds for a 1000-second creep test. If the horizontal strains are lower than 40 or higher than 120 microstrains at t= 30 seconds, the load is immediately removed from specimen. Specimens should be allowed to recover for a minimum of 3 minutes before reloading at a different level.

5) When the applied load is determined, the four displacements and the creep load were recorded in three stages. They are recorded at a rate of 10 Hz for the first 10 seconds, at 1 Hz for the next 290 seconds, and at 0.2 Hz for the remaining 700 seconds of the creep test.

In order to reduce the variability of the determined Poisson's ratio and creep compliance, 3 replicate samples are used to generate one value of Poisson's ratio and one value of creep compliance. The creep compliance and Poisson's ratio are calculated by the following steps:

1) The average thickness, diameter and maximum load for each set of 3 samples are computed.

2) Compute normalized horizontal and vertical deformations ($\Delta H_{(NORM)}$, and $\Delta V_{(NORM)}$) for each of the 6 specimen faces (3 specimens, 2 faces per specimen).

$$\Delta H_{(NORM)} = \Delta H \times C_{NORM}; \qquad \Delta V_{(NORM)} = \Delta V \times C_{NORM};$$

$$C_{NORM} = \frac{t_i \; D_i \; P_i}{t_{avg} \; D_{avg} \; P_{avg}}$$

where,

$\Delta H_{(NORM)}$ = normalized horizontal deformation
$\Delta V_{(NORM)}$ = normalized vertical deformation
C_{NORM} = normalized factor
t_i, D_i, P_i = thickness, diameter, and maximum load of specimen i (i=1 to 3)
t_{avg}, D_{avg}, P_{avg} = average thickness, diameter, and maximum load of three replicate specimens

3) Obtain the average normalized horizontal and vertical deformations, ΔH_{avg} and ΔV_{avg}, at halfway (500 sec) creep loading period for each of the 6 specimen faces.

4) Obtain the trimmed mean of the average normalized horizontal and vertical deformations by numerically ranking the 6 ΔH_{avg} and ΔV_{avg} values and averaging the

4 middle values. Thus, the highest and lowest values of the average normalized horizontal and vertical deformations are not included in the trimmed mean.

5) Obtain the ratio of horizontal to vertical deformations, X/Y, which is equal to the ratio of trimmed mean of the average normalized horizontal to vertical deformations.

6) compute creep compliance and Poisson's ratio by the following equations:

$$D(t) = \frac{\Delta H_{avg}\ t_{avg}\ D_{avg}\ C_{cmpl}}{P_{avg}\ GL}$$

$$v = -0.10 + 1.480\times(X/Y)^2 - 0.778\times(t_{avg}/D_{avg})^2\times(X/Y)^2$$

where,

D(t) = creep compliance at time t, 1/psi
v = resilient Poisson's ratio
GL = gage length, inch
ΔH_{avg} = trimmed mean of the average normalized horizontal deformation
(X/Y) = ratio of the average normalized horizontal to vertical deformations
$C_{cmpl} = 0.6354\times(X/Y)^{-1} - 0.332$

A computer program, which was written by R. Roque and W. Buttlar, was used to analyze these load and deflection data obtained by the data acquisition program to calculate creep compliance and Poisson's ratio. The creep compliance and Poisson's ratio obtained were tabulated in Table B.2 in the Appendix.

3.4.4 Indirect Tensile Strength Test

The indirect tensile strength is the maximum tensile stress that a specimen can tolerate before fracture. This mix property is useful for predicting thermal cracking

potential and characterizing the resistance to failure of asphalt concrete caused by tensile stresses. The tensile strength test was set up immediately after accomplishing the tensile creep test by changing load-control mode to displacement-control mode. The ramp movement to the specimen at a rate of 0.5-inch per minute for 4-inch-diameter specimens was used in this study. Data were collected at a rate of 20 Hz for the duration of the test. Both the horizontal and vertical deformations as well as the applied load can be recorded during the test. The maximum tensile strength then can be calculated as:

$$S_t = \frac{2\ P\ (C_{sx})}{\pi\ b\ D}$$

where,

C_{sx}	=	0.948 - 0.01114*(b/D) - 0.2693*(v) + 1.436*(b/D)(v)
S_t	=	maximum indirect tensile strength, psi
P	=	failure load at first crack, lbf
b	=	specimen thickness, inches
D	=	specimen diameter, inches
v	=	Poisson's ratio

The test procedure for determining the indirect tensile strength of the mixture is described in the AASHTO Provisional Standard TP9 [37].

3.4.5 Asphalt Extraction and Recovery Methods

After the mixtures were evaluated and failed by the indirect tensile strength test at -10°C, asphalt binders were extracted and recovered by means of the reflux, centrifuge and rotavapor methods, which are presently used by the Florida Department of Transportation. The extraction method used is the reflux method (ASTM D2172 Method

B [38]). The extracted solutions were centrifuged at a force of higher than 770 times gravity for at least 30 minutes accordance to ASTM D1856 [39] to eliminate mineral matter. The recovery apparatus used is the Buchi Rotavapor and the recovery method used is according to the "Standard Test Method for Recovery of Asphalt from Solution Using the Rotavapor Apparatus, Draft 9" [40]. The solvent used in this study is trichloroethylene which is used in the routine reflux/Abson procedure of FDOT.

CHAPTER 4
RESULTS OF CONVENTIONAL AND SHRP BINDER TESTS

4.1 Results of Conventional Binder Tests

The results of penetration tests at 25°C, absolute viscosity and Brookfield viscosity tests at 60 °C, Fraass breaking point tests, and Schweyer rheometer tests at 5, 15 and 25°C on the binders before and after the RTFOT and PAV processes, are listed in Appendices Table A.1 through Table A.5, respectively. These results were analyzed by using the statistical model as described in the following section. The percent retained penetration, the Fraass breaking point temperature, and the logarithm of aging indices at four different temperatures and three different tests were used as the response variables. Different evaluation parameters were analyzed separately. The weight of the samples were measured before and after the RTFOT and PAV+RTFOT aging processes and the data are included in this section.

4.1.1 Statistical Model

Statistical analysis using the ANOVA model was used to determine whether the effect of main factors and interactions of factors are significant. The effects of asphalt type and aging process were studied by means of this method. The test results from the binder tests were analyzed on the basis of a factorial experiment that included nine types of asphalt and two types of aging process. Asphalt (α) and aging process (β) are regarded

as fixed effects. The following linear model is assumed for any single response variable in the experiment :

$$Y_{ijk} = \mu + \alpha_i + \beta_j + (\alpha\beta)_{ij} + \epsilon_{ijk}$$

where

Y_{ijk} = the response of kth replicate, j^{th} aging process, and i^{th} asphalt

μ = the overall mean

α_i = the main effect of ith asphalt type

β_j = the main effect of jth aging process

$\alpha\beta_{ij}$ = the interaction effect

ϵ_{ijk} = the experimental error

i = 1 to 9 for nine asphalts

j = 1 to 3 for three aging processes

k = 1 to 2 for two replicates

SAS/STAT computer program was use to perform the analysis. A probability of Type I error (α) of 0.05 was used. Comparison of means was done by Duncan's multiple-range test at an α level of 0.05. However, some test data did not meet the assumption of homogeneity of variance as assumed by the ANOVA model, and the data had to be transformed to meet the requirement of homogeneity of variance. The usual approach for dealing with that kind of nonconstant variance is to apply a variance-stabilizing transformation and then to run the analysis of variance on the transformed data. If the data follows the log-normal distribution, then the logarithmic transformation is appropriate [41]. A logarithmic transformation was applied to the absolute viscosity and Brookfield

viscosity and the homogeneity of variance was improved through the logarithmic transformation of data.

4.1.2 Weight Change

The SHRP Pressure Aging Vessel (PAV) was performed on 9 binders (5 original and 4 modified asphalts). The weight changes of the samples during the RTFOT process and the subsequent PAV process were measured. The results are displayed in Table A.6 and Figure 4.1. It can be seen that all the samples experienced weight loss (possibly due to the loss of volatile) during the RTFOT process. However, they were all less than the maximum limit of 1%. It can also be noted that all the samples experienced weight gain (possibly due to oxidation) during the PAV process. The total weight changes are negative for four binders and positive for the other five binders.

4.1.3 Penetration

Table A.1 shows the results of the penetration test at 25°C of the binders before and after the RTFOT and PAV processes. Percent retained penetration, which is the ratio of the penetration of the aged residue to that of the unaged binder, was computed for the different binders. Figure 4.2 shows the graphical display of the average percent retained penetration of the different binders after the RTFOT and PAV processes. It can be seen that the C3GT (AC-30 + 10% GTR) binder has the lowest aging potential by having the highest percent retained penetration after the RTFOT and PAV processes.

The results of ANOVA on the percent retained penetration, which are displayed in Table 4.1, show that the nine asphalts have different degrees of effects on age-hardening processes and there is significant interaction effect between asphalt types and aging

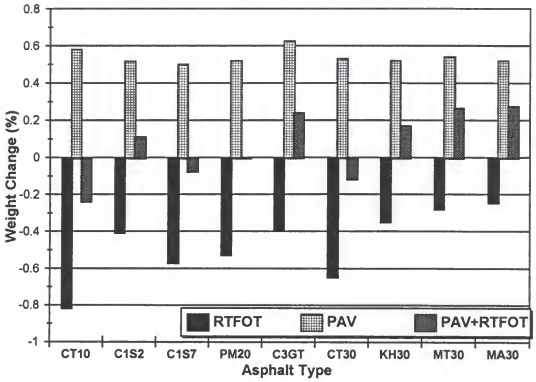

Note: CT10 - Coastal AC-10.
C1S2 - Coastal AC-10+3%SBR2879.
C1S7 - Coastal AC-10+3%SBR70.
PM20 - Ergon PMAC-20.
C3GT - Coastal AC-30+10%GTR.
CT30 - Coastal AC-30.
KH30 - Koch AC-30.
MT30 - Marathon AC-30.
MA30 - Mariani AC-30.

Figure 4.1 Weight Change of Nine Asphalts After RTFOT and PAV aging Processes

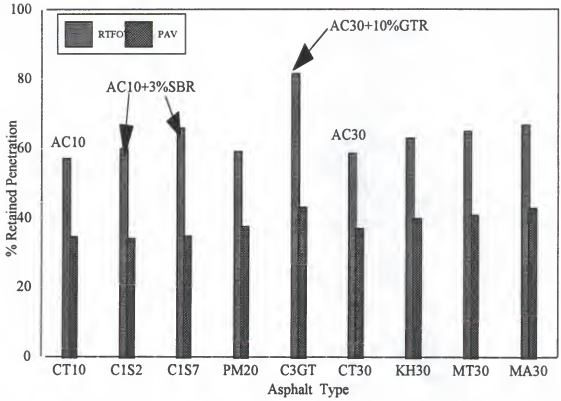

Note: CT10 - Coastal AC-10.
C1S2 - Coastal AC-10+3%SBR2879.
C1S7 - Coastal AC-10+3%SBR70.
PM20 - Ergon PMAC-20.
C3GT - Coastal AC-30+10%GTR.
CT30 - Coastal AC-30.
KH30 - Koch AC-30.
MT30 - Marathon AC-30.
MA30 - Mariani AC-30.

Figure 4.2 Percent Retained Penetration of Nine Asphalts Aged by the RTFOT and PAV

Table 4.1 Results of ANOVA and Duncan's Grouping on the Percent Retained Penetration in the comparison of RTFOT and PAV on Asphalt binders

Dependent Variable: **% retained penetration [Model = $\mu + \alpha_i + \beta_j + (\alpha\beta)_{ij} + \epsilon_{ijk}$]**

Source	DF	ANOVA SS	Mean Square	F Value	Pr > F
ASPHALT, α	8	927.165677	115.895710	59.79	0.0001
METHOD, β	1	5811.807262	5811.807262	2998.16	0.0001
INTERACTION, $\alpha\beta$	8	247.148552	30.893569	15.94	0.0001

R-Square= 0.995305

Duncan Grouping at METHOD=RTFOT

			Mean	N	ASPHALT*
	A		81.541	2	C3GT
	B		66.601	2	MA30
	B				
C	B		65.789	2	C1S7
C	B				
C	B		64.837	2	MT30
C					
C	D		62.823	2	KH30
	D				
E	D		59.921	2	C1S2
E					
E			59.098	2	PM20
E					
E			58.540	2	CT30
E					
E			57.104	2	CT10

Duncan Grouping at METHOD= PAV+RTFOT

			Mean	N	ASPHALT*
	A		43.041	2	C3GT
	A				
	A		42.000	1	MA30
	A				
B	A		40.856	2	MT30
B	A				
B	A	C	39.817	2	KH30
B		C			
B	D	C	37.487	2	PM20
	D	C			
	D	C	36.991	2	CT30
	D				
	D		34.782	2	C1S7
	D				
	D		34.639	2	CT10
	D				
	D		34.011	2	C1S2

Note: Means with the same letter are not significantly different at α=0.05.
* The meaning of the codes for the asphalt types can be found in Table 3.1.

processes. The Duncan's multiple range test was performed to compare the means of different asphalts and different aging processes (RTFOT and PAV) with a Type I error of 0.05 (α=0.05). The results of the Duncan's test are also shown in Table 4.1. The asphalts and processes which are denoted by the same letters are not significantly different from one another. It can be seen that the C3GT (AC-30+10%GTR) asphalt shows the highest percent retained penetration after both RTFOT and PAV processes. And the AC-10 based asphalts (CT10, C1S7 and C1S2) show severe aging due to low percent retained penetration after both RTFOT and PAV processes. The RTFOT process hardens the asphalts to approximately 60% of retained penetration and the RTFOT+PAV process hardens the asphalts to approximately 40% of retained penetration for all nine asphalt binders. Due to the insensitivity of penetration measurements at lower penetrations, the percent retained penetration may be an inappropriate parameter for comparing the aging severity of harder asphalts.

4.1.4 Absolute Viscosity and Brookfield Viscosity

Table A.2 and Table A.3 display the results of the absolute viscosity tests at 60 °C and the Brookfield viscosity tests at a shear rate of 1 s^{-1} and a temperature of 60 °C respectively. Figure 3.7 shows the plot the Brookfield viscosity at a shear rate of 1 s^{-1} versus the corresponding absolute viscosity. It can be seen that the Brookfield viscosity is very close to the absolute viscosity. However, when the viscosity is relative high, the Brookfield viscosity is lower than the absolute viscosity. A possible explanation for this difference lies in the shear susceptibility of the asphalts. When an asphalt is not severely aged and its viscosity is relatively low, the asphalt has a Newtonian flow behavior and the

viscosity does not change with shear rate. However, when an asphalt is severely aged and its viscosity is high, the asphalt tends to have a pseudo-plastic flow behavior and its viscosity would decrease as shear rate is increased. The absolute viscosity test is conducted at a lower shear rate than that of the Brookfield viscosity test. Thus, the Brookfield viscosity would tend to be lower than the absolute viscosity when an asphalt is severely aged.

Some modified asphalts, such as AC-10+3%SBR modified asphalt, were observed to climb up the spindle of the Brookfield viscometer during the test, resulting in a change in shearing area and incorrect test result. This phenomenon is known as the Weissenberg effect [11].

The result of ANOVA and Duncan's grouping on the Logarithm of absolute viscosity and Brookfield viscosity at 60°C is shown in Table 4.2. It can be seen that the C3GT (AC-30 +10%GTR) asphalt shows the highest viscosity and the CT10 (AC-10) asphalt shows the lowest viscosity before and after the aging processes. The SBR modified asphalts also have higher viscosity than that of the base asphalt.

The aging index (viscosity ratio), which is the ratio between the viscosity of the aged residue and that of the original asphalt, was used to represent the aging severity. Figure 4.3 shows the aging index of the RTFOT and PAV residues based on the absolute viscosity and Brookfield viscosity at 60 °C. It can be seen that the Ergon PMAC-20 has the lowest aging index and the Coastal AC-30 has the highest aging index among the nine binders evaluated.

Table 4.2 Results of ANOVA and Duncan's grouping on the Logarithm of Absolute Viscosity and Brookfield Viscosity in the comparison of RTFOT and PAV on asphalt binders

Dependent Variable: **Absolute Viscosity at 60°C [Model = $\mu + \alpha_i + \beta_j + (\alpha\beta)_{ij} + \epsilon_{ijk}$]**

Source	DF	ANOVA SS	Mean Square	F Value	Pr > F
ASPHALT, α	8	4.45313383	0.55664173	695.12	0.0001
PROCESS, β	2	14.24569874	7.12284937	8894.85	0.0001
ASPHALT*PROCESS, $\alpha\beta$	16	0.43247653	0.02702978	33.75	0.0001

R-Square=0.998871

Duncan Grouping at METHOD=Original

		Mean	N	ASPHALT*
	A	4.1983	2	C3GT
	B	3.9124	2	CT30
	C	3.5742	2	C1S2
	C			
D	C	3.5326	2	PM20
D				
D	E	3.5030	2	MA30
	E			
F	E	3.4761	2	MT30
F	E			
F	E	3.4739	2	KH30
F				
F		3.4321	2	C1S7
	G	3.0837	2	CT10

Duncan Grouping at METHOD=RTFOT

		Mean	N	ASPHALT*
	A	4.7664	2	C3GT
	B	4.3100	2	CT30
	B			
	B	4.3065	2	C1S2
	C	4.1660	2	PM20
	C			
	C	4.1396	2	C1S7
	D	3.9810	2	MT30
	D			
	D	3.9360	2	KH30
	D			
	D	3.9341	2	MA30
	E	3.7604	2	CT10

Note: * The meaning of the codes for the asphalt types can be found in Table 3.1.

Table 4.2 Continued

Duncan Grouping at METHOD=PAV+RTFOT

			Mean	N	ASPHALT*
	A		5.6099	2	C3GT
	B		5.0973	2	PM20
	C		4.8079	2	C1S2
	C				
D	C		4.7673	2	MT30
D	C				
D	C	E	4.7497	2	CT30
D		E			
D	F	E	4.7143	2	C1S7
	F	E			
	F	E	4.6995	2	KH30
	F				
	F		4.6643	2	MA30
	G		4.3823	2	CT10

Dependent Variable: **Brookfield Viscosity at 60°C [Model = $\mu + \alpha_i + \beta_j + (\alpha\beta)_{ij} + \epsilon_{ijk}$]**

Source	DF	ANOVA SS	Mean Square	F Value	Pr > F
ASPHALT, α	8	3.15599283	0.39449910	329.82	0.0001
PROCESS, β	2	12.98424580	6.49212290	5427.66	0.0001
ASPHALT*PROCESS, $\alpha\beta$	16	0.45237061	0.02827316	23.64	0.0001

R-Square=0.998057

Duncan Grouping at METHOD=Original

			Mean	N	ASPHALT*
	A		4.0564	2	C3GT
	B		3.8533	2	CT30
	C		3.5646	2	PM20
	C				
	C		3.5574	2	C1S2
	C				
D	C		3.5214	2	MA30
D	C				
D	C		3.5107	2	MT30
D					
D			3.4983	2	KH30
	E		3.4154	2	C1S7
	F		3.0855	2	CT10

Note: * The meaning of the codes for the asphalt types can be found in Table 3.1.

Table 4.2 Continued

Duncan Grouping at METHOD=RTFOT

		Mean	N	ASPHALT*
	A	4.6418	2	C3GT
	B	4.2340	2	C1S2
	B			
	B	4.2243	2	CT30
	C	4.1101	2	C1S7
	D	4.0344	2	PM20
	D			
E	D	3.9656	2	MT30
E				
E		3.9528	2	MA30
E				
E		3.9375	2	KH30
	F	3.7974	2	CT10

Duncan Grouping at METHOD=PAV+RTFOT

		Mean	N	ASPHALT*
	A	5.4913	2	C3GT
	B	4.9045	2	PM20
	C	4.7242	2	MT30
	C			
	C	4.7216	2	C1S2
	C			
D	C	4.6864	2	C1S7
D	C			
D	C	4.6613	2	MA30
D	C			
D	C	4.6545	2	KH30
D				
D		4.5887	2	CT30
	E	4.4211	2	CT10

Note: * The meaning of the codes for the asphalt types can be found in Table 3.1.
Means with the same letter are not significantly different at α=0.05

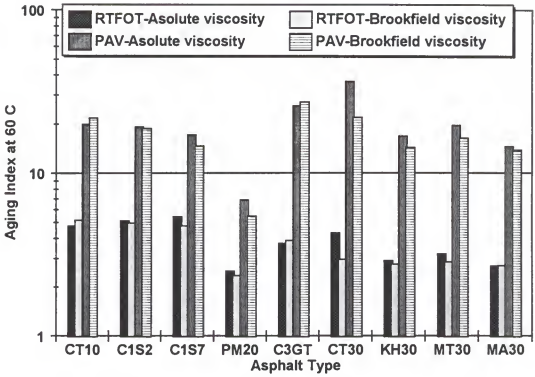

Note: CT10 - Coastal AC-10.
C1S2 - Coastal AC-10+3%SBR2879.
C1S7 - Coastal AC-10+3%SBR70.
PM20 - Ergon PMAC-20.
C3GT - Coastal AC-30+10%GTR.
CT30 - Coastal AC-30.
KH30 - Koch AC-30.
MT30 - Marathon AC-30.
MA30 - Mariani AC-30.

Figure 4.3 The Comparison of Aging Indices Based on Absolute and Brookfield Viscosity at 60°C

4.1.5 Constant Power Viscosity

The constant power viscosity at 5, 15, and 25°C of the different binders before and after the RTFOT and PAV processes are shown in Table A.5. Figure 4.4 displays the aging index of the RTFOT and PAV residues based on the constant power viscosity at 5, 15 and 25°C. It can be seen that the C3GT (AC-30+10%GTR) has the lowest aging index based on the viscosity at 5 and 15°C. The constant power viscosity at 5°C of the different aged asphalts are plotted in Figure 4.5. These viscosity values are compared with a limit of 2×10^{10} poises, which is usually used as the maximum allowable binder viscosity to avoid low temperature cracking of the asphalt mixture in service. As shown in Figure 4.5, three residues exhibit a viscosity value exceeding this limit. They are aged residues of MA30 (Mariani AC-30), MT30 (Marathon AC-30) and CT30 (Coastal AC-30).

To investigate the parallel shift pattern in the log-log plot of viscosity versus temperature, the Schweyer Rheometer tests were performed (with two replicates) at three temperatures, namely 5, 15 and 25 °C, on the nine asphalts and their residues aged by the RTFOT and PAV processes. Figure 4.6 shows the log-log plot of constant power viscosity ($\eta_{j=100}$) versus absolute temperature (°K) for the Coastal AC-30 asphalt. It is assumed that asphalts have Newtonian flow behavior at 60 °C and the absolute viscosity at 60 °C is equal to the constant power viscosity ($\eta_{j=100}$). With some variation, the parallel shift pattern are generally observed for all nine asphalts as similar to Figure 4.6.

Linear regression analyses were performed to estimate the viscosity-temperature relationship for the different asphalts before and after RTFOT and PAV processes. The purpose of these analyses is to determine how these relationships may change with aging.

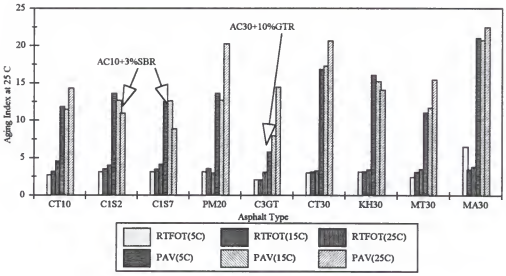

Note: CT10 - Coastal AC-10.
C1S2 - Coastal AC-10+3%SBR2879.
C1S7 - Coastal AC-10+3%SBR70.
PM20 - Ergon PMAC-20.
C3GT - Coastal AC-30+10%GTR.
CT30 - Coastal AC-30.
KH30 - Koch AC-30.
MT30 - Marathon AC-30.
MA30 - Mariani AC-30.

Figure 4.4 The Comparison of Aging Indices of Nine Asphalts Aged by the RTFOT and PAV

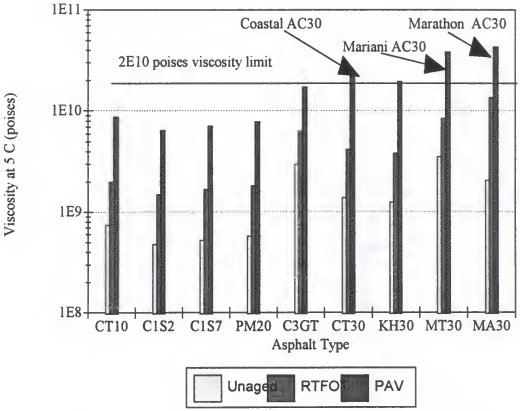

Note: CT10 - Coastal AC-10.
C1S2 - Coastal AC-10+3%SBR2879.
C1S7 - Coastal AC-10+3%SBR70.
PM20 - Ergon PMAC-20.
C3GT - Coastal AC-30+10%GTR.
CT30 - Coastal AC-30.
KH30 - Koch AC-30.
MT30 - Marathon AC-30.
MA30 - Mariani AC-30.

Figure 4.5 Constant Power Viscosity at 5°C of Nine Asphalts Aged by the RTFOT and PAV Processes

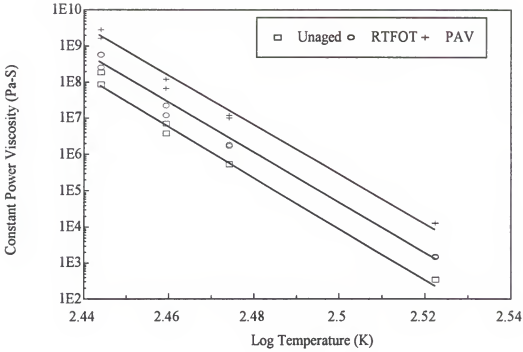

Regression Equation

Unaged: Log Viscosity = 178.28 - 69.70 × Log Temperature (°K), $R^2 = 0.993$

RTFOT: Log Viscosity = 173.74 - 67.65 × Log Temperature (°K), $R^2 = 0.992$

PAV: Log Viscosity = 168.18 - 65.08 × Log Temperature (°K), $R^2 = 0.992$

Figure 4.6 Relationship Between Constant Power Viscosity and Temperature for the Coastal AC-30 Asphalt

The summary of the results of the regression analyses are listed in Table 4.3. Good linear relationships ($R^2 > 0.98$) were found between the logarithm of viscosity (both constant-power and constant-stress) and the logarithm of absolute temperature in °K. The age hardening pattern indicated that the asphalt constant power viscosity-temperature relationship shifted upwards, and proximately parallel with aging. The amount of shifting from unaged to RTFOT process was found to be about 0.75 shifted upward and that of shifting from unaged to PAV process was found to be about 1.5 shifted upwards in this study.

The results of ANOVA and Duncan's grouping on the aging index which were calculated from the results of constant-power viscosities at 25°C, 15°C and 5°C are shown in Table 4.4. It can be seen that the MA30 (Marathon AC-30) asphalt shows the highest aging index after both RTFOT and PAV processes at these three temperatures. Due to significant interaction, these asphalts have different aging indexes for different combinations of aging and test temperature.

4.1.6 Fraass Breaking Test

The Fraass Breaking Point temperatures of the different binders before and after the RTFOT and PAV processes are shown in Table A.4 and displayed graphically in Figure 4.7. The C1S2 (AC-10+3%SBR2879) and C1S7 (AC-10+3%SBR70) binders can be seen to exhibit a significantly lower Fraass Breaking Point temperature than the other asphalts. The SBR and GTR modified binders first exhibited a very small crack (microcrack) and gradually formed total cracks on continuing the Fraass Breaking test.

Table 4.3 Summary of Results of Regression Analyses for the Viscosity-Temperature Relationship

Regression Equation:

$$\text{Log}(\eta) = B_0 + B_1 \times \log(\text{Temperature in } ^\circ\text{K})$$

Asphalt*	Aging Condition	B_0	B_1	R^2	DF[1]
Coastal AC-10	Unaged	183.31	-71.89	0.992	7
	STOA	176.66	-68.97	0.995	7
	LTOA	176.86	-68.82	0.989	7
Coastal AC-10+ 3%SBR2879	Unaged	167.49	-65.47	0.993	7
	STOA	161.45	-62.81	0.992	7
	LTOA	163.01	-63.21	0.985	7
Coastal AC-10+ 3%SBR70	Unaged	166.54	-65.02	0.999	7
	STOA	159.53	-61.97	0.995	7
	LTOA	163.41	-63.33	0.983	7
Ergon PMAC-20	Unaged	156.44	-60.90	0.992	7
	STOA	160.79	-62.47	0.993	7
	LTOA	167.19	-64.81	0.998	7
Coastal AC-30+ 10%GTR	Unaged	167.77	-65.30	0.981	7
	STOA	159.81	-61.92	0.981	7
	LTOA	148.51	-57.10	0.983	7
Coastal AC-30	Unaged	178.28	-69.70	0.993	7
	STOA	173.74	-67.65	0.992	7
	LTOA	168.18	-65.08	0.992	7
Koch AC-30	Unaged	178.75	-69.92	0.994	7
	STOA	180.46	-70.41	0.995	7
	LTOA	178.91	-69.50	0.992	7
Marathon AC-30	Unaged	191.79	-75.11	0.983	7
	STOA	189.61	-74.03	0.989	7
	LTOA	184.84	-71.84	0.983	7
Mariani AC-30	Unaged	186.88	-73.12	0.994	7
	STOA	194.31	-75.89	0.993	7
	LTOA	192.08	-74.71	0.995	7

Note: *: The meaning of the codes for the asphalt types can be found in Table 3.1.
1: Degree of freedom.

Table 4.4 Results of ANOVA and Duncan's Multiple Range Test on the Aging Index (constant-power viscosity) in the comparison of RTFOT and PAV on Asphalt binders

Dependent Variable: **Aging Index [Model = $\mu + \alpha_i + \beta_j + (\alpha\beta)_{ij} + \epsilon_{ijk}$]**

Temperature=25°C

Source	DF	ANOVA SS	Mean Square	F Value	Pr > F
ASPHALT, α	4	65.3249800	16.3312450	8.62	0.0028
METHOD, β	1	977.0622050	977.0622050	516.00	0.0001
ASPHALT*METHOD,$\alpha\beta$	4	55.9044200	13.9761050	7.38	0.0049

R-Square= 0.983052

Duncan Grouping at METHOD=RTFOT

	Mean	N	ASPHALT*
A	3.800	2	MA30
A			
A	3.500	2	MT30
A			
A	3.410	2	KH30
A			
A	3.280	2	CT30
A			
A	3.080	2	C3GT

Duncan Grouping at METHOD=PAV+RTFOT

	Mean	N	ASPHALT*
A	22.460	2	MA30
A			
A	20.640	2	CT30
B	15.430	2	MT30
B			
B	14.430	2	C3GT
B			
B	14.005	2	KH30

Temperature=15°C

Source	DF	ANOVA SS	Mean Square	F Value	Pr > F
ASPHALT, α	4	116.5151300	29.1287825	88.93	0.0001
METHOD,β	1	665.8580000	665.8580000	2032.78	0.0001
ASPHALT*METHOD,$\alpha\beta$	4	80.8956500	20.2239125	61.74	0.0001

R-Square= 0.982220

Duncan Grouping at METHOD=RTFOT

	Mean	N	ASPHALT*
A	3.475	2	MA30
A			
A	3.185	2	KH30
A			
A	3.145	2	MT30
A			
A	3.135	2	CT30
B	2.105	2	C3GT

Note: * The meaning of the codes for the asphalt types can be found in Table 3.1.

Table 4.4 Continued

Duncan Grouping at METHOD=PAV+RTFOT

	Mean	N	ASPHALT*
A	20.715	2	MA30
B	17.260	2	CT30
C	15.145	2	KH30
D	11.685	2	MT30
E	7.940	2	CT30

Temperature= 5°C

Source	DF	ANOVA SS	Mean Square	F Value	Pr > F
ASPHALT, α	4	216.4173200	54.1043300	60.00	0.0001
METHOD, β	1	572.2360200	572.2360200	634.62	0.0001
INTERACTION,αβ	4	82.5596800	20.6399200	22.89	0.0001

R-Square= 0.981756

Duncan Grouping at METHOD=RTFOT

		Mean	N	ASPHALT*
	A	6.475	2	MA30
	B	3.115	2	KH30
	B			
C	B	3.000	2	CT30
C				
C	D	2.450	2	MT30
	D			
	D	2.080	2	C3GT

Duncan Grouping at METHOD=PAV+RTFOT

	Mean	N	ASPHALT*
A	20.990	2	MA30
B	16.795	2	CT30
B			
B	16.020	2	KH30
C	11.030	2	MT30
D	5.775	2	C3GT

Note: * The meaning of the codes for the asphalt types can be found in Table 3.1.
Means with the same letter are not significantly different at α=0.05.

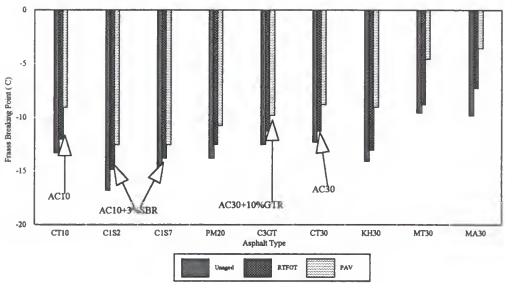

Note: CT10 - Coastal AC-10.
C1S2 - Coastal AC-10+3%SBR2879.
C1S7 - Coastal AC-10+3%SBR70.
PM20 - Ergon PMAC-20.
C3GT - Coastal AC-30+10%GTR.
CT30 - Coastal AC-30.
KH30 - Koch AC-30.
MT30 - Marathon AC-30.
MA30 - Mariani AC-30.

Figure 4.7 Fraass Breaking Point Temperature of Nine Asphalts Aged by the RTFOT and PAV

The Fraass Breaking Point temperature is defined as the temperature at which the first crack (or microcrack) is observed in the Fraass Breaking Point test.

The results of ANOVA and Duncan's multiple range test on the Fraass breaking point temperatures of asphalt after different aging methods are shown in Table 4.5. Both the effects of asphalt type and aging method are significant and the interaction effect is also significant. These results are similar to the results of ANOVA on the percent retained penetration. It is noticed that the MT30 (Mariani AC-30) and MA30 (Marathon AC-30) exhibit a significantly higher Fraass breaking point temperature than the other asphalts. The C1S2 (AC-10+3%SBR2879) and CIS7 (AC-10+3%SBR70) exhibit a significant lower Fraass breaking point temperature than the other asphalts. The Fraass breaking point temperature as read from the standard apparatus using a mercury thermometer is about 5.5°C higher than the temperature of the sample [29]. The Fraass breaking point temperature is related to thermal cracking temperature in the field. Therefore, the two SBR-modified asphalts exhibited a significantly improved capacity of resisting low-temperature cracking.

4.2 Results of SHRP Binder Tests

4.2.1 Dynamic Shear Rheometer Test

In SHRP testing for specification purposes, a standard testing frequency of 10 radians/second (1.59 Hertz) is specified. This frequency was used because it corresponds to a loading time of 0.1 seconds which simulates the effects of traffic loading [18]. In addition to the standard frequency of 10 radians/second (1.59 Hertz), a frequency sweep consisting of 7 different frequencies was also performed at the various temperatures.

Table 4.5 Results of ANOVA and Duncan's Grouping on the Fraass Breaking Point in the comparison of RTFOT and PAV on Asphalt binders

Dependent Variable: **FRAASS [Model = $\mu + \alpha_i + \beta_j + (\alpha\beta)_{ij} + \epsilon_{ijk}$]**

Source	DF	ANOVA SS	Mean Square	F Value	Pr > F
ASPHALT, α	8	317.0000000	39.6250000	122.27	0.0001
METHOD, β	2	153.3611111	76.6805556	236.61	0.0001
ASPHALT*METHOD, $\alpha\beta$	16	16.3888889	1.0243056	3.16	0.0041

R-Square =0.982341

Duncan Grouping at METHOD=Original

		Mean	N	ASPHALT*
	A	-9.500	2	MT30
	A			
	A	-9.750	2	MA30
	B	-12.250	2	CT30
	B			
	B	-12.500	2	C3GT
	B			
	B	-13.250	2	CT10
	B			
C	B	-13.750	2	PM20
C	B			
C	B	-14.000	2	KH30
C				
C		-15.000	2	C1S7
	D	-16.750	2	C1S2

Duncan Grouping at METHOD=RTFOT

		Mean	N	ASPHALT*
	A	-7.250	2	MA30
	B	-8.750	2	MT30
	C	-11.250	2	CT30
	C			
	C	-11.250	2	C3GT
	C			
D	C	-12.000	2	CT10
D				
D	E	-12.500	2	PM20
	E			
F	E	-13.000	2	KH30
F				
F		-13.750	2	C1S7
	G	-14.750	2	C1S2

Note: * The meaning of the codes for the asphalt types can be found in Table 3.1.

Table 4.5 Continued

Duncan Grouping at METHOD=PAV+RTFOT

		Mean	N	ASPHALT*
	A	-3.500	2	MA30
	A			
	A	-4.500	2	MT30
	B	-8.750	2	CT30
	B			
	B	-9.000	2	KH30
	B			
	B	-9.750	2	C3GT
	B			
C	B	-9.000	2	CT10
C				
C		-10.750	2	PM20
	D	-12.500	2	C1S7
	D			
	D	-12.500	2	C1S2

Note: * The meaning of the codes for the asphalt types can be found in Table 3.1.
Means with the same letter are not significantly different at α=0.05.

According to Christensen et al. [18], when interpreting the results of viscoelastic tests, such as the DSR, on asphalt binders in terms of pavement performance, isochronal plots should be used. An isochronal plot is a plot of viscoelastic parameters, such as complex shear modulus, versus temperature at a specified frequency. When the isochronal plot is created at a frequency equivalent to traffic loading, such as 10 radians/second (1.59 Hertz), the resulting plot has a direct correspondence to the expected response of the asphalt binder under actual traffic conditions [18].

In SHRP specification testing, the selected viscoelastic parameters are plotted against temperature for a frequency of 10 radians/second (1.59 Hertz). Figures 4.8 and 4.9 show the isochronal plots of dynamic complex modulus at a frequency of 10 rad/s for the unaged asphalts and the RTFOT-aged asphalts, respectively. It can be seen that the C3GT (AC-30+10%GTR) has a higher modulus than the others at the temperature range from 52 to 76° C. Figure 4.10 shows the isochronal plots of dynamic complex modulus for RTFOT+PAV aged asphalts at a frequency of 10 rad/s at lower temperatures from 13 to 34°C. It can be seen that the C1S2 (AC-10+3%SBR2879), C1S7 (AC-10+3%SBR70) and C3GT (AC-30+10%GTR) have substantially lower modulus than the others at these low temperatures, and the MT30 (Marathon AC-30) and MA30 (Mariani AC-30) have significantly higher modulus than the others at these low temperatures. Figures 4.11 through 4.13 show the plots of dynamic complex modulus, dynamic viscosity and phase angle as a function of frequency at a temperature of 76° C for the unaged asphalts. It can be seen that the C1S2 (AC-10+3%SBR2879), C1S7 (AC-10+3%SBR70) and PM20 (Ergon PMAC-20) have higher modulus and lower phase angle than the others at a low

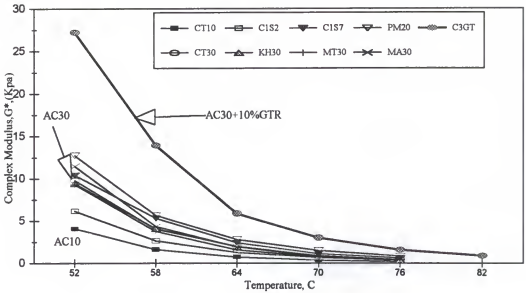

Note: CT10 - Coastal AC-10.
C1S2 - Coastal AC-10+3%SBR2879.
C1S7 - Coastal AC-10+3%SBR70.
PM20 - Ergon PMAC-20.
C3GT - Coastal AC-30+10%GTR.
CT30 - Coastal AC-30.
KH30 - Koch AC-30.
MT30 - Marathon AC-30.
MA30 - Mariani AC-30.

Figure 4.8 Isochronal Plots of Complex Modulus of Original Asphalt Binders at w=10 rad/sec

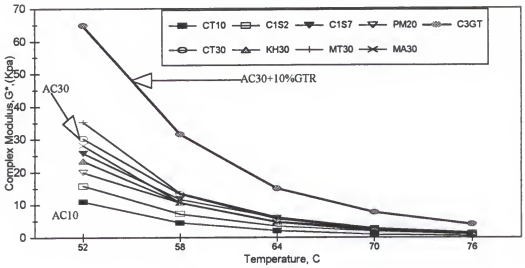

Note: CT10 - Coastal AC-10.
C1S2 - Coastal AC-10+3%SBR2879.
C1S7 - Coastal AC-10+3%SBR70.
PM20 - Ergon PMAC-20.
C3GT - Coastal AC-30+10%GTR.
CT30 - Coastal AC-30.
KH30 - Koch AC-30.
MT30 - Marathon AC-30.
MA30 - Mariani AC-30.

Figure 4.9 Isochronal Plots of Complex Modulus of RTFOT-aged Asphalt Binders at w=10 rad/sec

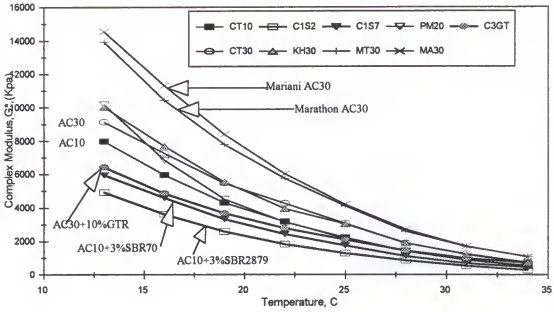

Note: CT10 - Coastal AC-10.
C1S2 - Coastal AC-10+3%SBR2879.
C1S7 - Coastal AC-10+3%SBR70.
PM20 - Ergon PMAC-20.
C3GT - Coastal AC-30+10%GTR.
CT30 - Coastal AC-30.
KH30 - Koch AC-30.
MT30 - Marathon AC-30.
MA30 - Mariani AC-30.

Figure 4.10 Isochronal Plots of Complex Modulus of PAV+RTFOT-aged Asphalt Binders at w=10 rad/sec

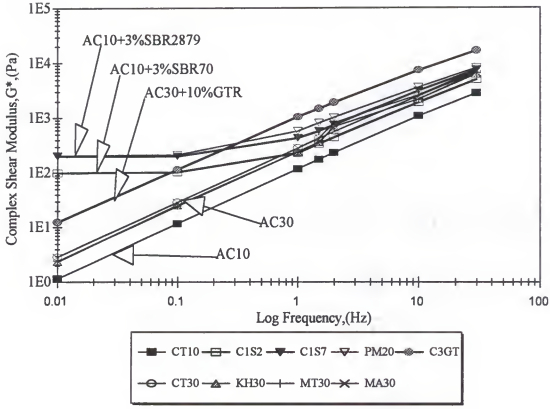

Note: CT10 - Coastal AC-10.
C1S2 - Coastal AC-10+3%SBR2879.
C1S7 - Coastal AC-10+3%SBR70.
PM20 - Ergon PMAC-20.
C3GT - Coastal AC-30+10%GTR.
CT30 - Coastal AC-30.
KH30 - Koch AC-30.
MT30 - Marathon AC-30.
MA30 - Mariani AC-30.

Figure 4.11 Plot of Complex Modulus at 76°C as a Function of Frequency for Unaged Asphalt Binders

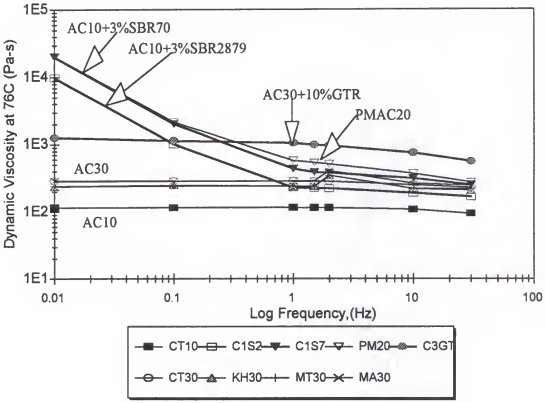

Note: CT10 - Coastal AC-10.
C1S2 - Coastal AC-10+3%SBR2879.
C1S7 - Coastal AC-10+3%SBR70.
PM20 - Ergon PMAC-20.
C3GT - Coastal AC-30+10%GTR.
CT30 - Coastal AC-30.
KH30 - Koch AC-30.
MT30 - Marathon AC-30.
MA30 - Mariani AC-30.

Figure 4.12 Plot of Dynamic Viscosity at 76°C as a Function of Frequency for Unaged Asphalt Binders

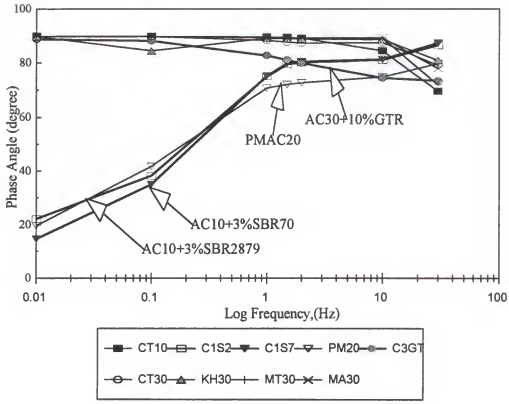

Note: CT10 - Coastal AC-10.
C1S2 - Coastal AC-10+3%SBR2879.
C1S7 - Coastal AC-10+3%SBR70.
PM20 - Ergon PMAC-20.
C3GT - Coastal AC-30+10%GTR.
CT30 - Coastal AC-30.
KH30 - Koch AC-30.
MT30 - Marathon AC-30.
MA30 - Mariani AC-30.

Figure 4.13 Plot of Phase Angle at 76°C as a Function of Frequency for Unaged Asphalt Binders

frequency of 0.01 Hz. For the unmodified asphalts, dynamic viscosity is relatively independent of deformation rate (frequency), indicating that the materials are purely viscous fluids. In contrast, the dynamic viscosity of the C1S2 (AC-10+3%SBR2879), C1S7 (AC-10+3%SBR70) and PM20 (Ergon PMAC-20) modified asphalts clearly decreases with increasing deformation rate, indicating that these materials have an elastic response as well as a viscous response.

The plots of dynamic complex modulus, dynamic viscosity and phase angle versus frequency for the RTFOT-aged asphalts at 76° C are shown in Figures 4.14 through 4.16. It can be seen that the C1S2 (AC-10+3%SBR2879), C1S7 (AC-10+3%SBR70) and C3GT (AC-30+10%GTR) have higher modulus and viscosity at low frequency, and the C1S2 and C1S7 have lower phase angle than the others at low frequency of 0.01 Hz. For unmodified RTFOT-aged residues, dynamic viscosity is relative independent of deformation rate (frequency), indicating that the materials are still purely viscous fluids. In contrast, dynamic viscosity of the C1S2 (AC-10 + 3%SBR2879) and C1S7 (AC-10 + 3% SBR70) modified asphalts clearly decreases with increasing deformation rate.

Figure 4.17 and 4.18 show the plots of dynamic complex modulus and phase angle as a function of frequency at a temperature of 3°C for the RTFOT+PAV-aged asphalts. It can be seen that the C1S2 (AC-10+3%SBR2879), C1S7 (AC-10+3%SBR70) and C3GT (AC-30+10%GTR) exhibit lower modulus and higher phase angle than the others at a high frequency of 30 Hz. This means that both SBR- and GTR- modified asphalts show higher modulus and more elastic behavior than unmodified asphalts at high temperatures, and

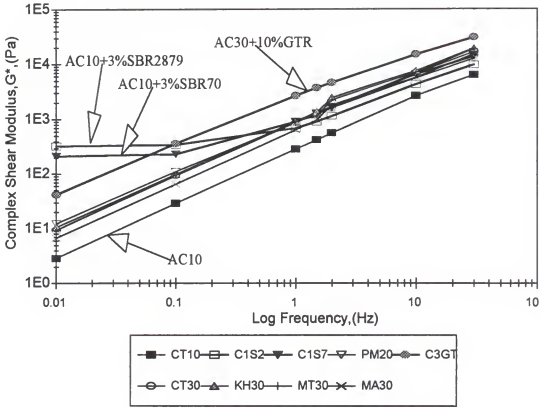

Note: CT10 - Coastal AC-10.
C1S2 - Coastal AC-10+3%SBR2879.
C1S7 - Coastal AC-10+3%SBR70.
PM20 - Ergon PMAC-20.
C3GT - Coastal AC-30+10%GTR.
CT30 - Coastal AC-30.
KH30 - Koch AC-30.
MT30 - Marathon AC-30.
MA30 - Mariani AC-30.

Figure 4.14 Plot of Complex Modulus at 76°C as a Function of Frequency for RTFOT-aged Asphalt Binders

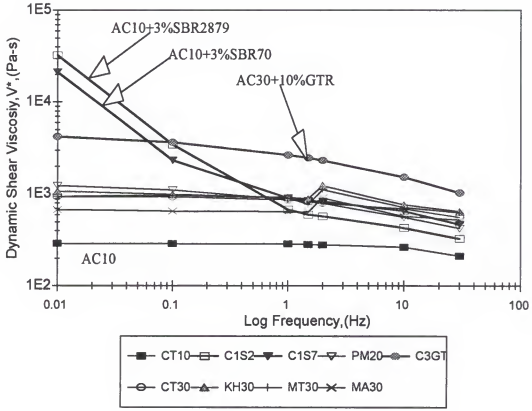

Note: CT10 - Coastal AC-10.
C1S2 - Coastal AC-10+3%SBR2879.
C1S7 - Coastal AC-10+3%SBR70.
PM20 - Ergon PMAC-20.
C3GT - Coastal AC-30+10%GTR.
CT30 - Coastal AC-30.
KH30 - Koch AC-30.
MT30 - Marathon AC-30.
MA30 - Mariani AC-30.

Figure 4.15 Plot of Dynamic Viscosity at 76°C as a Function of Frequency for RTFOT-aged Asphalt Binders

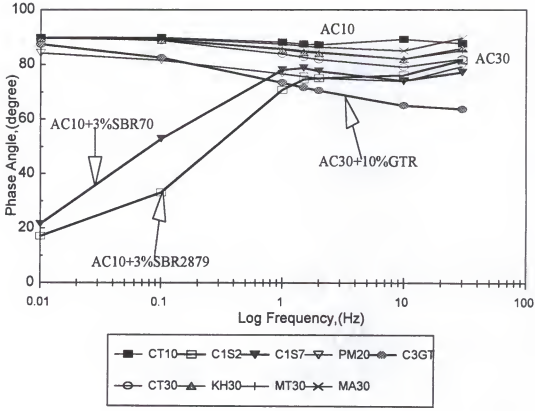

Note: CT10 - Coastal AC-10.
C1S2 - Coastal AC-10+3%SBR2879.
C1S7 - Coastal AC-10+3%SBR70.
PM20 - Ergon PMAC-20.
C3GT - Coastal AC-30+10%GTR.
CT30 - Coastal AC-30.
KH30 - Koch AC-30.
MT30 - Marathon AC-30.
MA30 - Mariani AC-30.

Figure 4.16 Plot of Phase Angle at 76°C as a Function of Frequency for RTFOT-aged Asphalt Binders

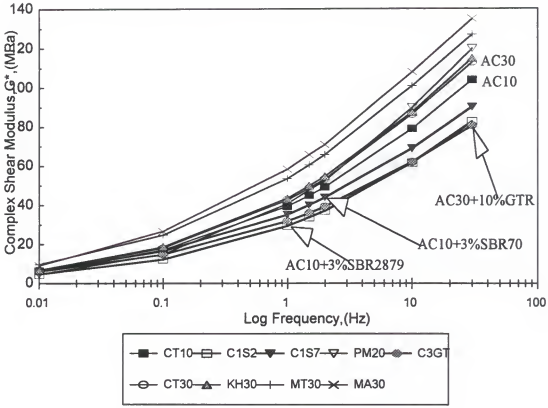

Note: CT10 - Coastal AC-10.
C1S2 - Coastal AC-10+3%SBR2879.
C1S7 - Coastal AC-10+3%SBR70.
PM20 - Ergon PMAC-20.
C3GT - Coastal AC-30+10%GTR.
CT30 - Coastal AC-30.
KH30 - Koch AC-30.
MT30 - Marathon AC-30.
MA30 - Mariani AC-30.

Figure 4.17 Plot of Complex Modulus at 3°C as a Function of Frequency for PAV+RTFOT-aged Asphalt Binders

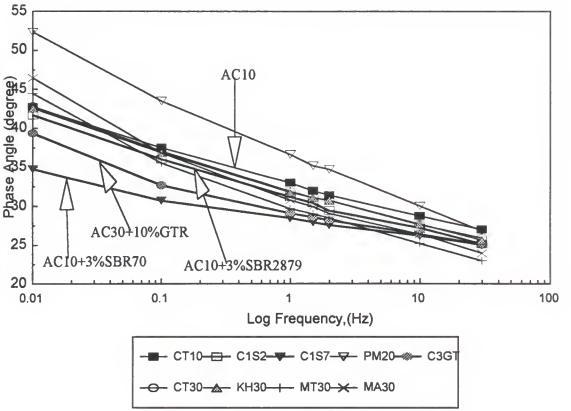

Note: CT10 - Coastal AC-10.
C1S2 - Coastal AC-10+3%SBR2879.
C1S7 - Coastal AC-10+3%SBR70.
PM20 - Ergon PMAC-20.
C3GT - Coastal AC-30+10%GTR.
CT30 - Coastal AC-30.
KH30 - Koch AC-30.
MT30 - Marathon AC-30.
MA30 - Mariani AC-30.

Figure 4.18 Plot of Phase Angle at 3°C as a Function of Frequency for PAV+RTFOT-aged Asphalt Binders

also show lower modulus and more viscous behavior than unmodified asphalts at low temperatures.

To investigate the variation of dynamic viscosity with respect to temperature, the Dynamic Shear Rheometer tests were performed at temperatures from 25 to 60 °C, on the nine asphalts and their residues aged by the RTFOT and PAV processes. The dynamic viscosity at a frequency of 1 Hz are shown in Table A.7. Linear regression analyses were performed to estimate the dynamic viscosity as a function of temperature. The following regression equation was used:

$$\log \eta^* = D_0 + D_1 \times \log(^\circ K)$$

where η^* = dynamic viscosity, Pa.S

D_0 , D_1 = constants

°K = degree Kelvin

Linear regression analyses were performed to estimate the viscosity-temperature relationship for the different asphalts before and after RTFOT and PAV processes. The purpose of these analyses is to determine how these relationships may change with aging. Good linear relationships ($R^2 \geq 0.99$) were found between the logarithm of dynamic viscosity and the logarithm of absolute temperature in °K. The relationships between $\log\eta^*$ and log°K are shown in Figure 4.19 and listed in Table 4.6. With some variation, the parallel shift patterns are generally similar to each other for all nine asphalts. The age hardening pattern indicated that the dynamic viscosity-temperature relationship shifted upwards, and proximately parallel with aging. The amount of shifting from unaged to RTFOT process was found to be about 0.5 shifted upward and that of shifting from

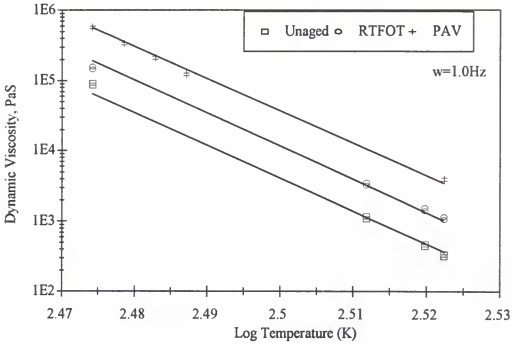

Regression Equation

Unaged: Log Viscosity = 129.68 - 50.41 × Log Temperature (°K), $R^2 = 0.999$

RTFOT: Log Viscosity = 114.44 - 44.16 × Log Temperature (°K), $R^2 = 0.996$

PAV: Log Viscosity = 115.47 - 44.36 × Log Temperature (°K), $R^2 = 0.997$

Figure 4.19 Relationship Between Dynamic Viscosity and Temperature for the Coastal AC-30 Asphalt

Table 4.6 Summary of Results of Regression Analyses for the Viscosity-Temperature Relationship

Regression Equation:

$$\text{Log}(\eta^*) = D_0 + D_1 \times \log(\text{Temperature in } ^\circ K)$$

Asphalt*	Aging Condition	D_0	D_1	R^2	DF[1]
Coastal AC-10	Unaged	135.11	-52.74	0.999	7
	STOA	123.16	-47.90	0.999	7
	LTOA	116.81	-45.27	0.999	9
Coastal AC-10+ 3%SBR2879	Unaged	123.16	-47.90	0.999	7
	STOA	119.4	-46.25	0.999	7
	LTOA	116.74	-44.97	0.997	9
Coastal AC-10+ 3%SBR70	Unaged	116.81	-45.27	0.999	7
	STOA	114.91	-44.37	0.999	7
	LTOA	104.7	-40.17	0.998	9
Ergon PMAC-20	Unaged	110.01	-42.55	0.999	7
	STOA	115.07	-44.47	0.999	7
	LTOA	117.35	-45.20	0.999	9
Coastal AC-30+ 10%GTR	Unaged	108.81	-41.92	0.998	7
	STOA	102.09	-39.11	0.999	7
	LTOA	98.39	-37.50	0.998	9
Coastal AC-30	Unaged	129.68	-50.41	0.999	7
	STOA	114.44	-44.16	0.996	7
	LTOA	115.47	-44.36	0.997	9
Koch AC-30	Unaged	138.99	-54.13	0.999	7
	STOA	133.91	-51.96	0.995	7
	LTOA	123.68	-47.68	0.998	9
Marathon AC-30	Unaged	144.48	-56.31	0.999	7
	STOA	133.97	-51.92	0.997	7
	LTOA	130.96	-50.56	0.999	9
Mariani AC-30	Unaged	147.36	-57.44	0.999	7
	STOA	138.37	-53.71	0.999	7
	LTOA	131.4	-50.74	0.999	9

Note: *: The meaning of the codes for the asphalt types can be found in Table 3.1.
1: Degree of freedom.

unaged to PAV process was found to be about 1.0 shifted upwards in this study. A shift of 1 on a log scale represents a ten-fold increase in values. Figure 4.20 shows the plot the constant-power viscosity at 25°C versus the corresponding dynamic viscosity at a frequency of 1 Hz. Good relationships ($R^2 = 0.88$) were found between the logarithm of dynamic viscosity and the logarithm of constant-power viscosity. If the material tested is purely viscous and has no elastic response, the dynamic viscosity would be equal to the true viscosity. However, if the material tested has an elastic response as well as viscous response, the dynamic viscosity would be lower than the true viscosity, and would decrease as the testing frequency, w, increases. It can be seen that the constant-power viscosity is about 10 times higher than the dynamic viscosity at 1 Hz. This difference can be attributed to the elastic response of the materials tested.

4.2.2 Bending Beam Rheometer Test

The SHRP Bending Beam Rheometer tests were run on standard-size asphalt binder beam specimens using a load of 980 ± 50 Newtons for a duration of 240 seconds to determine the low temperature stiffness of the asphalt binders. In SHRP specification testing, the BBR test is run at 10°C above the minimum asphalt pavement design temperature. For the north Florida region, the Florida Department of Transportation determined that a preliminary test temperature of -12°C will be used in BBR test for a minimum pavement temperature of -22°C (-7.6°F).

The plots of flexural creep stiffness versus loading time at test temperatures of -12, -18 and -24°C for the PAV+RTFOT-aged asphalts are shown in Figures 4.21 through 4.23. It can be seen that the C1S2 (AC-10+3%SBR2879), C1S7 (AC-10+3%SBR70) and

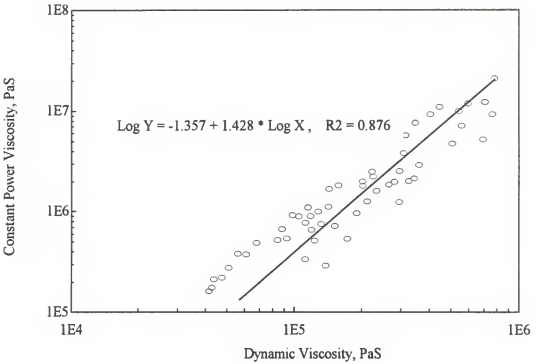

Figure 4.20 Relationship Between Dynamic Viscosity at 1 Hz and Constant Power Viscosity at 25°C

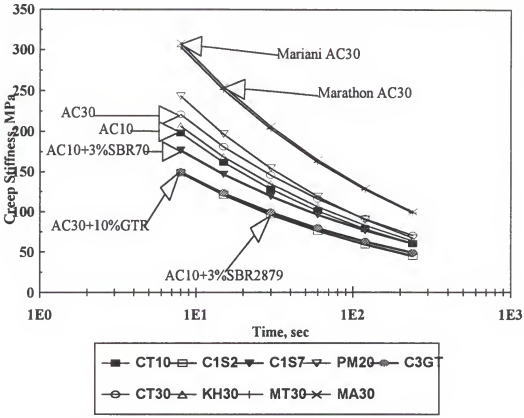

Note: CT10 - Coastal AC-10.
C1S2 - Coastal AC-10+3%SBR2879.
C1S7 - Coastal AC-10+3%SBR70.
PM20 - Ergon PMAC-20.
C3GT - Coastal AC-30+10%GTR.
CT30 - Coastal AC-30.
KH30 - Koch AC-30.
MT30 - Marathon AC-30.
MA30 - Mariani AC-30.

Figure 4.21 Plot of Creep Stiffness at -12°C Versus Loading Time for PAV+RTFOT-aged Asphalt Binders

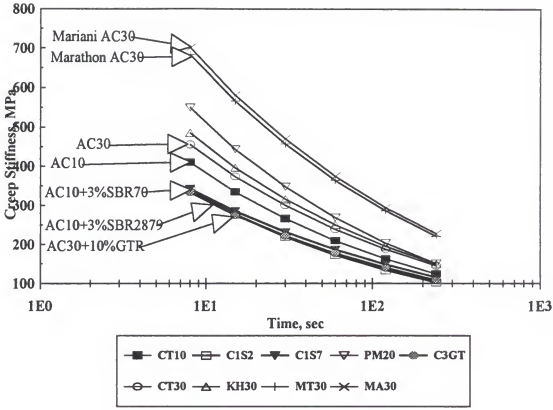

Note: CT10 - Coastal AC-10.
C1S2 - Coastal AC-10+3%SBR2879.
C1S7 - Coastal AC-10+3%SBR70.
PM20 - Ergon PMAC-20.
C3GT - Coastal AC-30+10%GTR.
CT30 - Coastal AC-30.
KH30 - Koch AC-30.
MT30 - Marathon AC-30.
MA30 - Mariani AC-30.

Figure 4.22 Plot of Creep Stiffness at -18°C Versus Loading Time for PAV+RTFOT-aged Asphalt Binders

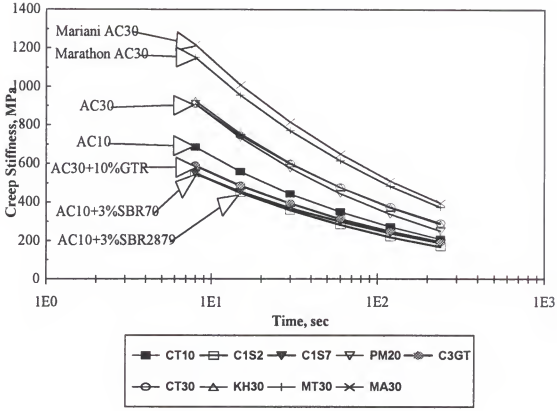

Note: CT10 - Coastal AC-10.
C1S2 - Coastal AC-10+3%SBR2879.
C1S7 - Coastal AC-10+3%SBR70.
PM20 - Ergon PMAC-20.
C3GT - Coastal AC-30+10%GTR.
CT30 - Coastal AC-30.
KH30 - Koch AC-30.
MT30 - Marathon AC-30.
MA30 - Mariani AC-30.

Figure 4.23 Plot of Creep Stiffness at -24°C Versus Loading Time for PAV+RTFOT-aged Asphalt Binders

C3GT (AC-30+10%GTR) have substantially lower stiffness than the others, and the MT30 (Marathon AC-30) and MA30 (Mariani AC-30) have significantly higher stiffness than the others at low temperatures. Also, the CT30 (Coastal AC-30) asphalt has a higher stiffness value than the CT10 (AC-10) asphalt at temperatures of -12, -18 and -24°C. Figure 4.24 shows the isochronal plots of flexural creep stiffness at a loading time of 60 sec for RTFOT+PAV-aged asphalts. It can be seen that the C3GT (AC-30+10%GTR), C1S2 (AC-10+3%SBR2879) and C1S7 (AC-10+3%SBR70) have substantially lower stiffness than the others at very low temperatures, and the MT30 (Marathon AC-30) and MA30 (Mariani AC-30) have significantly higher stiffness than the others at low temperatures. The SHRP binder specification requires that the flexural creep stiffness cannot exceed 300 MPa at a loading time of 60 seconds. The limiting stiffness temperature (below which low-temperature cracking would occur) is 10°C below the temperature at which the binder reaches this stiffness. Results of the BBR test at a loading time of 60 seconds and their predictive limiting stiffness temperatures are shown in Table 4.7.

Based on the limiting stiffness temperatures from BBR test, CT10 (AC-10) shows the lowest cracking temperature among the five unmodified asphalts. The GTR- and SBR-modified asphalts have lower cracking temperatures than the unmodified asphalts, as seen from the limiting stiffness temperatures. These results show that SBR and GTR modifiers can be used to improve the resistance to low-temperature cracking.

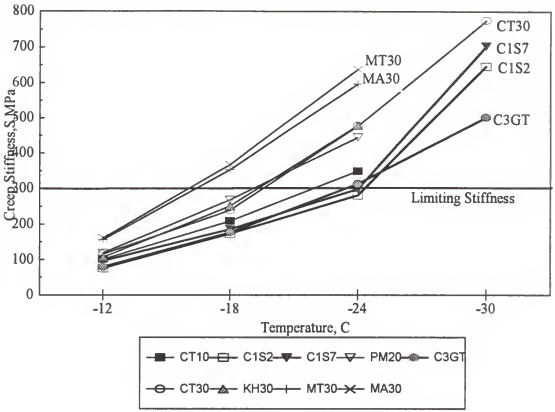

Note: CT10 - Coastal AC-10.
C1S2 - Coastal AC-10+3%SBR2879.
C1S7 - Coastal AC-10+3%SBR70.
PM20 - Ergon PMAC-20.
C3GT - Coastal AC-30+10%GTR.
CT30 - Coastal AC-30.
KH30 - Koch AC-30.
MT30 - Marathon AC-30.
MA30 - Mariani AC-30.

Figure 4.24 Isochronal Plot of Creep Stiffness at 60 sec Loading Time for PAV+RTFOT-aged Asphalt Binders

Table 4.7 Results of Bending Beam Rheometer Test on PAV+RTFOT-aged Asphalt Binders

Asphalt Binders*	CT10	C1S2	C1S7	PM20	C3GT	CT30	KH30	MT30	MA30
Creep Stiffness at -12°C (MPa)	101.2	75.9	96.1	119.1	79.4	115.9	106.8	157.0	161.6
Creep Stiffness at -18°C (MPa)	209.8	173.3	186.9	268.8	177.4	239.2	251.2	353.5	367.9
Creep Stiffness at -24°C (MPa)	349.9	281.5	298.9	444.4	313.8	476.8	478.1	596.3	638.1
Creep Stiffness at -30°C (MPa)	-	647.5	703.7	-	501.4	774.9	-	-	-
Slope, m -value, at -12°C	0.356	0.358	0.352	0.338	0.342	0.341	0.359	0.355	0.338
Slope, m -value, at -18°C	0.308	0.339	0.335	0.319	0.301	0.302	0.305	0.274	0.273
Slope, m -value, at -24°C	0.281	0.303	0.302	0.263	0.250	0.248	0.247	0.222	0.221
Slope, m -value, at -30°C	-	0.236	0.216	-	0.215	0.206	-	-	-
Temp. at 300 MPa Stiffness,°C	-21.9	-25	-24.1	-19.1	-23.4	-19.5	-19.3	-16.4	-16
Limiting Stiffness Temperature,°C	-31.9	-35	-34.1	-29.1	-33.4	-29.5	-29.3	-26.4	-26
PG Grade	58-28	64-34	70-34	70-28	76-28	64-28	64-28	64-22	64-22

*Note: The meaning of the codes for the asphalt types can be found in Table 3.1.

4.2.3 Direct Tension Test

In the Direct Tension Test (DTT), the asphalt binder test specimen was loaded in tension at a constant rate to determine the strain at failure. In SHRP specification testing, the critical temperature for the DTT test was the same as that for the BBR test which is 10°C below the minimum asphalt pavement design temperature.

The SHRP binder specification establishes the failure criterion as a fracture strain of 1.0 % or less when the sample is pulled in tension at 1.0 mm/min strain rate. Results of the DTT test and their predictive limiting strain temperatures are shown in Table 4.8. The predictive limiting strain temperatures are higher as compared with the predictive limiting stiffness temperatures from the BBR test. This means that the DTT is more conservative than the BBR test.

It can be noted that the C1S2 (AC-10+3%SBR2879), C1S7 (AC-10+3% SBR70) and C3GT (AC-30+10%GTR) have substantially higher failure strain value than the others at low temperatures, and the MT30 (Marathon AC-30) and MA30 (Mariani AC-30) have significantly lower failure strain value than the others at low temperatures. These results are consistent with those of BBR test in showing that SBR and GTR modifiers can be used to improve the resistance to low-temperature cracking.

4.2.4 SHRP Binder Performance Grading

There are two forms of testing associated with the proposed SHRP binder specification : conformance testing and classification testing. The conformance testing is an accept/reject form of testing where the properties of a binder sample are compared to the required properties for a single grade. In classification testing, a coordinated series of

Table 4.8 Results of Direct Tension Test on PAV+RTFOT-aged Asphalt Binders

Asphalt Binders*		CT10	C1S2	C1S7	PM20	C3GT	CT30	KH30	MT30	MA30
Failure Stress (Mpa)	-12°C	2.14	2.57	2.11	1.84	1.73	1.79	2.61	2.13	2.34
	-18°C	2.24	2.86	2.13	2.69	1.77	1.76	2.68	2.2	2.38
	-24°C	2.46	2.95	2.16	2.89	2.17	2.33	2.89	1.86	2.43
Failure Strain (%)	-12°C	1.378	3.848	1.683	0.965	1.514	0.834	1.257	0.700	0.740
	-18°C	0.402	1.102	0.608	0.368	0.465	0.327	0.457	0.280	0.289
	-24°C	0.360	0.581	0.365	0.307	0.294	0.286	0.367	0.162	0.189
Temperature at 1% Failure Strain (°C)		-14.2	-19.2	-15.8	-11.7	-14.9	-10.0	-13.9	-7.7	-8.5
Limiting Strain Temperature, °C		-24.2	-29.2	-25.8	-21.7	-24.9	.20.0	-23.9	-17.7	-18.5
PG Grade		58-28	64-34	70-34	70-28	76-28	64-28	64-28	64-22	64-22

*Note: The meaning of the codes for the asphalt types can be found in Table 3.1.

tests must be performed to classify the unknown material according to the SHRP binder specification. The classification testing is employed in this study to classify performance grades of asphalt binders according to AASHTO MP1, "Standard Specification for Performance Graded Asphalt Binder," and AASHTO PP6, "Standard Practice for Grading or Verifying the Performance Grade of an Asphalt Binder." All nine asphalt binders were evaluated by the SHRP classification testing. The test results are displayed in Table A.8. The nine asphalt binders are classified into seven PG grades. Both CT30 (Coastal AC-30) and KH30 (Koch AC-30) can be classified as a PG64-28 grade, while MT30 (Marathon AC-30) and MA30 (Mariani AC-30) can be classified as a PG64-22 grade. It can be noted that the C3GT (Coastal AC-30+10%GTR) is classified as a PG76-28 grade, as compared with a PG64-28 grade for the unmodified CT30 (Coastal AC-30). The SHRP PG grading shows that the GTR addition improves the high-temperature performance while the low-temperature performance is unaffected. It can also be noted that the C1S2 (AC-10+3%SBR2879) and C1S7 (AC-10+3%SBR70) are classified as PG64-34 and PG70-34 grades, respectively, as compared with a PG58-28 grade for the unmodified CT10 (AC-10). This means that the SBR modification has improved both the high-temperature and the low-temperature performance of the binder.

4.2.5 Comparison of PG Grade and Bitumen Test Data Chart

The Bitumen Test Data Chart (BTDC) consists of one horizontal scale for the temperature and two vertical scales for the penetration and viscosity, respectively. The consistency of an asphalt binder at different temperatures can be plotted on the BTDC to show its temperature susceptibility. The BTDC basically allows one to take different

physical property measurements (viscosity, penetration, Fraass temperature, and/or softening point) and, from these, predict the consistency of the material over a wide temperature range. Additionally, it is a good idea to use family curves of the BTDC which could show the effects of aging on an asphalt binder over a wide temperature range. Figures 4.25 through 4.27 show the BTDC plots of the unaged, RTFOT-aged, and PAV-aged asphalt binders. It can be seen that the slopes of the BTDC plot show their temperature susceptibility and can be used to compare the characteristics of the original asphalt binders with those of their RTFOT-aged and PAV-aged residues. It also shows that a PG Grade with a wide temperature range will display less temperature susceptibility in the BTDC plots. As seen from the slopes of the BTDC plots, the temperature susceptibilities of the C3GT (Coastal AC-30+10% GTR) and C1S7 (Coastal AC-10+3% SBR70) modified asphalts are significantly lower than those of the unmodified asphalts before or after aging processes. It can also be seen that the GTR and SBR modified asphalts have substantially higher viscosity than those of the unmodified asphalts at high temperatures, while the effect of GTR and SBR modifiers are small at low temperatures.

4.3 Summary of Findings

Based on the results of conventional binder tests and SHRP binder tests, the following conclusions are made:

1. Asphalts generally exhibit weight loss (possibly due to the loss of volatile) during the RTFOT process and weight gain (possibly due to oxidation) during the PAV process.

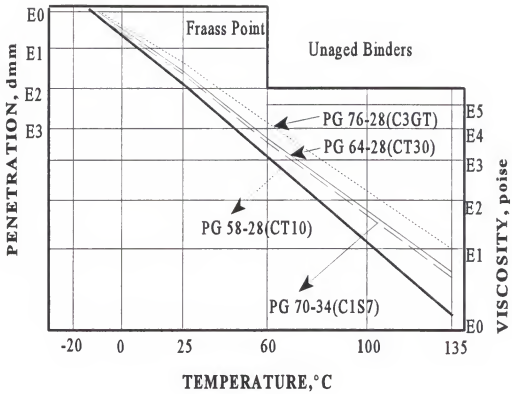

Note: CT10 - Coastal AC-10.
C1S7 - Coastal AC-10+3%SBR70.
C3GT - Coastal AC-30+10%GTR.
CT30 - Coastal AC-30.

Figure 4.25 Bitumen Test Data Charts for Unaged Asphalt Binders

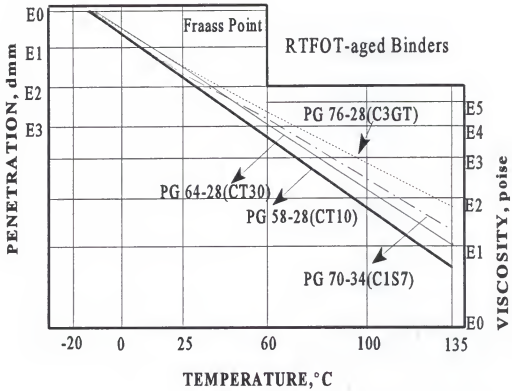

Note: CT10 - Coastal AC-10.
C1S7 - Coastal AC-10+3%SBR70.
C3GT - Coastal AC-30+10%GTR.
CT30 - Coastal AC-30.

Figure 4.26 Bitumen Test Data Charts for RTFOT-aged Asphalt Binders

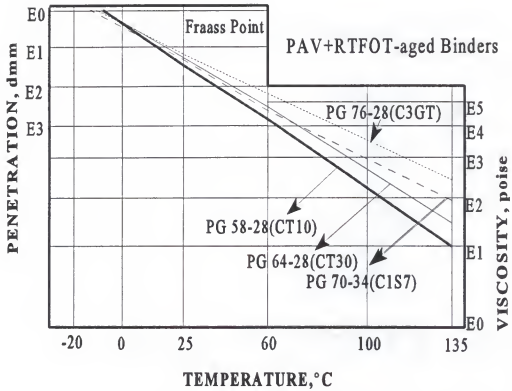

Note: CT10 - Coastal AC-10.
C1S7 - Coastal AC-10+3%SBR70.
C3GT - Coastal AC-30+10%GTR.
CT30 - Coastal AC-30.

Figure 4.27 Bitumen Test Data Charts for PAV+RTFOT-aged Asphalt Binders

2. The GTR-modified asphalt (AC-30+10%GTR) showed the lowest aging potential based on penetration and Schweyer viscosity as compared with the other asphalt binders.
3. The Brookfield rheometer can be used to measure the viscosity of asphalt binder at 60°C. This testing apparatus is much easier to perform than the conventional capillary tube.
4. The SBR-modified asphalts exhibited a significant improvement in capacity of resisting thermal cracking based on Fraass breaking point, BBR and DTT tests.
5. The results from the DSR test indicate that the modified asphalt binders, such as SBR- and GTR-modified asphalts, show high modulus and more elastic behavior than unmodified asphalt at high temperature, and also show lower modulus and more viscous behavior than the unmodified asphalts at low temperature.
6. The cracking temperatures as predicted by SHRP limiting stiffness temperature from the BBR test and the limiting strain temperature from the DTT are generally lower than the cracking temperature as predicted by constant power viscosity.
7. The results from the BTDC indicate that a PG grade with a wide temperature range will display a low temperature susceptibility in the BTDC. Family curves of the BTDC could be used to compare the characteristics of a binder as it ages.

8. Bitumen Test Data Chart (BTDC) of the tested binders show that the SBR- and GTR-modified binders have a substantially lower temperature susceptibility as compared with their corresponding unmodified binders at the unaged, RTFOT-aged and PAV-aged conditions.

CHAPTER 5
RESULTS OF MIXTURE STRENGTH TESTS

5.1 Introduction

An experimental program was conducted to evaluate the effects of different modifiers and aging conditions on the indirect tensile strength, creep compliance, resilient modulus, and fracture energy of compacted asphalt mixtures. An appropriate statistical model was used to analyze the data and compare different modifiers and aging conditions at three different temperatures.

5.2 Statistical Model

Statistical analysis using the ANOVA model was used to determine whether the effect of main factors and interactions of factors are significant. The effects of asphalt type and aging method were studied by means of this experiment design. The test results from the mixture strength tests were analyzed according to the factorial experimental design that included three types of asphalt and three types of aging process. Asphalt (α) and aging method (β) are regarded as fixed effects. The following linear model is assumed for any single response variable in the experiment:

$$Y_{ijk} = \mu + \alpha_i + \beta_j + (\alpha\beta)_{ij} + \epsilon_{ijk}$$

where

Y_{ijk} = the response of kth replicate, j^{th} aging process, and i^{th} asphalt

μ= the overall mean

α_i= the main effect of ith asphalt type

β_j= the main effect of jth aging process

$\alpha\beta_{ij}$= the interaction effect

ϵ_{ijk}= the experimental error

i= 1 to 3 for three asphalts

j= 1 to 3 for three aging processes

k= 1 to 3 for three replicates

5.3 Results Of Diametral Resilient Modulus Test

The resilient modulus is defined as the ratio of applied stress to corresponding instantaneous or total recoverable strain during repeated loading. Mixtures with high resilient modulus at a low temperature are considered to be too brittle to resist the thermal and load associated cracking. At low temperatures, a low elastic modulus is beneficial to prevent a rapid accumulation of tensile stresses and strains during temperature drops. The numerical values of the measured total and instantaneous resilient modulus at test temperatures of 0, -10 and -20°C for all mixtures before and after the STOA and LTOA aging processes are shown in Table B.1 in Appendix B. Because of the very short loading time (0.1 second) and very low temperatures involved in the resilient modulus test, some test results were inconsistent at temperatures of -10 and -20°C. The cause of the inconsistency might be due to micro damage sustained in the asphalt mixture upon cooling to low temperatures, or that the LVDT was frozen and could not respond normally. The inconsistency could also be due to different air void contents of the mixtures at different

aging conditions. In general, both the STOA and LTOA aging processes tend to increase the resilient modulus at temperatures of 0, -10 and -20°C. The instantaneous resilient moduli are slightly higher than the total resilient modulus for all mixtures before and after the STOA and LTOA aging processes. Comparisons of the instantaneous and total resilient moduli plots for unmodified and modified asphalt mixtures with similar air void content at 0, -10 and -20°C are shown in Figures 5.1 and 5.2. It can be seen that the GTR-modified asphalt mixtures before and after the LTOA process have lower instantaneous and total resilient moduli as compared with the unmodified mixtures. The mixtures with SBR-modified asphalt have lower air void content and exhibit approximately the same instantaneous and total resilient moduli as compared with the unmodified mixtures.

5.4 Results Of Indirect Tensile Creep Tests

Asphalt mixtures exhibit viscoelastic behavior. Viscoelastic deformation is the result of the combined elastic and viscous response of the material when subjected to an applied load. The rheological behavior of asphalt mixtures can be modeled by using different combinations of Hookean springs and Newtonian dashpots. Maxwell, Kelvin, Van der Poel, Burgers, and Kuhn and Rigden models are well-known rheological models which make use of a combination of Hookean springs and Newtonian dashpots. Among these models, the Burgers model is a simple model that can model this behavior well. The slope and intercept from the Burgers model were used to evaluate and analyze indirect tensile creep data in this study. This model is illustrated in Figure 5.3. In this model, the top spring models the purely elastic deformation, the combined middle spring and dashpot

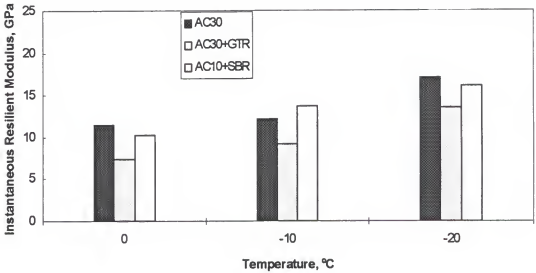

(a) Unaged Samples at Initial Compaction

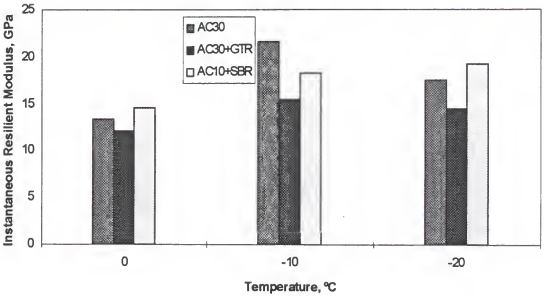

(b) LTOA Samples at Ultimate Compaction

Figure 5.1 Comparison of Instantaneous Resilient Moduli of Mixtures

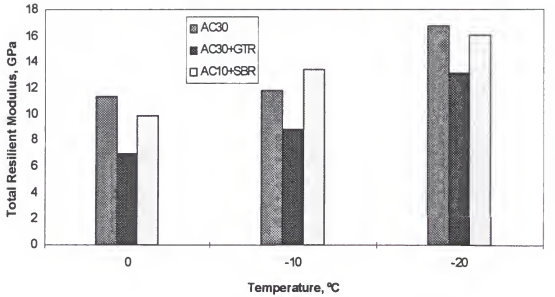

(a) Unaged Samples at Initial Compaction

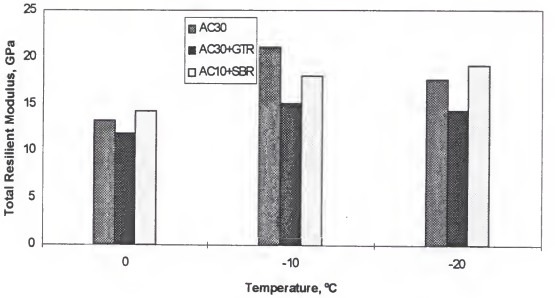

(b) LTOA Samples at Ultimate Compaction

Figure 5.2 Comparison of Total Resilient Moduli of Mixtures

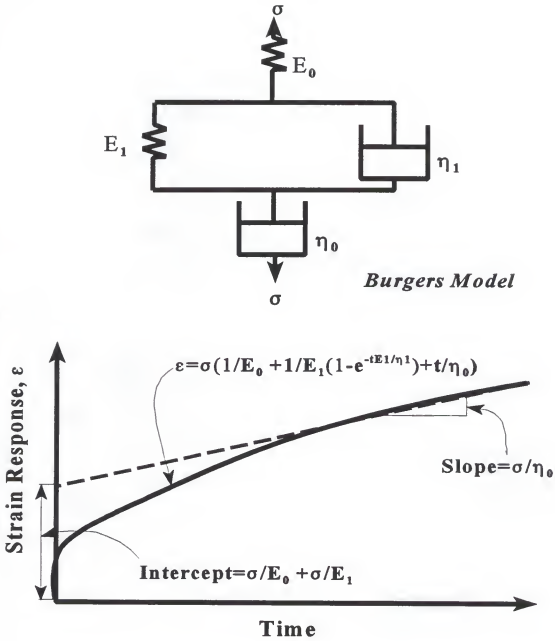

Figure 5.3 Response of a Burgers Model Subjected to a Unit Load

model the delayed elastic deformation, and the lower dashpot models the purely viscous flow. Creep testing of asphalt mixtures provides information on elastic, delayed elastic and viscous components. The creep compliance from a creep test represents the strain caused by a unit stress. It can be represented by the response of a Burgers model subject to a unit applied stress. The creep compliance can be expressed as: $1/E_0 + 1/E_1 \times (1-e^{-tE1/\eta 1}) + t/\eta_0$. It can be noted that at large t the slope of the creep compliance plot approaches $1/\eta_0$. The intercept of the creep compliance plot with the vertical axis is equal to $(1/E_0 + 1/E_1)$, which can be considered to be equal to 1/(total elastic stiffness) of the mixture.

Results of the indirect tensile creep tests at test temperatures of 0, -10 and -20°C for all mixtures before and after the STOA and LTOA processes are shown in Table B.2 in Appendix B. The values of creep compliance at 19 different times and one average Poisson's ratio are reported. Comparisons of creep compliance at 1000 seconds for all mixtures at different temperatures and after different aging effects are shown in Figures 5.4 and 5.5. In general, the creep compliance reduces as temperature decreases for all mixtures. The creep compliance also slightly decreases after the STOA or LTOA process for all mixtures.

An investigation was made to determine when the creep compliance versus time plot reaches a steady state. The instantaneous slopes at different times were compared to the slope at 1000 seconds. It was found that in general at times beyond 500 seconds, the observed slope changes by less than 1%, which is of the same magnitude as the expected experimental error from this test. Thus, it was concluded that, in most cases, steady state condition was reached at 500 seconds.

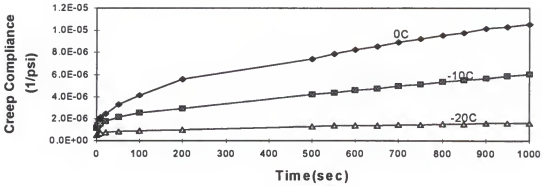

(a) AC30+GTR Unaged Samples at Initial Compaction

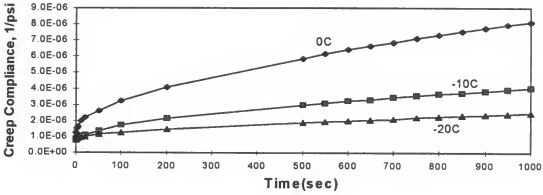

(b) AC30+GTR STOA Samples at Initial Compaction

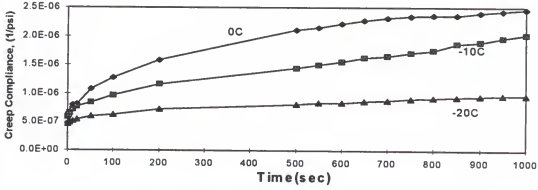

(c) AC30+GTR LTOA Samples at Initial Compaction

Figure 5.4 Comparison of Creep Compliance of Mixtures at Different Temperatures

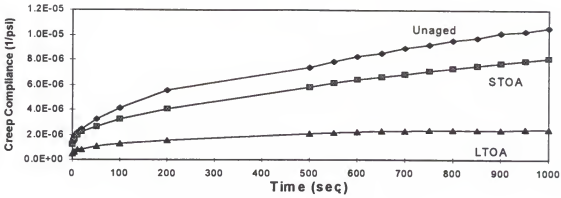

(a) 0°C (AC30+GTR at Initial Compaction)

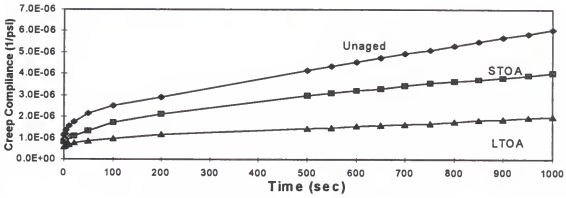

(b) -10°C (AC30+GTR at Initial Compaction)

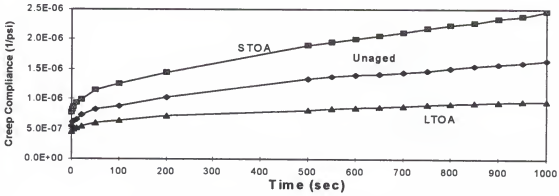

(c) -20°C (AC30+GTR at Initial Compaction)

Figure 5.5 Comparison of Creep compliance of Mixtures at Different Aged Conditions

Tables 5.1 and 5.2 summarize the air void contents of the mixtures, and the intercepts and slopes of the creep compliance plots, R^2 of the regression line for determination of slopes and intercepts, and Poisson's ratio at 0, -10 and -20°C for all mixtures tested at initial and ultimate compaction conditions. Comparisons of the slopes of the creep compliance versus time plots for unmodified and modified asphalt mixtures with similar air void content at 0, -10 and -20°C are shown in Figure 5.6. At 0°C, the SBR modified asphalt mixtures after the LTOA process have lower creep compliance slopes as compared with the unmodified mixtures. At the test temperatures of -10 and -20°C, the mixtures with SBR- or GTR-modified asphalt exhibit substantially higher creep compliance slopes as compared with the unmodified mixtures. A mixture with higher creep compliance slope (ie. low viscous stiffness) would strain more through viscous deformation and not build up tensile stresses at low temperatures. Also, comparisons of the intercepts of the creep compliance versus time plots for unmodified and modified asphalt mixtures with similar air void content at 0, -10 and -20°C are shown in Figure 5.7. It can be seen that the GTR modified asphalt mixtures before and after the LTOA process have higher creep compliance intercepts as compared with the unmodified mixtures. The mixtures with SBR modified asphalt have lower air void content and exhibit approximately the same creep compliance intercepts as compared with the unmodified mixtures at -10 and -20°C.

5.5 Results Of Indirect Tensile Strength Tests

The indirect tensile strength is the maximum tensile stress that a specimen can tolerate before fracture. It indicates the resistance to failure of asphalt concrete caused by

Table 5.1 Results of Analysis of Creep Compliance Data for Samples of Initial Compaction

Asphalt	Aging Condition	Temp. (C)	Air Void (%)	Intercept (1/psi)	Slope (1/psi)	R^2	Poisson's Ratio
AC30	Unaged	0	8.5	2.035E-06	3.634E-09	0.997	0.16
		-10	8.4	1.614E-06	1.040E-09	0.995	0.19
		-20	8.3	7.115E-07	1.565E-10	0.958	0.25
	STOA	0	11	2.683E-06	3.162E-09	1.000	0.21
		-10	11.3	1.26E-06	1.032E-09	0.994	0.24
		-20	11.6	8.577E-07	4.572E-10	0.998	0.29
	LTOA	0	11.4	1.515E-06	2.197E-09	0.989	0.24
		-10	11.3	1.208E-06	9.604E-10	0.997	0.29
		-20	11.2	7.013E-07	5.472E-10	0.997	0.31
AC30 +GTR	Unaged	0	7	4.496E-06	6.210E-09	0.995	0.21
		-10	6.8	2.311E-06	3.752E-09	1.000	0.23
		-20	6.6	1.031E-06	6.003E-10	0.995	0.24
	STOA	0	7.4	3.714E-06	4.469E-09	0.998	0.12
		-10	7.6	1.958E-06	2.097E-09	0.998	0.18
		-20	7.8	1.341E-06	1.108E-09	0.999	0.23
	LTOA	0	7.7	1.810E-06	6.664E-10	0.972	0.44
		-10	7.8	8.733E-07	1.140E-09	0.997	0.33
		-20	7.9	6.656E-07	3.152E-10	0.988	0.32
AC10 +SBR	Unaged	0	6.7	3.255E-06	4.120E-09	0.998	0.21
		-10	6.8	1.486E-06	2.364E-09	0.999	0.25
		-20	6.9	7.278E-07	3.243E-10	0.998	0.4
	STOA	0	7.2	3.148E-06	4.482E-09	0.999	0.22
		-10	7	1.071E-06	6.928E-10	0.998	0.33
		-20	6.8	5.892E-07	2.920E-10	0.998	0.33
	LTOA	0	6.8	2.005E-06	1.964E-09	0.990	0.38
		-10	7	1.105E-06	9.447E-10	0.997	0.3
		-20	7.2	7.340E-07	3.862E-10	0.994	0.26

Table 5.2 Results of Analysis of Creep Compliance Data for Samples of Ultimate Compaction

Asphalt	Aging Condition	Temp. (C)	Air Void (%)	Intercept (1/psi)	Slope (1/psi)	R^2	Poisson's Ratio
AC30	Unaged	0	4.5	2.975E-06	2.811E-09	0.994	0.16
		-10	4.5	2.401E-06	1.993E-09	0.999	0.14
		-20	4.6	1.108E-06	6.091E-10	0.996	0.29
	STOA	0	5.1	2.086E-06	3.176E-09	0.998	0.33
		-10	4.8	1.323E-06	1.030E-09	0.992	0.3
		-20	4.5	4.421E-07	1.293E-10	0.971	0.5/0.57
	LTOA	0	4.5	1.772E-06	1.228E-09	0.994	0.12
		-10	4.7	7.217E-07	2.370E-10	0.993	0.32
		-20	4.9	5.921E-07	2.465E-10	0.984	0.26
AC30 +GTR	Unaged	0	4.7	2.394E-06	2.473E-09	0.997	0.22
		-10	4.6	1.280E-06	7.591E-10	0.996	0.2
		-20	4.5	5.151E-07	1.680E-10	0.997	0.5/0.80
	STOA	0	4.8	2.180E-06	1.366E-09	0.983	0.18
		-10	4.9	1.132E-06	3.722E-10	0.952	0.17
		-20	5	6.461E-07	2.149E-10	0.977	0.31
	LTOA	0	4.7	1.936E-06	1.558E-09	0.993	0.25
		-10	4.9	9.341E-07	7.406E-10	0.998	0.32
		-20	5.1	6.904E-07	2.531E-10	0.994	0.26
AC10 +SBR	Unaged	0	3.5	2.433E-06	2.684E-09	0.998	0.33
		-10	3.6	1.628E-06	1.372E-09	0.989	0.35
		-20	3.7	6.687E-07	4.324E-10	0.999	0.32
	STOA	0	3.8	2.614E-06	3.219E-09	0.998	0.22
		-10	3.7	1.315E-06	9.600E-10	0.996	0.25
		-20	3.6	5.165E-07	1.547E-10	0.980	0.50/0.51
	LTOA	0	3.6	1.338E-06	9.645E-10	0.993	0.41
		-10	3.7	8.080E-07	5.392E-10	0.994	0.29
		-20	3.9	5.580E-07	3.073E-10	0.995	0.25

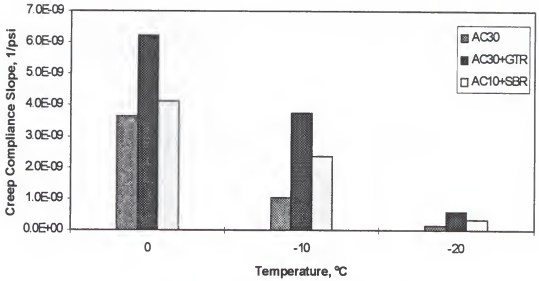

(a) Unaged Samples at Initial Compaction

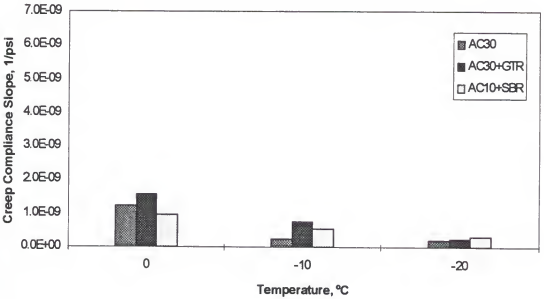

(b) LTOA Samples at Ultimate Compaction

Figure 5.6 Comparison of the Creep Compliance Slopes for Different Asphalt Mixes

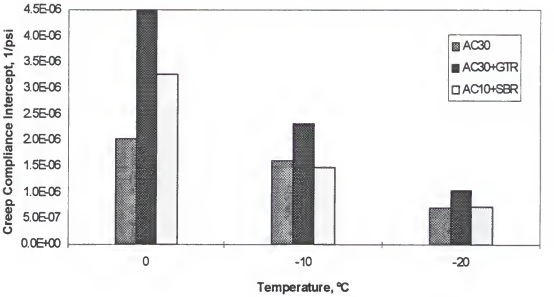

(a) Unaged Samples at Initial Compaction

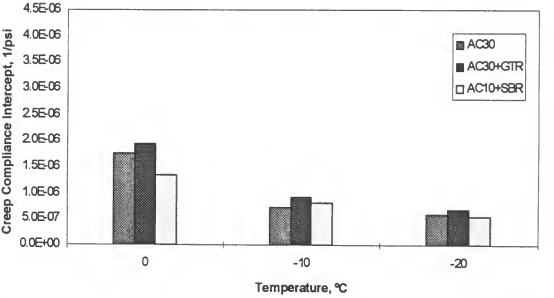

(b) LTOA Samples at Ultimate Compaction

Figure 5.7 Comparison of the Creep Compliance Intercepts for Different Asphalt Mixes

tensile stresses and can be used for predicting the thermal cracking potential of a mixture. Asphalt mixtures that can tolerate high strains prior to failure are more likely to resist cracking than the mixes that cannot tolerate high strains. Results of the indirect tensile strength tests at -10°C for all mixtures at initial and ultimate compaction conditions are shown in Tables 5.3 and 5.4. Reported are air void content, tensile strength, horizontal strains at failure, and fracture energy. These results were analyzed by using the statistical model as described in the previous section. This test was only performed at -10°C on samples which had previously been tested by resilient modulus and indirect tensile creep tests. It can be seen that the air void content of the samples strongly affects their tensile strength. Mixes with higher air voids tend to have lower tensile strengths. However, horizontal strain at failure is apparently not affected by air void content. Results of ANOVA and Duncan's grouping on the indirect tensile strengths for all mixtures before and after STOA and LTOA processes are shown in Table 5.5. The test results indicated that the SBR modified mixtures have higher tensile strength at both initial and ultimate compaction. The high tensile strengths of SBR modified samples are partly attributed to the low air void content of the compacted samples. However, the aging processes did not have significant effects on the tensile strengths of the samples.

Comparisons of tensile strengths for all of the test mixtures are shown in Figure 5.8. These plots again show that the SBR-modified mixtures have higher tensile strengths than the other mixtures at similar compaction and aging conditions.

Results of ANOVA and Duncan's grouping of the failure strains for all mixtures are shown in Table 5.6. It can be seen that the SBR and GTR modified mixtures have

Table 5.3 Results of Indirect Tensile Strength Test on Samples of Initial Compaction

Mixture	Aging Condition	Air Voids (%)	Tensile Strength (psi)	Failure Strain (10^{-6} inch)	Fracture Energy (psi)
AC30	Unaged	9.9	258.6	462.3	0.755
	Unaged	7.0	426.6	762.3	1.510
	Unaged	8.3	378.6	621.0	1.122
	STOA	10.7	334.6	485.7	0.719
	STOA	11.4	259.4	386.3	0.429
	STOA	11.8	240.5	493.1	0.524
	LOTA	10.6	358.4	483.0	0.727
	LOTA	11.7	254.0	245.9	0.280
	LOTA	11.6	272.4	506.3	0.630
AC30 +GTR	Unaged	6.9	274.5	818.9	1.158
	Unaged	6.9	276.2	661.4	0.704
	Unaged	6.6	302.4	1013.0	1.496
	STOA	8.8	336.2	627.5	1.000
	STOA	7.0	415.5	890.6	1.686
	STOA	7.6	387.9	663.5	1.106
	LOTA	7.0	454.9	604.0	1.266
	LOTA	8.2	364.0	581.7	0.834
	LOTA	8.2	359.8	817.2	1.419
AC10 +SBR	Unaged	7.2	387.6	1052.2	2.062
	Unaged	6.7	440.1	759.4	1.589
	Unaged	6.5	460.6	1054.3	2.419
	STOA	7.1	507.9	356.2	0.465
	STOA	6.9	555.4	1096.6	3.025
	STOA	7.0	539.5	767.2	1.997
	LOTA	7.2	495.1	389.7	0.560
	LOTA	7.2	492.2	657.1	1.487
	LOTA	6.6	581.4	1151.6	3.229

Table 5.4 Results of Indirect Tensile Strength Test on Samples of Ultimate Compaction

Mixture	Aging Condition	Air Voids (%)	Tensile Strength (psi)	Failure Strain (10^{-6} inch)	Fracture Energy (psi)
AC30	Unaged	4.0	327.6	741.4	1.032
	Unaged	5.5	197.2	529.6	0.472
	Unaged	4.0	367.7	589.1	0.968
	STOA	5.4	237.6	448.6	0.430
	STOA	4.8	494.4	674.9	1.582
	STOA	4.0	607.5	948.9	2.661
	LOTA	4.8	527.6	586.8	1.414
	LOTA	4.5	591.8	773.5	2.071
	LOTA	4.8	475.2	483.0	1.039
AC30 +GTR	Unaged	4.5	455.1	799.8	1.801
	Unaged	4.5	460.0	808.2	1.718
	Unaged	4.8	434.9	814.7	1.701
	STOA	4.7	467.4	531.5	1.019
	STOA	5.0	375.8	739.3	1.423
	STOA	5.0	372.6	583.6	0.995
	LOTA	5.0	391.3	643.0	1.211
	LOTA	4.8	355.1	457.0	0.757
	LOTA	4.9	380.2	679.0	1.257
AC10 +SBR	Unaged	3.7	410.8	861.5	1.521
	Unaged	3.6	536.5	1128.6	2.809
	Unaged	3.5	567.9	830.4	1.985
	STOA	3.7	577.9	876.0	2.142
	STOA	3.6	578.7	895.5	2.293
	STOA	3.8	571.1	1080.6	3.497
	LOTA	3.8	580.5	785.0	2.305
	LOTA	3.7	589.6	819.9	1.953
	LOTA	3.6	647.1	1103.8	2.873

Table 5.5 Results of ANOVA and Duncan's Grouping on Indirect Tensile Strength

Model $Y_{ijk} = \mu + \alpha_i + \beta_j + (\alpha\beta)_{ij} + \epsilon_{ijk}$

Dependent Variable: Indirect Tensile Strength
Compact Condition: **Initial**

Source	DF	ANOVA SS	Mean Square	F Value	Pr > F
ASPHALT, α	2	171187.3505	85593.6753	34.39	0.0001
AGING, β	2	11984.9457	5992.4728	2.41	0.1184
INTERACTION	4	38621.6847	9655.4212	2.88	0.0692

R-Square = 0.831970, C.V.= 12.93395

Duncan Grouping	Mean	N	ASPHALT
A	495.52	9	AC10+SBR
B	352.36	9	AC30+GTR
B			
B	309.22	9	AC30

Compact Condition: **Ultimate**

Source	DF	ANOVA SS	Mean Square	F Value	Pr > F
ASPHALT, α	2	126316.3399	63158.1699	9.65	0.0014
AGING, β	2	35193.1472	17596.5736	2.69	0.0952
INTERACTION	4	73478.5111	18369.6278	2.81	0.0569

R-Square = 0.665980, C.V.= 17.36866

Duncan Grouping	Mean	N	ASPHALT
A	562.23	9	AC10+SBR
B	425.16	9	AC30
B			
B	410.26	9	AC30+GTR

Note: Means with the same letter are not significantly different at α=0.05.

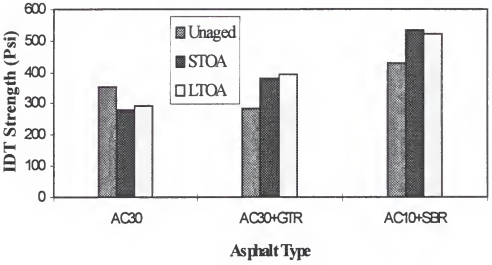

(a) Initial Compaction

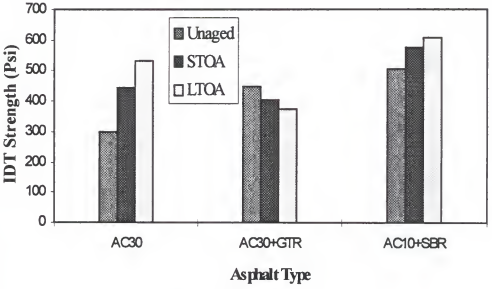

(b) Ultimate Compaction

Figure 5.8 Comparison of Indirect Tensile Strengths of Mixtures

Table 5.6 Results of ANOVA and Duncan's Grouping on Failure Strains

$$\textbf{Model} \quad Y_{ijk} = \mu + \alpha_i + \beta_j + (\alpha\beta)_{ij} + \epsilon_{ijk}$$

Dependent Variable: Failure Strains
Compact Condition: **Initial**

Source	DF	ANOVA SS	Mean Square	F Value	Pr > F
ASPHALT, α	2	992979.8070	496489.9035	6.59	0.0031
AGING, β	2	392876.9404	196438.4702	2.61	0.0849
INTERACTION	4	18926.8396	4731.7099	0.06	0.9925

R-Square = 0.392920, C.V.= 40.26501

Duncan Grouping	Mean	N	ASPHALT
A	809.34	18	AC10+SBR
A			
A	741.96	18	AC30+GTR
B	493.97	18	AC30

Duncan Grouping	Mean	N	METHOD
A	800.51	18	Unage
A			
B A	640.72	18	STOA
B			
B	604.04	18	LOTA

Compact Condition: **Ultimate**

Source	DF	ANOVA SS	Mean Square	F Value	Pr > F
ASPHALT, α	2	909173.1470	454586.5735	10.05	0.0002
AGING, β	2	66834.0781	33417.0391	0.74	0.4835
INTERACTION	4	127631.6419	31907.9105	0.71	0.5926

R-Square =0.451506 , C.V.= 28.41441

Duncan Grouping	Mean	N	ASPHALT
A	931.23	18	AC10+SBR
B	672.88	18	AC30+GTR
B			
B	641.72	18	AC30

Note: Means with the same letter are not significantly different at α=0.05.

higher failure strains as compared with the unmodified samples. The high failure strains may be due to the more elastic behavior of the mixtures. Although the LTOA mixtures have higher tensile strengths, they are more brittle as shown by their low failure strains.

5.6 Fracture Energy

Fracture energy is the energy required to cause fracture of an asphalt mixture. It is determined by calculating the total area under the stress-strain curve from an indirect tensile strength test. Comparisons of fracture energies at test temperature of -10°C for different material effects and different aging effects are shown in Figures 5.9 and 5.10. The results of ANOVA on the measured fracture energy at -10°C along with the Duncan's Multiple Range test results for all mixtures are shown in Table 5.7. The test results indicated that the fracture energy slightly decreases after the STOA or LTOA process for the samples of initial compaction at -10°C. This shows that the fracture energy value decreases as the asphalt binder hardens. As seen from these plots, all the SBR-modified asphalt mixtures have higher fracture energy at -10°C than that of mixtures containing the unmodified AC-30. At initial compaction condition, the GTR-modified mixture has significantly higher fracture energy than the unmodified mix. However, at ultimate compaction condition, the difference is statistically insignificant as seen from the results of Duncan Grouping.

5.7 Summary of Findings

The conclusions from the results of the mixture studies are summarized as follows:

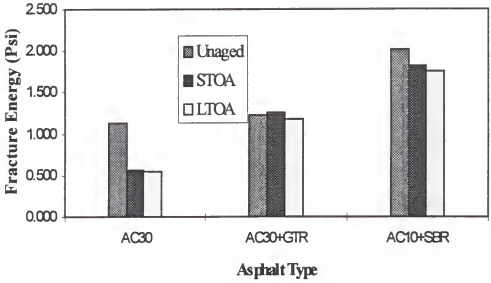

Figure 5.9 Comparison of Fracture Energies of Mixtures at Initial Compaction

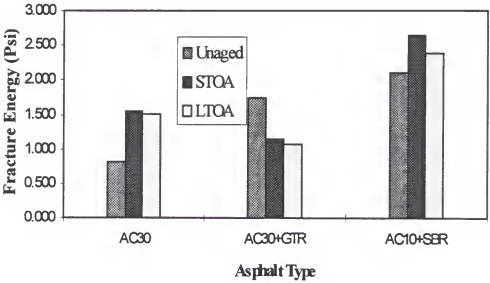

Figure 5.10 Comparison of Fracture Energies of Mixtures at Ultimate Compaction

Table 5.7 Results of ANOVA and Duncan's Grouping on Fracture Energy

Model $Y_{ijk} = \mu + \alpha_i + \beta_j + (\alpha\beta)_{ij} + \epsilon_{ijk}$

Dependent Variable: Fracture Energy
Compact Condition: **Initial**

Source	DF	ANOVA SS	Mean Square	F Value	Pr > F
ASPHALT, α	2	11594463.49	5797231.75	10.57	0.0002
AGING, β	2	698578.32	349289.16	0.64	0.5337
INTERACTION	4	924682.12	231170.53	0.42	0.7923

R-Square = 0.348736, C.V.= 58.47566

Duncan Grouping	Mean	N	ASPHALT
A	1870.3	18	AC10+SBR
B	1185.4	18	AC30+GTR
C	744.0	18	AC30

Compact Condition: **Ultimate**

Source	DF	ANOVA SS	Mean Square	F Value	Pr > F
ASPHALT, α	2	13662802.07	6831401.03	15.15	0.0001
AGING, β	2	463749.58	231874.79	0.51	0.6014
INTERACTION	4	4027370.68	1006842.67	2.23	0.0904

R-Square =0.47225 , C.V.= 40.35258

Duncan Grouping	Mean	N	ASPHALT
A	2375.2	18	AC10+SBR
B	1320.1	18	AC30+GTR
B			
B	1296.6	18	AC30

Note: Means with the same letter are not significantly different at α=0.05.

(1) The instantaneous resilient modulus is slightly higher than the total resilient modulus for all mixtures before and after the STOA and LTOA aging processes. It is important to specify the type of resilient modulus measured.

(2) In general, both STOA and LTOA aging processes increase the resilient modulus at temperatures of 0, -10 and -20°C.

(3) The creep compliance decreases as temperature decreases and also slightly decreases after the STOA or LTOA process for all mixtures.

(4) The creep compliance of a mixture at a later time could be predicted by extrapolation of a linear regression equation after it reaches a steady state condition, which usually occurs at a testing time of approximately 500 sec.

(5) The slope and intercept from the Burgers model can be used to help analyzed the creep compliance versus time data. The intercept of the steady state line with the vertical axis at a time of zero represent 1/(total elastic stiffness) of the mixture.

(6) At 0°C, the SBR-modified asphalt mixtures did not exhibit a lower viscosity (low creep compliance slope) than the unmodified mixtures after the LTOA process. However, at -10 and -20°C, the SBR-modified mixtures exhibit substantially lower viscosity (higher creep compliance slope) than the unmodified mixtures.

(7) The GTR-modified asphalt mixtures have lower resilient moduli and lower elastic stiffness (higher creep compliance intercepts) as compared with the unmodified mixtures before and after the LTOA process. The SBR-modified asphalt mixtures exhibit approximately the same elastic stiffness (creep compliance intercepts) and

resilient moduli as compared with the unmodified mixtures at -10 and -20°C before and after the LTOA process.

(8) The SBR-modified mixtures have higher tensile strengths than the GTR-modified and the unmodified mixtures. Both the SBR and GTR modified asphalt mixtures have higher failure strains than the unmodified samples.

(9) The fracture energy of asphalt mixtures at -10°C decreases slightly after the STOA or LTOA process. The SBR-modified asphalt mixtures have higher fracture energy at -10°C than that of mixtures containing the unmodified AC-30. The GTR-modified asphalt mixtures show higher fracture energy than the unmodified mixtures at initial compaction. However, at ultimate compaction condition, the difference is statistically insignificant.

(10) On the basis of indirect tensile creep compliance, tensile strength, failure strain and fracture energy, the SBR-modified mixtures show a greater potential to resist low temperature cracking as compared with the unmodified mixtures.

CHAPTER 6
RESULTS OF RHEOLOGICAL TESTS ON RECOVERED ASPHALT RESIDUES

In order to establish the relationship between the properties of the asphalt mixtures and those of binders, asphalt binders were extracted and recovered from various asphalt mixtures and evaluated for the rheological properties. Asphalt binders were extracted and recovered from the STOA and LTOA-aged mixtures by means of the reflux, centrifuge and rotavapor methods, which are presently used by the Florida Department of Transportation. All of the recovered STOA and LTOA residues were evaluated by (1) Penetration test at 25°C, (2) Brookfield viscosity test at 60°C, (3) Dynamic Shear Rheometer (DSR) test at high service temperatures from 52 to 70°C on the STOA residues and at intermediate temperatures from 13 to 31°C on the LTOA residues, (4) Bending Beam Rheometer (BBR) test at low service temperatures of -10 and -24°C. This chapter presents the results of these rheological tests on the recovered binders. It also presents the comparisons between the aging effects of the SHRP STOA, LTOA, RTFOT and PAV.

6.1 Results Of Conventional and SHRP Binder Tests

Results from the Penetration, Brookfield viscosity and Bending Beam Rheometer (BBR) tests on the recovered binders are listed in Table 6.1. The analysis of these results are presented in following sections.

6.1.1 Penetration

The penetration test on the recovered binders was performed at 25°C according to ASTM D5 Standard Test Method. The data as shown in Table 6.1 indicate that the penetration of the recovered binder residues are lower than those of original binders. Figure 6.1 shows the graphical display of the average percent retained penetration of the different binder residues after the STOA and LTOA processes. It can be seen that the Coastal AC-30 +10%GTR binder has the lowest aging potential by having the highest percent retained penetration after the STOA and LTOA processes.

6.1.2 Brookfield Viscosity

The benefit of using Brookfield Rheometer instead of capillary tube is the convenience of sample preparation and cleaning of the equipment after the test. The viscosities at a shear rate of 1 sec^{-1} obtained in the Brookfield rheometer at 60°C are well correlated with their corresponding absolute viscosity. The aging index which is the ratio between the viscosity of the aged residue and that of the original asphalt, was used to represent the aging severity. Figure 6.2 shows the aging index of the STOA and LTOA residues based on the Brookfield viscosity. It can be observed that the Coastal AC-30 +10%GTR and Coastal AC-10+3%SBR2879 binders have a lower aging index as compared with Coastal AC-30 after the STOA and LTOA processes.

6.1.3 Bending Beam Rheometer (BBR)

The SHRP binder specification requires that the flexural creep stiffness cannot exceed 300 MPa at a loading time of 60 seconds. The limiting stiffness temperature (below which low-temperature cracking would occur) is 10°C below the temperature at

Table 6.1 Results of Tests on STOA and LTOA Recovered Binder

Asphalt Binder	Penetration @25°C, 5sec, 100g, (dmm)	Viscosity @60°C, at shear rate=1/s, (poise)	Creep Stiffness at 60sec, (MPa)	
			@-10°C	@-24°C
STOA Residue				
CT30	30.8 27.7	43569 84477	64.3 67.1	436.7 448.5
C3GT	31.5 29.7	84743 131245	42.5 50.1	288.5 352.3
C1S2	42.0 39.6	16117 24603	52.8 57.8	326.5 352.0
LTOA Residue				
CT30	23.8 23.1	86578 96582	81.2 85.4	444.1 483.1
C3GT	29.5 27.5	80304 163069	58.6 67.6	295.2 356.8
C1S2	33.2 30.7	32536 43212	56.7 64.9	332.9 354.1

NOTE: **CT30**: Coastal AC-30
C3GT: Coastal AC-30 + 10%GTR
C1S2: Coastal AC-10 + 3%SBR(UP2879)

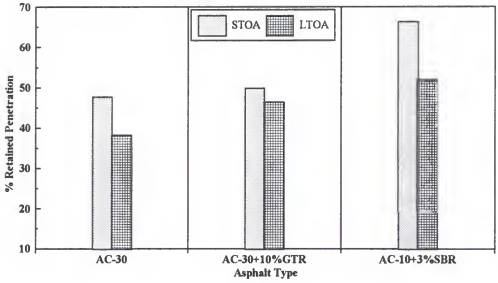

Figure 6.1 Percent Retained Penetration of three Asphalts Aged by the STOA and LTOA Processes

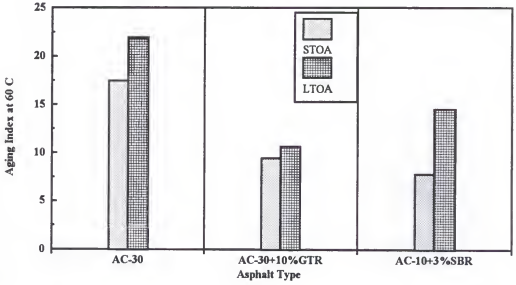

Figure 6.2 The Comparison of Aging Indices of three Asphalts Aged by the STOA and LTOA Processes

which the binder reaches this stiffness. Results of the BBR test at a loading time of 60 seconds on the recovered binders are also shown in Table 6.1. Figures 6.3 and 6.4 show the plots of flexural creep stiffness at a loading time of 60 seconds at -10 and -24°C for the STOA and LTOA residues. It can be seen that the Coastal AC-30+10%GTR and Coastal AC-10+3%SBR binders have a lower stiffness value as compared with Coastal AC-30 binder at -10 and -24°C after either the STOA or LTOA process. Figure 6.5 and 6.6 show the plots of m-value at a loading time of 60 seconds at -10 and -24°C for the STOA and LTOA residues. It can be observed that the Coastal AC-30 binder has the lowest m-value among all the binders at -10 and -24°C after either the STOA or LTOA process.

6.1.4 Dynamic Shear Rheometer (DSR)

An isochronal plot is a plot of viscoelastic parameters, such as complex shear modulus or phase angle, versus temperature at a specified frequency. In testing at high service temperatures, the selected viscoelastic parameters at a lower frequency are plotted against temperature. Figures 6.7 and 6.8 show the isochronal plots of complex shear modulus and phase angle at a frequency of 0.01 Hertz for the STOA residues at high service temperatures. It can be seen that the Coastal AC-30 + 10%GTR binder has the highest modulus and lowest phase angle among all the binders at temperatures ranging from 52 to 70°C. In testing at intermediate to low service temperatures, the selected viscoelastic parameters at a higher frequency are plotted against temperature. Figures 6.9 and 6.10 show the isochronal plots of complex shear modulus and phase angle at a frequency of 30 Hertz for the LTOA residues at intermediate service temperatures,

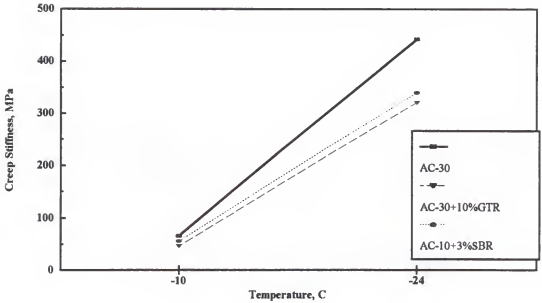

Figure 6.3 Isochronal Plot of Creep Stiffness at 60 sec Loading Time of STOA Residues

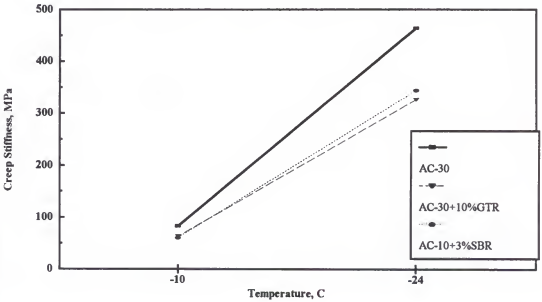

Figure 6.4 Isochronal Plot of Creep Stiffness at 60 sec Loading Time of LTOA Residues

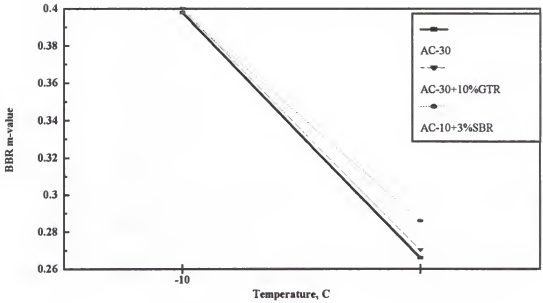

Figure 6.5 Isochronal Plot of m-value at 60 sec Loading Time of STOA Residues

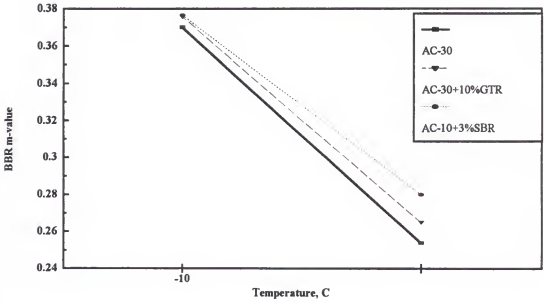

Figure 6.6 Isochronal Plot of m-value at 60 sec Loading Time of LTOA Residues

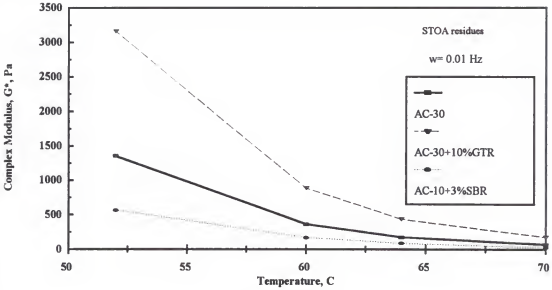

Figure 6.7 Isochronal Plot of Complex Modulus of STOA Residues at w=0.01 Hz

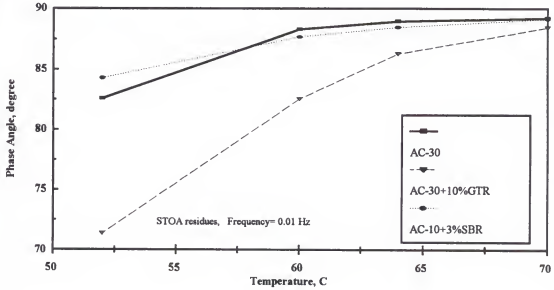

Figure 6.8 Isochronal Plot of Phase Angle of STOA Residues at w=0.01 Hz

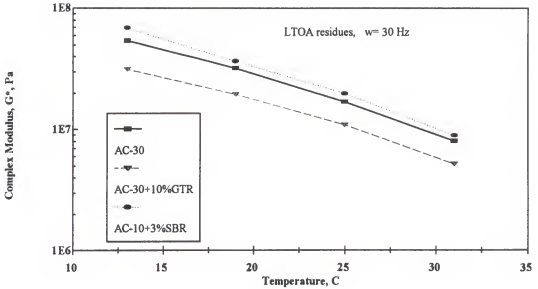

Figure 6.9 Isochronal Plot of Complex Modulus of LTOA Residues at w=30 Hz

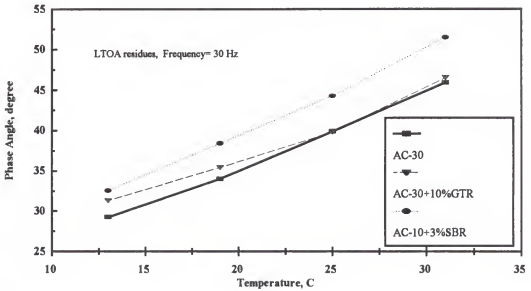

Figure 6.10 Isochronal Plot of Complex Modulus of LTOA Residues at w=30 Hz

respectively. It can be seen that the Coastal AC-30+10%GTR binder has the lowest modulus and similar phase angle among the binders tested at temperatures ranging from 13 to 31°C. This means that GTR- modified asphalts show higher modulus and more elastic behavior than unmodified asphalts at high temperatures, and also have lower modulus and similar phase angle to unmodified asphalts at intermediate to low temperatures.

6.2 Comparison Between the SHRP Aging Processes for Asphalt Mixtures and Those for Asphalt Binders

The Strategic Highway Research Program (SHRP) has proposed a Short-Term Oven Aging (STOA) process to simulate the aging effects of hot mixing and construction process on asphalt mixtures, and a Long-Term Oven Aging (LTOA) process to simulate the effects of additional aging of asphalt mixtures in service for 5 to 10 years. The SHRP STOA process basically involves heating a loose asphalt mixture in a forced-draft oven for four hours at a temperature of 135°C. The LTOA process involves compacting the mixtures after the STOA process and aging the compacted specimens in a forced-draft oven at 85°C for five days.

In the SHRP Superpave binder specification, the conventional Rolling Thin Film Oven Test (RTFOT) is used to simulate the effects of the hot-mix process on a binder, and the Pressure Aging Vessel (PAV) is used to simulate additional aging of the binder in service. In this section, the effects of the SHRP STOA and LTOA were evaluated by comparing their effects on the asphalt binders to those produced by the RTFOT and the PAV processes. Three different asphalt binders were used in this study. The three

different asphalt binders were blended with an aggregate with a fixed gradation and at a fixed asphalt content (6.5% by weight of mix) in the laboratory to produce mixtures complying with the specifications for a dense-graded surface mixture used in Florida. After the mixtures were subjected to the STOA and the LTOA processes, asphalt binders were extracted and recovered by means of the reflux, centrifuge and rotavapor methods. The same original asphalt binders were also subjected to the RTFOT and PAV processes. In order to compare and evaluate the relationships among the aging effects of RTFOT, PAV, STOA and LTOA on Florida asphalt cements, three asphalts were evaluated by Penetration test, Brookfield viscosity test, Dynamic Shear Rheometer (DSR) test, and Bending Beam Rheometer (BBR) test. Results from the Penetration, Brookfield viscosity, and BBR tests on RTFOT, PAV, STOA and LTOA residues are listed in Tables 6.2 and 6.3. Figure 6.11 shows the percent retained penetration of the different binder residues by the processes of RTFOT, PAV, STOA and LTOA. It can be seen that, based on relative percent retained penetration, the order of aging severity, from highest to lowest, is PAV, LTOA, STOA, and RTFOT. Figure 6.12 shows the aging index of the different binder residues by the processes of RTFOT, PAV, STOA and LTOA. It can be seen that, based on the aging index as computed from Brookfield viscosity at 60°C, the order of aging severity is PAV, LTOA, STOA, and RTFOT. This order of aging severity is the same as that based on percent retained penetration. The STOA residues are more severely aged than the RTFOT residues, and the PAV residues are more severely aged than the LTOA residues. Figures 6.13 and 6.14 show the plots of flexural creep stiffness at a loading time of 8, 60 and 240 seconds at -10 and -24°C for the RTFOT, PAV,

Table 6.2 Conventional Binder Test Results by Different Aging Processes

Asphalt Binder	Penetration @25°C, 5sec, 100g, (dmm)	Viscosity @60°C, at shear rate=1/s, (poise)
Unaged Binder		
CT30	61.5	3674
C3GT	44.1	11404
C1S2	86.3	2603
RTFOT Residue		
CT30	36.0	10849
C3GT	36.0	43937
C1S2	51.7	12889
PAV+RTFOT Residue		
CT30	22.8	80650
C3GT	19.0	310481
C1S2	29.3	48660
STOA Residue		
CT30	29.3	64023
C3GT	30.6	107994
C1S2	40.8	20360
LTOA Residue		
CT30	23.5	91580
C3GT	28.5	121687
C1S2	31.9	37874

NOTE: **CT30**: Coastal AC-30
C3GT: Coastal AC-30 + 10%GTR
C1S2: Coastal AC-10 + 3%SBR(UP2879)

Table 6.3 Results of BBR Test on Binders aged by Different Processes

Asphalt Binder (Temperature, °C)	Loading Time (sec)	Creep Stiffness (MPa)			
		RTFOT	**STOA**	**PAV**	**LTOA**
CT30(-10)	8	129.5	139.0	181.1	167.4
	60	57.5	65.7	90.6	83.3
	240	31.4	36.8	55.5	48.5
C3GT(-10)	8	75.7	80.8	119.2	128.0
	60	39.3	46.3	61.7	63.1
	240	21.8	26.0	35.1	36.4
C1S2(-10)	8	73.9	116.1	120.5	123.4
	60	38.2	55.5	59.5	60.3
	240	18.9	31.2	34.6	35.6
CT30(-24)	8	723.3	717.9	745.8	728.0
	60	440.8	442.6	476.8	463.6
	240	289.9	298.3	329.4	302.5
C3GT(-24)	8	487.6	532.0	497.0	535.8
	60	292.9	320.4	313.8	326.0
	240	192.0	211.5	217.1	211.5
C1S2(-24)	8	567.9	570.9	584.5	581.4
	60	329.1	339.3	341.5	343.5
	240	210.1	221.3	225.3	228.8

NOTE: **CT30**: Coastal AC-30
C3GT: Coastal AC-30 + 10%GTR
C1S2: Coastal AC-10 + 3%SBR(UP2879)

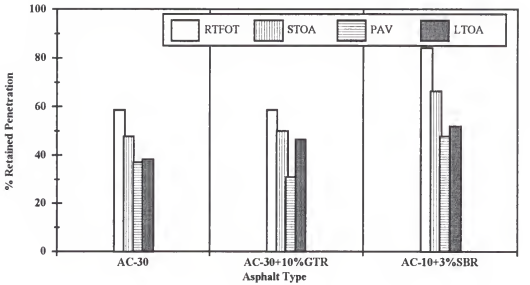

Figure 6.11 Percent Retained Penetration of three Asphalts Aged by the RTFOT, STOA, PAV and LTOA Processes

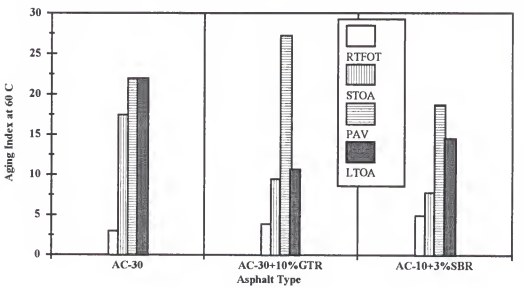

Figure 6.12 The Comparison of Aging Indices of three Asphalts Aged by the RTFOT, STOA, PAV and LTOA Processes

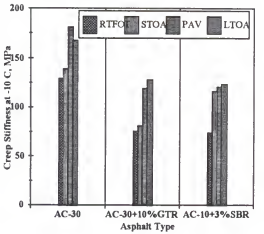

(a) 8 seconds

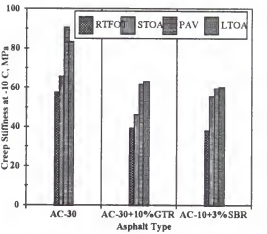

(b) 60 seconds

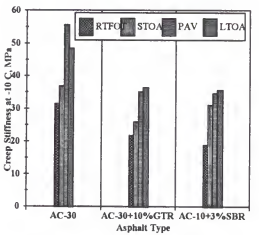

(c) 240 seconds

Figure 6.13 The Comparison of Creep Stiffness at 8, 60 and 240 seconds Loading Time at -10°C of Binders aged by RTFOT, STOA, PAV, and LTOA Processes

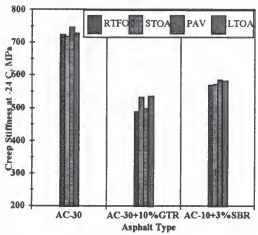

(a) 8 seconds

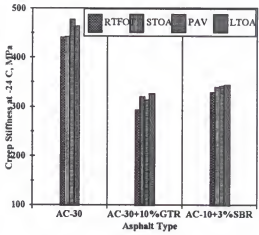

(b) 60 seconds

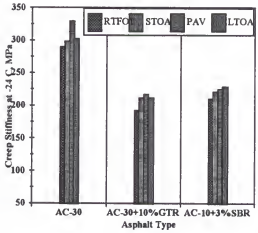

(c) 240 seconds

Figure 6.14 The Comparison of Creep Stiffness at 8, 60 and 240 seconds Loading Time at -24°C of Binders aged by RTFOT, STOA, PAV, and LTOA Processes

STOA, and LTOA residues. It can be seen that, based on creep stiffness values at -10°C, the order from highest to lowest, is PAV, LTOA, STOA, and RTFOT. However, the residues from the four different aging processes have very close stiffness value at a temperature of -24°C. It also can be observed that the same aging order is observed at different loading times at -10°C or -24°C. Figures 6.15 and 6.16 show the plots of m-value at a loading time of 60 seconds at -10 and -24°C for the RTFOT, PAV, STOA, and LTOA residues. It can be observed that the order based on the m-value at -10 and -24°C from lowest to highest is PAV, LTOA, STOA, and RTFOT. This order of m-value is the same as those of percent retained penetration and aging index. Figure 6.17 shows the plots of $G^*/\sin\delta$ at a frequency of 10 rad/sec at high service temperatures for the RTFOT and STOA residues. It can be observed that the STOA residues have higher $G^*/\sin\delta$ values as compared with the RTFOT residues at the temperature range from 52 to 70°C. Figure 6.18 shows the plots of $G^*\times\sin\delta$ at a frequency of 10 rad/sec at intermediate service temperatures for the PAV and LTOA residues. It can be seen that the LTOA residues have slightly higher $G^*\times\sin\delta$ values as compared with the PAV residues at temperatures ranging from 13 to 31°C.

6.3 Summary of Findings

The main conclusions from this chapter are summarized as follows:

(1) The results from the Penetration and Brookfield viscosity indicated that the GTR-modified and SBR-modified recovered binders have a lower aging potential than the unmodified binder.

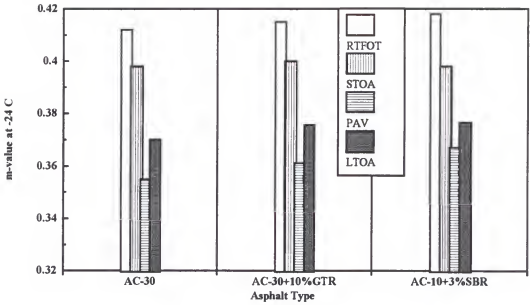

Figure 6.15 The Comparison of m-value at 60 sec Loading Time at -10°C of Binders aged by RTFOT, STOA, PAV, and LTOA Processes

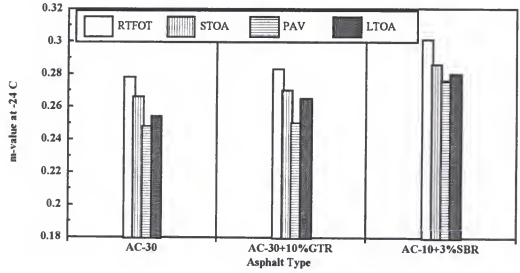

Figure 6.16 The Comparison of m-value at 60 sec Loading Time at -24°C of Binders aged by RTFOT, STOA, PAV, and LTOA Processes

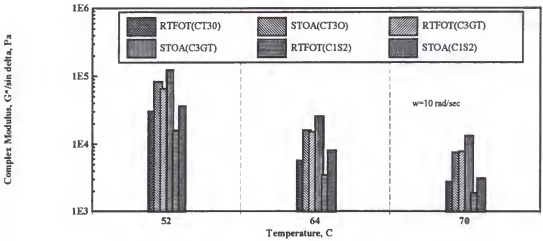

Figure 6.17 The Comparison of G*/sinδ of RTFOT and STOA Residues at w=10 rad/sec at High Service Temperatures

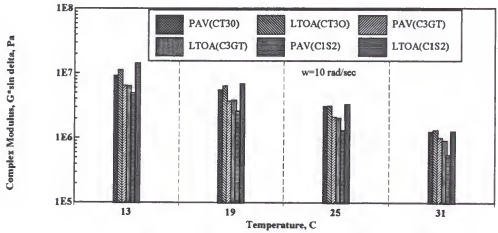

Figure 6.18 The Comparison of G*×sinδ of PAV and LTOA Residues at w=10 rad/sec at Intermediate Service Temperatures

Note: CT30: Coastal AC-30
C3GT: Coastal AC-30 + 10%GTR
C1S2: Coastal AC-10 + 3%SBR

(2) The GTR-modified and SBR-modified recovered binders exhibited a lower stiffness and higher m-value as compared with the unmodified one at -10 and -24°C.

(3) The GTR-modified recovered binder showed higher modulus and more elastic behavior than the unmodified asphalts at high temperatures and also exhibited lower modulus and similar phase angle as compared with the unmodified asphalts at intermediate and low temperatures.

(4) Based on the Penetration, Brookfield viscosity and m-value, the STOA residues are more severely aged than the RTFOT residues and the PAV residues are more severely aged than the LTOA residues.

(5) The results from the BBR test indicate that the residues from the four different aging processes have very close stiffness values at a temperature of -24°C. However, based on creep stiffness values at -10°C, the order of aging severity from highest to lowest, is PAV, LTOA, STOA and RTFOT, but it may vary for different mixtures. It also can be observed that different loading times give the same aging order trend at -10°C and -24°C. It is to be stressed that the aging order is only applicable to the mixtures used in this study.

(6) The results from the DSR test indicate that the STOA residues have a higher modulus and lower phase angle than the RTFOT residues at temperatures ranging from 52 to 70°C and the LTOA residues have a higher modulus and phase angle than the PAV residues at temperatures ranging from 13 to 31°C.

CHAPTER 7
RELATIONSHIP BETWEEN THE BINDER AND MIXTURE PROPERTIES

This chapter presents the comparison between the results of SHRP and conventional binder tests on typical asphalts used in Florida. The relationships between binder and mixture properties were also evaluated and presented in this chapter.

7.1 Comparison of Results of SHRP and Conventional Binder Tests on Florida Asphalt Cements

7.1.1 Binder Rheological Properties at High Service Temperature

Asphalt mixtures are more susceptible to rutting and shoving at high service temperature when the mixture has a lower viscosity and is more easy to creep under heavy loading. At high pavement service temperature when the binder is relatively soft, the strength of the mixture would be predominantly affected by the characteristics of the aggregate. However, when the aggregate factor is fixed, an asphalt binder with a harder stiffness or higher viscosity should give better rutting resistance to the asphalt mixture.

For all unmodified asphalts, and most modified asphalts, oxidative aging results in increased G^* values and decreased δ values. These changes result in more resistance to deformation and more elasticity, which means more contribution to rutting resistance. It is reasonable that the SHRP specification has minimum limits of $G^*/\sin\delta$ on the unaged and the oven-aged binders to control tenderness and rutting. However, Reese and Goodrich

[42, 43] found that G*/sinδ did not explain the rutting which occurred at the laboratory creep test studies and the Needles test road.

The values of G*/sinδ for Florida asphalts were compared to their penetrations and viscosities at similar high service temperatures. Figure 7.1 shows the plot of Brookfield viscosity at a shear rate of 1 s^{-1} and a temperature of 60°C versus the G*/sinδ at 64°C for all nine asphalt binders before and after the RTFOT process. G*/sinδ increases as the viscosity increases. The correlation is quite good (R^2=0.90).

7.1.2 Binder Rheological Properties at Intermediate Service Temperature

At intermediate service temperature, an asphalt binder behaves partially as a solid and partially as a liquid. As an asphalt binder hardens with time, the stiffness of the asphalt concrete would increase. A stiffer asphalt concrete would cause the maximum load-induced stress to increase, and increase the cracking potential of the pavement. Tayebali [44] stated that asphalt-aggregate mixtures with lower stiffness are likely to demonstrate better fatigue resistance under controlled-strain loading than their counterparts with higher stiffness. Conversely, laboratory stress-controlled fatigue testing implies that stiffer binders are more resistant to fatigue cracking [45].

The SHRP binder properties used for control of the fatigue performance of asphalt binders is the loss modulus, G*sinδ, which is measured at the intermediate pavement temperatures ranging from 4 to 40°C. It is based on the dissipated energy theory which is directly proportional to the G*sinδ [46]. However, Reese and Goodrich [4] found that G*sinδ did not adequately explain a binder's contribution to fatigue cracking resistance at the laboratory flexural beam studies and the Needles test road.

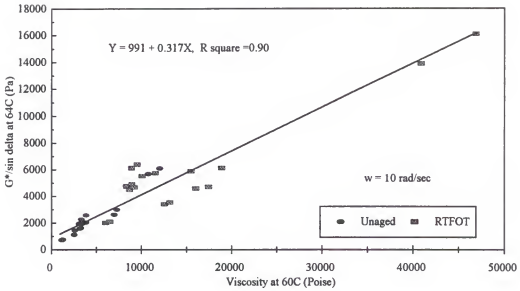

Figure 7.1 Relationship Between Brookfield Viscosity at 60°C and G*/sinδ at 64°C

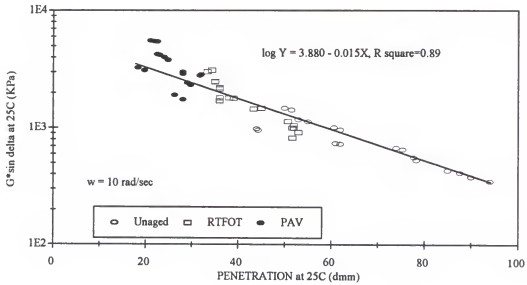

Figure 7.2 Relationship Between Penetration and G*sinδ before and after RTFOT and PAV at 25°C

The values of G*sinδ for Florida asphalts were compared to their penetrations and viscosities at intermediate pavement temperatures. Figure 7.2 shows the penetration versus the G*sinδ at 25°C for all nine asphalt binders before and after the RTFOT and PAV processes. G*sinδ (loss modulus) increases as the penetration decreases. The relationship is quite good (R^2=0.88). The verification of results between penetration and G* at 25°C was plotted in Figure 7.3 [47]. It can be seen that two regression equations are very close to each other. G* increases as the penetration decreases.

Figure 7.4 shows the Schweyer constant power viscosity versus the G*sinδ at 25°C for all nine asphalt binders before and after the RTFOT and PAV processes. G*sinδ (loss modulus) increases as the constant power viscosity increases. The correlation is quite good (R^2=0.85).

7.1.3 Binder Rheological Properties at Low Service Temperature

When an asphalt pavement surface is cooled down by weather, contraction strains are induced in the asphalt concrete. Thermal cracking will occur when these thermal contraction strains exceed the maximum fracture strain of the asphalt concrete, and is normally manifested by transverse cracks on the asphalt pavement.

Because of the complex rheological behavior of asphalt cement at low temperatures, it is generally acknowledged that there is a need for an accurate and reliable measurement of its consistency at low temperatures. The simple and conventional approach taken to reduce thermal cracking is to use low AC-grade asphalts, which tend to be less stiff at low temperatures. Many researchers [11,13,15] have recommended limiting viscosity or stiffness values of asphalt cement or HMA for a particular temperature range

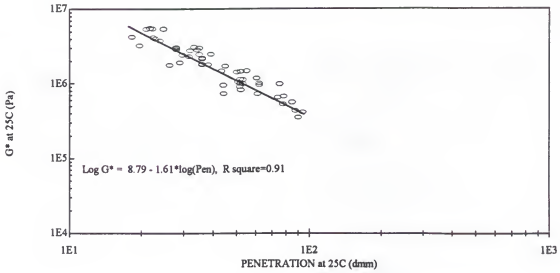

(a) Result from this study

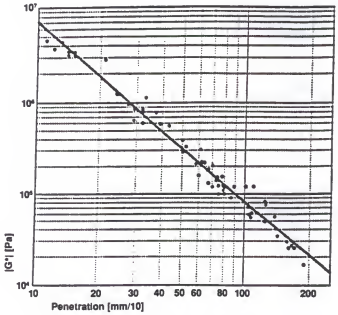

Regression line: log(G*) = 8.80 - 1.95*log(Pen)

(b) Result from another study [47]

Figure 7.3 Verification of Results Between Penetration and G* at 25°C

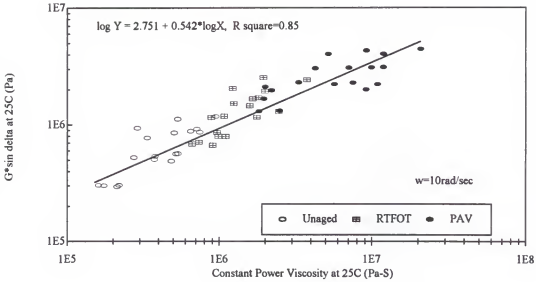

Figure 7.4 Relationship Between Constant Power Viscosity and G*sinδ before and after RTFOT and PAV at 25°C

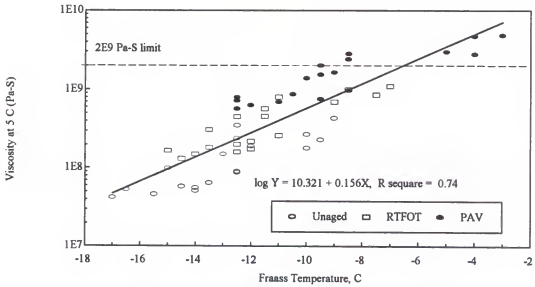

Figure 7.5 Relationship Between Constant Power Viscosity at 5°C and Fraass Temperature before and after RTFOT and PAV

based on field experiments. A stiffness limit of 300 MPa for a loading time of 2 hours or a failure strain limit of 1.0 % for an elongation rate of 1.0 mm/min has been used in the recent SHRP specification to reduce low temperature cracking. In this study, four different test parameters namely Fraass breaking temperature, viscosity limit, stiffness limit and failure strain limit were used to evaluate the low temperature cracking potential of the asphalt cement.

Figure 7.5 shows the plots of constant power viscosity at 5°C versus the Fraass temperature for all nine asphalt binders before and after the RTFOT and PAV processes. Viscosity increases as the Fraass breaking temperature increases. The relationship is fair (R^2=0.75). If a limiting viscosity of 2×10^9 Pa-S is used to predict low temperature cracking [13], the estimated cracking temperature would likely be much higher than the Fraass temperature.

Figure 7.6 and 7.7 show the plots of creep stiffness and failure strain at -12, -18 and -24°C versus the Fraass temperature for all nine asphalt residues after the PAV process. Creep stiffness increases as the Fraass breaking temperature increases. The relationship is fair (R^2 from 0.78 to 0.81). Failure strain decreases as the Fraass breaking temperature increases. The relationship is poor (R^2 from 0.42 to 0.65) as compared with the relationship between failure strain and the Fraass temperature.

Figure 7.8 shows the creep stiffness versus the failure strain at -12, -18 and -24°C for all nine asphalt residues after the PAV process. Creep stiffness decreases as failure strain increases. The relationship is quite good (R^2 = 0.86) as compared with the others.

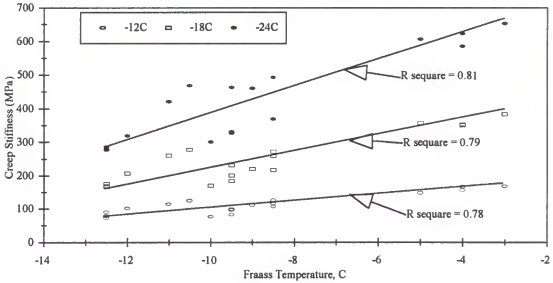

Figure 7.6 Relationship Between Fraass Temperature and Creep Stiffness at -12, -18, and -24°C after PAV

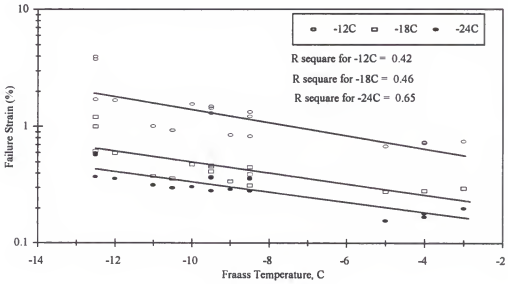

Figure 7.7 Relationship Between Fraass Temperature and Failure Strain at -12, -18, and -24°C after PAV

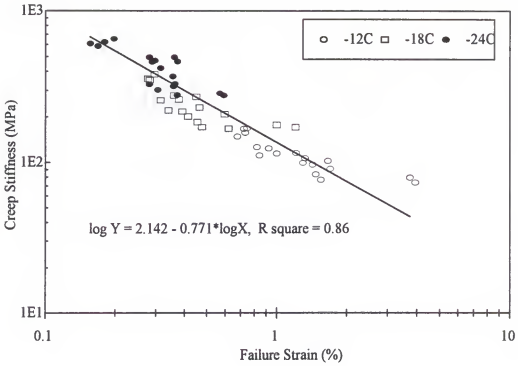

Figure 7.8 Relationship Between Creep Stiffness and Failure Strain at -12, -18, and -24°C after PAV

The Fraass breaking temperatures, predictive limiting stiffness temperatures, and predictive limiting strain temperatures of the binders are shown in Table 7.1. The low-temperature cracking temperature as predicted by the Fraass breaking temperature is higher than the SHRP predictive limiting strain temperature and limiting stiffness temperature. The cracking temperature as predicted by the SHRP predictive limiting stiffness temperature is higher than the predictive limiting strain temperature.

7.2 Relationships Between SHRP Binder and Mixture Properties at low Temperatures

In this study, three different asphalt binders (conventional and modified) were used. The three different asphalt binders were blended with an aggregate with a fixed gradation and at a fixed asphalt content (6.5 percent by weight of mix) in the laboratory to produce mixtures complying with the Florida specifications for a dense-graded structural (S-1) mixture. Marshall-size specimens were compacted in the Gyratory Testing Machine (GTM) to two compaction levels. One is achieved by 18 revolutions with the GTM and is to simulate the initial field compaction. The other is achieved by 200 GTM revolutions, and is to simulate the condition after five to ten years of traffic on the pavement.

The GTM compacted asphalt mixture samples were evaluated by the resilient modulus, indirect tensile creep and strength tests. After the mixtures were evaluated and tested by the indirect tensile strength test at -10°C, asphalt binders were extracted and recovered by means of the reflux, centrifuge and rotavapor methods, which are presently used by the Florida Department of Transportation. All of the recovered STOA and LTOA residues were evaluated by Bending Beam Rheometer (BBR) test at a low service temperature of -10°C.

Table 7.1 Results of Direct Tension Test on PAV+RTFOT-aged Asphalt Binders

Asphalt Binders		Coastal AC-10	Coastal AC-10+ 3% SBR2879	Coastal AC-10+ 3%SBR70	Ergon PMAC 20	Coastal AC-30+ 10%GTR	Coastal AC-30	Koch AC-30	Marathon AC-30	Mariani AC-30
Failure Strain (%)	**-12°C**	**1.378**	**3.848**	**1.683**	**0.965**	**1.514**	**0.834**	**1.257**	**0.700**	**0.740**
	-18°C	**0.402**	**1.102**	**0.608**	**0.368**	**0.465**	**0.327**	**0.457**	**0.280**	**0.289**
	-24°C	**0.360**	**0.581**	**0.365**	**0.307**	**0.294**	**0.286**	**0.367**	**0.162**	**0.189**
Temperature at 1% Failure Strain (°C)		**-14.2**	**-19.2**	**-15.8**	**-11.7**	**-14.9**	**-10.0**	**-13.9**	**-7.7**	**-8.5**
Limiting Strain Temperature,°C		**-24.2**	**-29.2**	**-25.8**	**-21.7**	**-24.9**	**-20.0**	**-23.9**	**-17.7**	**-18.5**
Limiting Stiffness Temperature,°C		**-31.9**	**-35.0**	**-34.1**	**-29.1**	**-33.4**	**-29.5**	**-29.3**	**-26.4**	**-26.0**
Fraass Breaking Temperature,°C		**-9.0**	**-12.5***	**-12.3***	**-10.8**	**-9.8***	**-8.8**	**-9.3**	**-4.5**	**-3.5**
PG Grade		**58-28**	**64-34**	**70-34**	**70-28**	**76-28**	**64-28**	**64-28**	**64-22**	**64-22**

Note: * Temperature was recorded at the first appearance of a mircocrack.

Figures 7.9 and 7.10 show the plots of binder creep stiffness versus mixture stiffness by indirect tensile creep test at -10°C for samples of both compaction conditions. Binder stiffness increases as mixture stiffness increases. The relationship is good (R^2 from 0.77 to 0.80). Comparison of the prediction equations for binder stiffness versus mixture stiffness relationship shows that the equation for the samples of ultimate compaction has a higher intercept and slope. This means that for the same binder stiffness, the mixtures at a higher compaction level would have a higher stiffness.

The comparisons of the relationships between binder and mixture stiffness at -10°C for mixtures aged by the STOA and LTOA processes are shown in Figure 7.11 and 7.12, for initially compacted and ultimately compacted samples, respectively. It can be seen that the LTOA-aged samples have higher binder and mixture modulus as compared with the STOA-aged ones.

Figures 7.13 and 7.14 show the plots of binder m-value versus mixture stiffness at -10°C for initially compacted and ultimately compacted samples, respectively. Binder m-value decreases as mixture stiffness increases. The correlation is better for the initially compacted specimens (with $R^2 = 0.85$) than for the ultimately compacted samples (with $R^2 = 0.42$).

Other mixture properties were plotted against the corresponding binder stiffness in an attempt to find possible relationships. Figures 7.15 through 7.18 show plots of mixture instantaneous resilient modulus, tensile strength, failure strain, and fracture energy versus binder stiffness at -10°C for both STOA- and LTOA-aged samples. The correlations between these mix properties and the binder stiffness appear to be fairly poor.

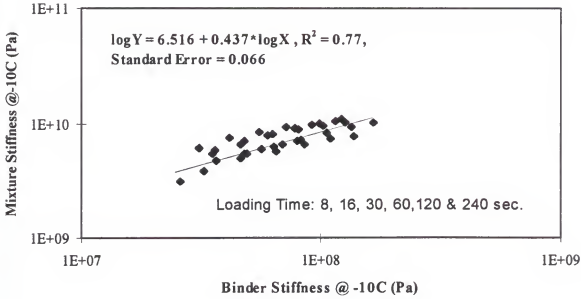

Figure 7.9 Relationship Between Mixture and Binder Stiffness at -10°C for samples at Initial Compaction

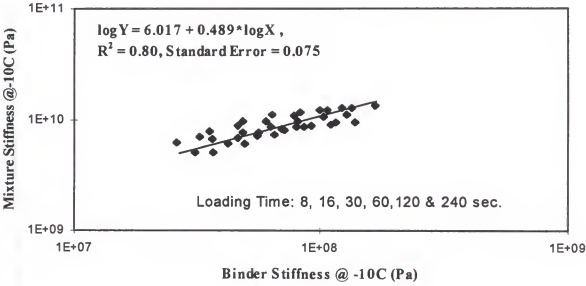

Figure 7.10 Relationship Between Mixture and Binder Stiffness at -10°C for samples at Ultimate Compaction

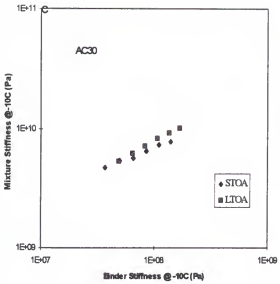

(a) AC-30

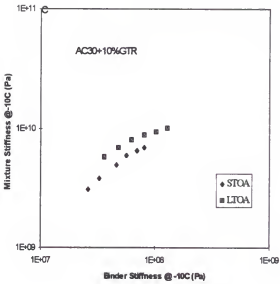

(b) AC-30+10%GTR

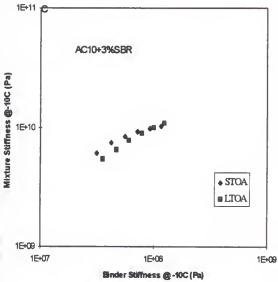

(c) AC-10+3%SBR

Figure 7.11 Relationships Between Mixture and Binder Stiffness for Initially Compacted Samples Aged by the STOA and LTOA Processes

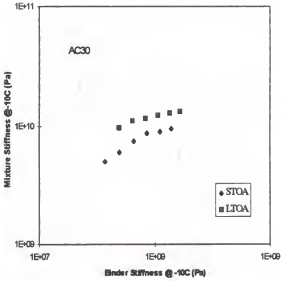

(a) AC-30

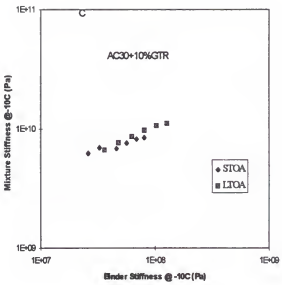

(b) AC-30+10%GTR

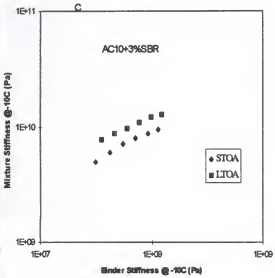

(c) AC-10+3%SBR

Figure 7.12 Relationships Between Mixture and Binder Stiffness for Ultimately Compacted Samples Aged by the STOA and LTOA Processes

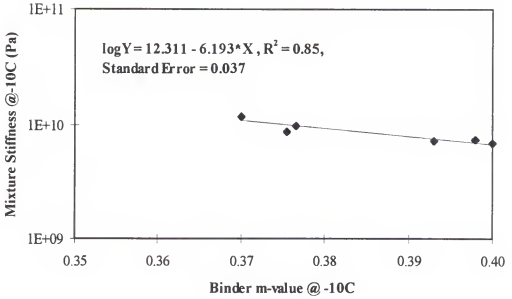

Figure 7.13 Relationships Between Mixture and Binder m-value at 60 Seconds Loading Time for Initially Compacted Samples

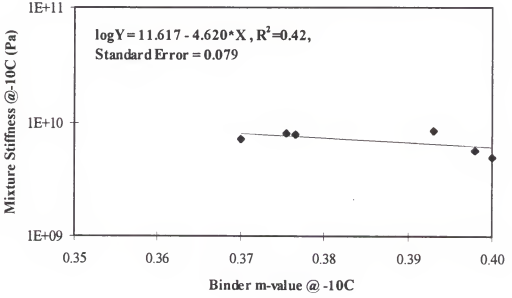

Figure 7.14 Relationships Between Mixture and Binder m-value at 60 Seconds Loading Time for Ultimately Compacted Samples

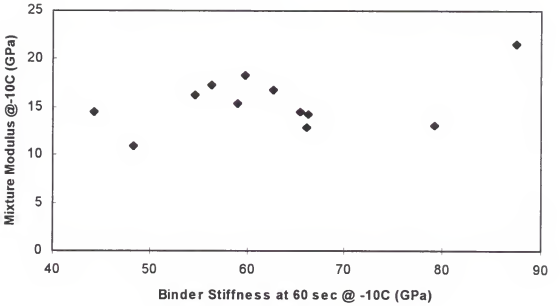

Figure 7.15 Plot of Mixture Resilient Modulus versus Binder Stiffness at -10°C

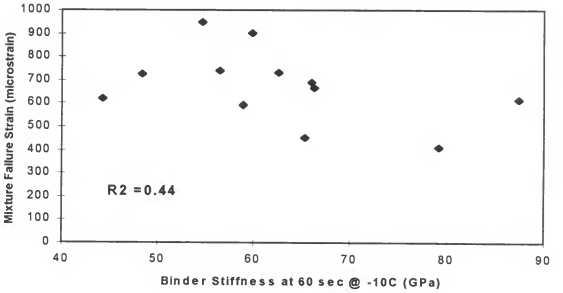

Figure 7.16 Plot of Mixture Failure Strain versus Binder Stiffness at -10°C

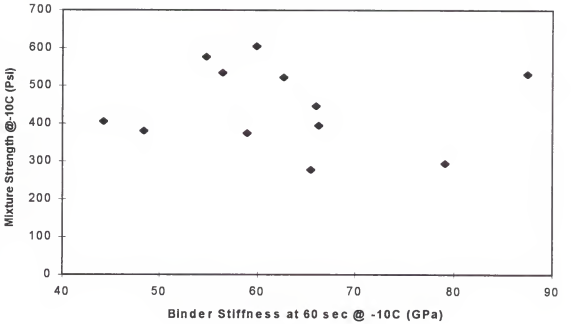

Figure 7.17 Plot of Mixture Tensile Strength versus Binder Stiffness at -10°C

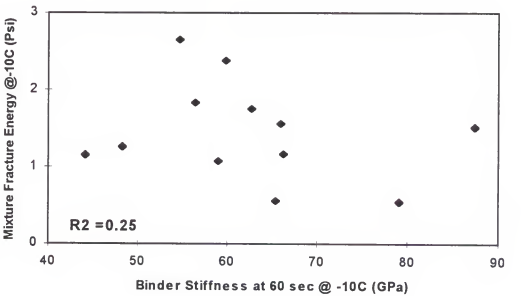

Figure 7.18 Plot of Mixture Fracture Energy versus Binder Stiffness at -10°C

Figure 7.19 shows plots of mixture instantaneous resilient modulus versus mixture stiffness at 1 second as determined by the indirect tensile creep test for all mixture samples. It can be seen that the resilient modulus is very close to the stiffness of the mixture. The correlation is quite good (R^2=0.80).

7.3 Summary of Findings

The main findings from this part of the study are summarized as follows:

(1) There exists a good relationship between the Brookfield viscosity at 60°C and the G*/sinδ at 64°C for all nine asphalt binders before and after the RTFOT process. G*/sinδ increases as the viscosity increases.

(2) The penetration and constant power viscosity show a good correlation with the G*sinδ (loss modulus) at 25°C for all nine asphalt binders before and after the RTFOT and PAV processes.

(3) The Fraass temperature shows a fair correlation with the creep stiffness at -12, -18 and -24°C and with the constant power viscosity at 5°C for all nine asphalt residues after the PAV process. Hence, Fraass temperature could be used as an indicator of low temperature cracking resistance as the creep stiffness.

(4) A good relationship was found between the SHRP creep stiffness and the failure strain at -12, -18 and -24°C for all nine asphalt residues after the PAV process. Creep stiffness decreases as failure strain increases.

(5) The cracking temperature as predicted by the Fraass breaking point temperature is higher than the SHRP limiting stiffness temperature and limiting strain temperature.

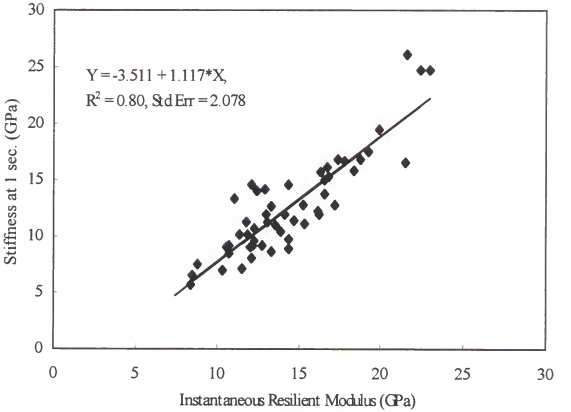

Figure 7.19 Plot of Mixture instantaneous resilient modulus versus Mixture Stiffness at 1 second as determined by the indirect tensile creep test

(6) A good relationship was found between the SHRP binder creep stiffness and the mixture stiffness at -10°C. Binder stiffness increases as mixture stiffness increases. With the same binder stiffness, the more densified mixtures show higher mixture stiffness.

(7) The LTOA aged mixtures have higher mixture resilient modulus, binder stiffness and lower binder m-value as compared with the STOA aged ones.

(8) The relationship between binder creep stiffness and mixture creep stiffness is good. However, there are poor correlations between the binder stiffness and the mixture's resilient modulus, tensile strength, failure strain, and fracture energy.

CHAPTER 8
CONCLUSIONS AND RECOMMENDATIONS

8.1 Conclusions

A laboratory study was conducted to evaluate the relationships between the results of the SHRP binder tests and the cracking resistance of the asphalt mixtures under Florida conditions. The scope of the study covers six different base asphalts from five different refinery sources and three types of modifiers, namely a ground tire rubber (GTR), styrene-butadiene rubber (SBR) and styrene block copolymer. The main findings from this study are summarized in following sections.

8.1.1 Relationship Between SHRP Binder and Conventional Binder Test Results

The SHRP dynamic shear rheometer (DSR) test measures the viscoelastic properties of a binder at intermediate and high pavement service temperatures. Results of the DSR tests compare well to results of conventional tests on the same binders at similar temperatures. The $G^*\sin\delta$ and G^* values were found to be inversely proportional to the penetration at 25 °C, with R^2 values of 0.89 and 0.91, respectively. The $G^*\sin\delta$ value is linearly proportional to the constant power viscosity at 25 °C ($R^2 = 0.87$). The dynamic viscosity (η^*) measured at 1 Hz is linearly proportional to the constant power viscosity at 25 °C ($R^2 = 0.88$). The $G^*/\sin\delta$ value at 64 °C is found to be linearly proportional to the viscosity at 60 °C ($R^2 = 0.90$). While the data for viscosity at 64 °C were not available

for comparison purpose, it is expected that the $G^*/\sin\delta$ value at 64 °C should correlate well to the viscosity at 64 °C.

The SHRP bending beam rheometer (BBR) test measures the stiffness of a binder at low service temperatures. The creep stiffness as measured by the BBR at low temperatures correlates well with the Fraass breaking point temperature, with R^2 values ranging from 0.78 to 0.81. The creep stiffness at -12, -18 and -24 °C increases as the Fraass breaking point temperature decreases. However, the cracking temperature as predicted by the Fraass breaking point temperature is slightly higher than that predicted by the SHRP limiting stiffness as measured by the BBR.

The SHRP direct tension test (DTT) measures the failure strain of a binder at low service temperature. The failure strain as measured by the DTT at low temperatures correlates poorly to the Fraass breaking point temperature (with R^2 values ranging from 0.42 to 0.65). The cracking temperature as predicted by the SHRP limiting strain as measured by the DTT is slightly lower than that predicted by the Fraass temperature, but slightly higher than that predicted by the SHRP limiting stiffness as determined by the BBR.

The conventional Bitumen Test Data Chart (BTDC) could be used to display the temperature susceptibility of an asphalt binder. The range of service temperature of a SHRP PG grade asphalt can be clearly shown on a BTDC. The changes of the characteristics of a binder as it ages could also be clearly shown on a BTDC.

8.1.2 Relationship Between Binder and Mixture Properties

The SHRP indirect tensile creep test measures the creep compliance of an asphalt

mixture at low temperatures. The slope and intercept from the Burgers model were used to analyze the creep compliance versus time data. The creep compliance as a function of time (t) can be expressed as: $1/E_0 + 1/E_1 \times (1 - e^{-tE1/\eta 1}) + t/\eta_0$. At a large t, the slope of the creep compliance plot approaches $1/\eta_0$ or 1/(viscosity of the mix). The interception of the creep compliance plot with the vertical axis is equal to $(1/E_0 + 1/E_1)$, which can be considered to be equal to 1/(total elastic stiffness of the mixture). It was found that, for most of the mixtures tested, the change in creep compliance reached a steady state at a time of 500 seconds, and it was possible to predict the creep compliance at 1000 seconds or beyond by running the creep test only up to 500 seconds.

The mixture stiffness at 8, 16, 30, 60, 120 and 240 seconds as determined by the indirect tensile creep test at -10°C was found to be linearly related to the binder creep stiffness at the same loading time (with R^2 values ranging from 0.77 to 0.86).

The tensile strength, failure strain and fracture energy of the mixtures at -10°C as measured by the indirect tensile strength tests were found to be not related to the binder creep stiffness at the same temperature.

Diametral resilient modulus tests were run using the test set-up for the SHRP indirect tensile test. The resilient modulus was found to be close and related to the stiffness of the mixture at 1 second as determined by the indirect tensile creep test. Thus, it is possible to estimate the resilient modulus from the mixture stiffness at 1 second as determined by the indirect tensile creep test.

8.1.3 Comparison Between SHRP Aging Processes for Asphalt Binders and Mixtures

In the SHRP Superpave specification, the Rolling Thin Film Oven Test (RTFOT)

is intended to simulate the effects of the hot-mix process on a binder, and the Short-Term Oven Aging (STOA) process is to simulate the aging effects of hot mixing and construction process on asphalt mixtures. Based on the penetration, viscosity and creep stiffness of the aged binders, the STOA was seen to be a more severe aging process as compared with the RTFOT.

The SHRP Pressure Aging Vessel (PAV) is intended to simulate additional aging of the binder in service, and the Long-Term Oven Aging (LTOA) process is to simulate the effects of additional aging of asphalt mixtures in service for 5 to 10 years. Based on the penetration, viscosity and creep stiffness of the aged binders, the PAV was seen to be a more severe aging process as compared with the LTOA.

Based on creep stiffness values of the aged binders at -10°C, the order of aging severity from highest to lowest, is PAV, LTOA, STOA and RTFOT. It also can be observed that different loading times give the same aging order trend.

The results from the DSR test indicate that the STOA residues have a higher modulus and lower phase angle than the RTFOT residues at temperatures ranging from 52 to 70°C and the LTOA residues have a higher modulus and phase angle than the PAV residues at temperatures ranging from 13 to 31°C.

8.1.4 Effects of GTR and SBR Additives on Asphalt Binders

As compared with the base asphalts, the SBR- and GTR-modified asphalts were seen to have lower Fraass temperatures, lower stiffness and higher failure strains at low temperatures, higher penetration, higher viscosity and higher $G^*\sin\delta$ at intermediate to high temperatures.

Plots of the SBR- and GTR-modified binders on a BTDC show that they are lower temperature susceptibility as compared with their corresponding unmodified binders at the unaged, RTFOT-aged and PAV-aged conditions.

8.1.5 Effects of GTR and SBR Additives on Asphalt Mixtures

As compared with the unmodified asphalts mixtures, the SBR-modified asphalt mixtures were seen to have higher creep compliance, tensile strength, failure strain and fracture energy at low temperatures, which indicate a greater potential to resist low temperature cracking. The GTR-modified asphalt mixtures showed lower resilient modulus than that of the unmodified mixtures.

It was found that the SBR-modified asphalt mixtures did not exhibit a lower viscosity (low creep compliance slope) than the unmodified mixtures after the LTOA process at 0°C. However, at -10 and -20°C, the SBR-modified mixtures exhibit substantially lower viscosity (higher creep compliance slope) than the unmodified mixtures. The GTR-modified asphalt mixtures have lower elastic stiffness (higher creep compliance intercepts) as compared with the unmodified mixtures before and after the LTOA process. The SBR-modified asphalt mixtures exhibit approximately same elastic stiffness (creep compliance intercepts) and resilient moduli as compared with the unmodified mixtures at -10 and -20°C before and after the LTOA process.

8.2 Recommendations for Further Research

Based on the results of this study, the following recommendations for further research are suggested:

(1) Additional research is needed to evaluate the slope and interception of the creep compliance versus time plots of the asphalt mixtures tested in the indirect tensile creep test. These parameters might be able to be used to estimate the elastic modulus and the viscosity of the asphalt mixture.

(2) Results of other research have suggested that SHRP test parameters such as, $G^*/\sin\delta$ and $G^* \times \sin\delta$ of the binder, might not correlate with the performance of the asphalt mixture in the field. Further evaluation of these parameters are needed, especially on their applicability to local conditions.

(3) Two problems might occur, when the modified asphalt binders are extracted and recovered by means of the reflux, centrifuge and rotavapor methods. First, the extracted asphalt might have a higher viscosity because of solvent aging. Second, the extracted binder might have a lower viscosity caused by incomplete extraction. The modifiers, such as ground tire rubber, might clog the filter of reflux during extraction. Further work addressing these problems is needed.

Table A.1 Penetration of Asphalt at 25°C before and after the RTFOT and PAV processes

ASPHALT TYPE*	Penetration of original binder		Penetration of RTFOT aged residues		Penetration of PAV aged residues	
	replicates	mean	replicates	mean	replicates	mean
CT10	90	92	53	52.5	32	31.85
	94		52		31.7	
C1S2	87.6	86.3	51.7	51.7	29.7	29.3
	85		51.7		29	
C1S7	77.8	78.1	50.7	51.4	26.3	27.1
	78.3		52		28	
PM20	74	74.7	43.3	44.2	28	28
	75.4		45		28	
C3GT	44	44.1	36	36	19.7	19
	44.3		36		18.3	
CT30	61	61.5	36	36	22.5	22.75
	62		36		23	
KH30	62	61.3	38	38.5	24	24.4
	60.6		39		24.8	
MT30	53	54	35	35	22.3	22.05
	55		35		21.8	
MA30	50	50.7	33.3	33.8	21	21.75
	51.5		34.3		22.5	

*Note: The meaning of the codes for the asphalt types can be found in Table 3.1.

Table A.2 Absolute Viscosity of Asphalts at 60°C before and after the RTFOT and PAV processes.

ASPHALT TYPE*	Viscosity of original binder (poise)		Viscosity of RTFOT age residues (poise)		Viscosity of PAV+ RTFOT age residues (poise)	
	replicates	mean	replicates	mean	replicates	mean
CT10	1184	1213	5564	5762	23430	24124
	1242		5961		24817	
C1S2	2676	2705	13380	13798	52873	51810
	2734		14216		50747	
C1S7	3549	3758	18809	20311	63912	64257
	3966		21813		64602	
PM20	8093	8174	21041	20427	57062	56200
	8256		19814		55339	
C3GT	14481	15847	52131	58770	367221	409425
	17213		65409		451629	
CT30	3432	3409	15100	14660	126768	125127
	3386		14221		123486	
KH30	2943	2978	8240	8639	51860	50092
	3013		9039		48324	
MT30	2982	2993	9244	9578	57730	58526
	3004		9913		59321	
MA30	3123	3185	8119	8605	48650	46224
	3247		9091		43797	

*Note: The meaning of the codes for the asphalt types can be found in Table 3.1.

Table A.3 Brookfield Viscosity of Asphalts at 60°C before and after the RTFOT and PAV processes.

ASPHALT TYPE*	Viscosity of original binder (poise)		Viscosity of RTFOT age residues (poise)		Viscosity of PAV+ RTFOT age residues (poise)	
	replicates	mean	replicates	mean	replicates	mean
CT10	1185	1218	6046	6276	25750	26376
	1251		6507		27002	
C1S2	2636	2603	13183	12889	51597	48660
	2570		12596		45723	
C1S7	3861	3617	18923	17222	59271	53040
	3374		15521		46810	
PM20	6988	7134	16074	16774	35460	38946
	7281		17475		42432	
C3GT	10775	11403	40948	43937	327942	310481
	12032		46926		293020	
CT30	3487	3674	10114	10849	88626	80650
	3861		11584		72674	
KH30	3098	3150	8366	8665	42988	45190
	3202		8965		47393	
MT30	3185	3242	8919	9243	52128	52999
	3299		9568		53871	
MA30	3287	3322	8712	8973	49412	45976
	3357		9234		42541	

*Note: The meaning of the codes for the asphalt types can be found in Table 3.1.

Table A.4 Results of Fraass Breaking Point Test

Asphalt Type*	Fraass Breaking Point Temperature in °C		
	Unaged binder	**RTFOT residues**	**PAV residues**
CT10	-12.5	-12	-9.5
	-14	-12	-8.5
C1S2#	-17	-14.5	-12.5
	-16.5	-15	-12.5
C1S7#	-15.5	-14	-13
	-14.5	-13.5	-12
PM20	-14	-12.5	-11
	-13.5	-12.5	-10.5
C3GT#	-12.5	-11.5	-10
	-12.5	-11	-9.5
CT30	-12.5	-11.5	-9
	-12	-11	-8.5
KH30	-13	-12.5	-9.5
	-15	-13.5	-8.5
MT30	-9	-8.5	-4
	-10	-9	-5
MA30	-9.5	-7	-4
	-10	-7.5	-3

Note: # Temperatures at the first occurrence of mircocrack are recorded.
* The meaning of the codes for the asphalt types can be found in Table 3.1.

Table A.5 Results of Schweyer Constant Stress Rheometer Test

Asphalt Type	Constant Power Viscosity in Pa-S		
Unaged	**5°C**	**15°C**	**25°C**
Coastal AC10	5.55e+07	1.95e+06	1.61e+05
	9.00e+07	2.90e+06	2.13e+05
Coastal AC-10	5.27e+07	2.51e+06	2.20e+05
+3%SBR(2879)	4.20e+07	2.10e+06	1.75e+05
Coastal AC-10	5.80e+07	4.27e+06	4.85e+05
+3%SBR(UP70)	4.60e+07	3.57e+06	3.75e+05
Ergon	6.38e+07	4.69e+06	2.76e+05
PMAC-20	5.10e+07	3.93e+06	3.79e+05
Coastal AC-30	2.40e+08	8.10e+06	6.50e+05
+10%GTR	3.50e+08	1.60e+07	7.45e+05
Coastal AC-30	8.71e+07	3.82e+06	5.19e+05
	1.90e+08	7.00e+06	5.36e+05
Koch AC-30	9.85e+07	4.33e+06	5.07e+05
	1.50e+08	4.66e+06	3.37e+05
Marathon	2.70e+08	4.73e+06	7.15e+05
AC-30	4.30e+08	1.40e+07	2.90e+05
Mariani AC-30	2.30e+08	5.53e+06	9.52e+05
	1.80e+08	1.60e+07	5.34e+05

Table A.5 Results of Schweyer Constant Stress Rheometer Test (continued)

Asphalt Type	Constant Power Viscosity in Pa-S		
RTFOT-aged	**5°C**	**15°C**	**25°C**
Coastal AC10	1.75e+08	6.35e+06	7.35e+05
	2.20e+08	9.01e+06	9.68e+05
Coastal AC-10	1.66e+08	6.67e+06	9.07e+05
+3%SBR(2879)	1.30e+08	9.46e+06	6.64e+05
Coastal AC-10	1.83e+08	1.13e+07	1.11e+06
+3%SBR(UP70)	1.50e+08	1.60e+07	9.83e+05
Ergon	2.01e+08	1.25e+07	8.87e+05
PMAC-20	1.60e+08	1.80e+07	1.08e+06
Coastal AC-30	4.54e+08	1.71e+07	2.47e+06
+10%GTR	8.00e+08	3.40e+07	1.76e+06
Coastal AC-30	2.60e+08	1.20e+07	1.66e+06
	5.70e+08	2.20e+07	1.81e+06
Koch AC-30	3.09e+08	1.38e+07	1.59e+06
	4.50e+08	1.50e+07	1.24e+06
Marathon	6.90e+08	1.58e+07	1.99e+06
AC-30	1.00e+09	4.00e+07	1.23e+06
Mariani AC-30	8.54e+08	1.90e+07	3.76e+06
	1.10e+09	5.70e+07	1.95e+06

Table A.5 Results of Schweyer Constant Stress Rheometer Test (continued)

Asphalt Type	Constant Power Viscosity in Pa-S		
PAV-aged	**5°C**	**15°C**	**25°C**
Coastal AC10	7.55e+08	2.05e+07	2.01e+06
	9.70e+08	3.50e+07	3.33e+06
Coastal AC-10	7.17e+08	2.15e+07	2.49e+06
+3%SBR(2879)	5.70e+08	3.70e+07	1.83e+06
Coastal AC-10	7.89e+08	3.66e+07	2.21e+06
+3%SBR(UP70)	6.30e+08	6.20e+07	1.97e+06
Ergon	8.68e+08	4.03e+07	5.69e+06
PMAC-20	6.90e+08	6.90e+07	7.57e+06
Coastal AC-30	1.38e+09	6.38e+07	9.20e+06
+10%GTR	2.00e+09	1.30e+08	1.10e+07
Coastal AC-30	1.64e+09	6.63e+07	9.98e+06
	2.80e+09	1.20e+08	1.20e+07
Koch AC-30	1.54e+09	6.96e+07	7.09e+06
	2.40e+09	6.60e+07	4.73e+06
Marathon	2.98e+09	5.15e+07	9.27e+06
AC-30	4.70e+09	1.70e+08	5.19e+06
Mariani AC-30	4.84e+09	1.16e+08	2.10e+07
	2.80e+09	3.30e+08	1.20e+07

Table A.6 Weight Changes of Asphalts after the RTFOT and PAV processes.

ASPHALT TYPE	Weight Loss in RTFOT (%)		Weight Gain in PAV (%)		Total Weight Change (%)
	replicates	mean	replicates	mean	
COASTAL AC-10	0.83	0.815	0.60	0.58	-0.235
	0.80		0.56		
COASTAL AC-10	0.57	0.57	0.48	0.50	-0.07
+ 3% SBR (UP70)	0.57		0.52		
COASTAL AC-10	0.31	0.405	0.51	0.515	+0.11
+3% SBR(UP2879)	0.50		0.52		
COASTAL AC-30	0.63	0.645	0.54	0.53	-0.115
	0.66		0.52		
COASTAL AC-30	0.37	0.385	0.62	0.625	+0.24
+ 10% GTR	0.40		0.63		
ERGON PMAC-20	0.54	0.525	0.51	0.52	-0.005
	0.51		0.53		
KOCH AC-30	0.37	0.35	0.50	0.52	+0.165
	0.34		0.54		
MARATHON	0.26	0.275	0.52	0.54	+0.265
AC-30	0.29		0.56		
MARIANI	0.26	0.245	0.52	0.52	+0.275
AC-30	0.23		0.52		

Table A.7 Results of Dynamic Shear Rheometer Test

Asphalt Type	Dynamic Viscosity at Frequency = 1.0 Hz (Pa-S)			
Unaged	**25°C**	**52°C**	**58°C**	**60°C**
Coastal AC10	4.39e+04	4.17e+02	1.67e+02	1.29e+02
	4.17e+04	4.58e+02	1.59e+02	1.23e+02
Coastal AC-10 +3%SBR(2879)	4.77e+04	6.42e+02	2.75e+02	2.19e+02
	4.29e+04	7.07e+02	3.03e+02	2.41e+02
Coastal AC-10 +3%SBR(UP70)	6.81e+04	1.09e+03	5.49e+02	4.06e+02
	6.12e+04	1.20e+03	6.03e+02	4.46e+02
Ergon PMAC-20	5.10e+04	1.32e+03	5.95e+02	4.80e+02
	5.61e+04	1.25e+03	5.65e+02	5.28e+02
Coastal AC-30 +10%GTR	1.20e+05	2.81e+03	1.46e+03	1.19e+03
	1.32e+05	3.10e+03	1.60e+03	1.31e+03
Coastal AC-30	8.47e+04	1.08e+03	4.31e+02	3.10e+02
	9.32e+04	1.18e+03	4.74e+02	3.41e+02
Koch AC-30	1.13e+05	9.81e+02	4.23e+02	2.86e+02
	1.24e+05	1.08e+03	4.64e+02	2.58e+02
Marathon AC-30	1.39e+05	9.65e+02	3.93e+02	2.91e+02
	1.53e+05	1.06e+03	4.32e+02	2.62e+02
Mariani AC-30	1.73e+05	1.13e+03	4.50e+02	3.10e+02
	1.91e+05	1.24e+03	4.95e+02	2.79e+02

Table A.7 Results of Dynamic Shear Rheometer Test (continued)

Asphalt Type	Dynamic Viscosity at Frequency = 1.0 Hz (Pa-S)			
RTFOT-aged	**25°C**	**52°C**	**58°C**	**60°C**
Coastal AC10	1.19e+05	1.16e+03	4.82e+02	3.64e+02
	1.13e+05	1.09e+03	4.58e+02	3.46e+02
Coastal AC-10 +3%SBR(2879)	9.84e+04	1.65e+03	7.54e+02	5.99e+02
	8.86e+04	1.49e+03	6.78e+02	5.40e+02
Coastal AC-10 +3%SBR(UP70)	1.43e+05	2.67e+03	1.23e+03	9.38e+02
	1.28e+05	2.94e+03	1.35e+03	1.03e+03
Ergon PMAC-20	1.05e+05	2.10e+03	1.06e+03	7.84e+02
	1.16e+05	1.99e+03	1.01e+03	8.62e+02
Coastal AC-30 +10%GTR	2.04e+05	6.63e+03	3.21e+03	2.77e+03
	2.24e+05	7.29e+03	3.53e+03	3.04e+03
Coastal AC-30	1.44e+05	3.18e+03	1.40e+03	1.05e+03
	1.58e+05	3.50e+03	1.54e+03	1.16e+03
Koch AC-30	2.13e+05	2.50e+03	1.14e+03	5.98e+02
	2.34e+05	2.75e+03	1.26e+03	5.38e+02
Marathon AC-30	2.96e+05	3.71e+03	1.47e+03	8.71e+02
	3.25e+05	4.08e+03	1.62e+03	7.84e+02
Mariani AC-30	2.81e+05	2.81e+03	1.03e+03	7.65e+02
	3.10e+05	3.10e+03	1.14e+03	6.88e+02

Table A.7 Results of Dynamic Shear Rheometer Test (continued)

Asphalt Type	Dynamic Viscosity at Frequency = 1.0 Hz (Pa-S)				
PAV-aged	**25°C**	**28°C**	**31°C**	**34°C**	**60°C**
Coastal AC10	3.63e+05	2.05e+05	1.26e+05	6.81e+04	1.47e+03
	3.44e+05	2.16e+05	1.19e+05	7.17e+04	1.39e+03
Coastal AC-10 +3%SBR(2879)	2.96e+05	1.73e+05	1.04e+05	9.37e+04	2.02e+03
	2.66e+05	1.91e+05	1.15e+05	8.52e+04	1.82e+03
Coastal AC-10 +3%SBR(UP70)	2.26e+05	1.55e+05	8.44e+04	6.31e+04	2.34e+03
	2.03e+05	1.41e+05	9.29e+04	5.74e+04	2.57e+03
Ergon PMAC-20	3.16e+05	1.99e+05	1.26e+05	9.69e+04	2.08e+03
	3.48e+05	2.19e+05	1.38e+05	8.81e+04	2.29e+03
Coastal AC-30 +10%GTR	4.07e+05	2.92e+05	1.78e+05	1.48e+05	6.14e+03
	4.48e+05	2.66e+05	1.96e+05	1.34e+05	6.75e+03
Coastal AC-30	5.44e+05	3.20e+05	2.20e+05	1.16e+05	4.10e+03
	5.98e+05	3.52e+05	2.00e+05	1.28e+05	3.69e+03
Koch AC-30	5.09e+05	3.34e+05	1.96e+05	1.09e+05	2.75e+03
	5.60e+05	3.04e+05	2.15e+05	9.94e+04	2.48e+03
Marathon AC-30	6.96e+05	4.56e+05	2.56e+05	1.70e+05	2.80e+03
	7.66e+05	4.15e+05	2.82e+05	1.54e+05	2.52e+03
Mariani AC-30	7.11e+05	4.91e+05	2.59e+05	1.55e+05	2.83e+03
	7.82e+05	4.47e+05	2.85e+05	1.41e+05	2.55e+03

Table A.8 Results of Classification Testing of Asphalt Binders

Asphalt Binders*	Spec.	CT10	C1S2	C1S7	CT3O	C3GT
Tests on unaged material						
Brookfield,135C Pas	<3	0.2	0.263	0.516	0.566	1.055
Flash point, C	>230	273	278	280	295	310
G*/sin δ@52C,10rad/s, kPa	>1	4.09	6.17	10.41	9.79	27.22
G*/sin δ@58C,10rad/s, kPa	>1	1.61	2.64	5.31	4.05	13.94
G*/sin δ@64C,10rad/s, kPa	>1	0.74	1.27	2.42	2	5.88
G*/sin δ@70C,10rad/s, kPa	>1	0.36	0.67	1.13	0.88	2.99
G*/sin δ@76C,10rad/s, kPa	>1	0.18	0.36	0.61	0.45	1.57
G*/sin δ@82C,10rad/s, kPa	>1					0.89
Tests on RTFO residue						
Mass Loss,%	<1.0	0.82	0.41	0.57	0.64	0.39
G*/sin δ@52C,10rad/s, kPa	>2.2	10.99	15.86	25.81	30.22	64.82
G*/sin δ@58C,10rad/s, kPa	>2.2	4.54	7.23	11.76	13.31	31.47
G*/sin δ@64C,10rad/s, kPa	>2.2	2.04	3.48	5.99	5.63	15
G*/sin δ@70C,10rad/s, kPa	>2.2	0.91	1.89	2.71	2.77	7.74
G*/sin δ@76C,10rad/s, kPa	>2.2	0.45	0.93	1.37	1.3	4.05
Tests on PAV (&RTFO) residue						
G*sin δ@13C,10rad/s, kPa	<5000	7975.9	4931	5964	9128.5	6423
G*sin δ@16C,10rad/s, kPa	<5000	5963.6	3639	4603.4	7276.5	4863.6
G*sin δ@19C,10rad/s, kPa	<5000	4307	2600.9	3339.6	5470	3676.7
G*sin δ@22C,10rad/s, kPa	<5000	3189.9	1846.5	2450.1	4270	2791.8
G*sin δ@25C,10rad/s, kPa	<5000	2205	1306.2	1767.4	3083.5	2105.4
G*sin δ@28C,10rad/s, kPa	<5000	1412	865.4	1113.2	1900.9	1443.7
G*sin δ@31C,10rad/s, kPa	<5000	877	550.4	703.7	1258.5	1008
G*sin δ@34C,10rad/s, kPa	<5000	529.6	290	459.9	771.8	713.6
Bending Beam						
Creep Stiffness,S, 60s.-12C,MPa	<300	101.2	75.9	96.1	115.9	79.4
Creep Stiffness,S, 60s.-18C,MPa	<300	209.8	173.3	186.9	239.2	177.4
Creep Stiffness,S, 60s.-24C,MPa	<300	349.9	281.5	298.9	476.8	313.8
Creep Stiffness,S, 60s.-30C,MPa	<300	-	647.5	703.7	774.9	501.4
Slope,m,60s,-12C	>0.30	0.356	0.358	0.322	0.341	0.342
Slope,m,60s,-18C	>0.30	0.308	0.339	0.335	0.302	0.301
Slope,m,60s,-24C	>0.30	0.281	0.303	0.302	0.248	0.25
Slope,m,60s,-30C	>0.30	-	0.216	0.181	0.206	0.215
Direct Tension						
Failure Strain,-12C,MPa	>1%	1.378	3.848	1.683	0.834	1.514
Failure Strain,-18C,MPa	>1%	0.402	1.102	0.608	0.327	0.465
Failure Strain,-24C,MPa	>1%	0.36	0.581	0.365	0.286	0.294
Most extreme PG grade passed		PG58-28	PG64-34	PG70-34	PG64-28	PG76-28

*Note: The meaning of the codes for the asphalt types can be found in Table 3.1.

Table A.8 Results of Classification Testing of Asphalt Binders (Continued)

Asphalt Binders*	Spec.	PM20	KH30	MT30	MA3O
Tests on unaged material					
Brookfield,135C Pas	<3	0.598	0.475	0.492	0.542
Flash point, C	>230	272	303	313	308
G*/sin δ@52C,10rad/s, kPa	>1	12.76	9.43	9.3	11.5
G*/sin δ@58C,10rad/s, kPa	>1	5.67	4.11	3.73	4.37
G*/sin δ@64C,10rad/s, kPa	>1	2.81	1.96	1.59	1.91
G*/sin δ@70C,10rad/s, kPa	>1	1.5	0.74	0.75	0.89
G*/sin δ@76C,10rad/s, kPa	>1	0.84	0.37	0.38	0.45
G*/sin δ@82C,10rad/s, kPa	>1				
Tests on RTFO residue					
Mass Loss,%	<1.0	0.53	0.35	0.27	0.24
G*/sin δ@52C,10rad/s, kPa	>2.2	20	23.47	35.22	28.12
G*/sin δ@58C,10rad/s, kPa	>2.2	10.65	10.73	13.56	10.75
G*/sin δ@64C,10rad/s, kPa	>2.2	4.64	4.82	6.25	4.58
G*/sin δ@70C,10rad/s, kPa	>2.2	2.43	2.77	2.8	2.1
G*/sin δ@76C,10rad/s, kPa	>2.2	1.34	1.41	1.55	0.99
Tests on PAV (&RTFO) residue					
G*sin δ@13C,10rad/s, kPa	<5000	10187.7	10025.6	13947.3	14570.3
G*sin δ@16C,10rad/s, kPa	<5000	6860.6	7691.6	10435.9	11319.9
G*sin δ@19C,10rad/s, kPa	<5000	4516.3	5527.3	7786.5	8399
G*sin δ@22C,10rad/s, kPa	<5000	3174.8	3958.2	5753.8	6015.7
G*sin δ@25C,10rad/s, kPa	<5000	2237.7	3045.8	4108.6	4218
G*sin δ@28C,10rad/s, kPa	<5000	1433.3	1923.1	2626.5	2733.3
G*sin δ@31C,10rad/s, kPa	<5000	912.6	1208.5	1706.9	1726.2
G*sin δ@34C,10rad/s, kPa	<5000	589	706.1	1093.2	1078.9
Bending Beam					
Creep Stiffness,S, 60s.-12C,MPa	<300	119.1	106.8	157	161.6
Creep Stiffness,S, 60s.-18C,MPa	<300	268.8	251.2	361.2	385.3
Creep Stiffness,S, 60s.-24C,MPa	<300	444.4	478.1	596.3	638.1
Creep Stiffness,S, 60s.-30C,MPa	<300	-	-	-	-
Slope,m,60s,-12C	>0.30	0.388	0.359	0.355	0.338
Slope,m,60s,-18C	>0.30	0.319	0.305	0.297	0.285
Slope,m,60s,-24C	>0.30	0.263	0.247	0.222	0.221
Slope,m,60s,-30C	>0.30	-	-	-	-
Direct Tension					
Failure Strain,-12C,MPa	>1%	0.965	1.257	0.700	0.740
Failure Strain,-18C,MPa	>1%	0.368	0.457	0.280	0.289
Failure Strain,-24C,MPa	>1%	0.307	0.367	0.162	0.189
Most extreme PG grade passed		PG70-28	PG64-28	PG64-22	PG64-22

*Note: The meaning of the codes for the asphalt types can be found in Table 3.1.

Table A.9 Height, %Air Voids, Gyratory Shear, %VMA, and Bulk Density of the GTM Specimens

Mixture	ID #	Height (in.)	Air Void (%)	Gyratory Shear (psi)	%VMA	Bulk Density (psi)
AC30 Initial Compaction Unaged	1	1.91	8.3	51.5	18.3	130.5
	2	1.94	9.9	50.8	18.9	129.7
	3	1.94	9.1	51.2	18.6	130.1
	4	2.03	7.0	52.0	18.0	130.9
	5	2.00	8.1	51.6	18.3	130.5
	6	2.00	7.5	51.8	18.2	130.7
	7	1.91	7.8	51.7	18.2	130.6
	8	1.97	8.6	51.0	18.8	130.7
	9	2.00	8.3	51.3	18.8	130.6
AC30 Initial Compaction STOA	1	2.00	11.2	47.9	20.9	127.2
	2	2.00	11.8	47.4	21.5	126.2
	3	1.94	11.5	47.6	21.2	126.7
	4	2.00	10.9	47.5	21.4	126.5
	5	2.06	11.2	47.6	21.3	126.6
	6	2.00	11.1	47.5	21.3	126.5
	7	2.00	10.7	48.9	20.1	128.4
	8	1.88	11.3	48.2	20.7	127.7
	9	2.24	11.8	47.5	21.2	127.0
AC30 Initial Compaction LTOA	1	2.03	11.5	47.9	20.9	127.4
	2	1.94	10.5	47.7	21.1	127.2
	3	1.88	11.0	47.8	21.0	127.3
	4	1.94	10.8	47.7	21.0	127.2
	5	1.88	11.6	48.5	20.1	126.8
	6	1.91	11.2	48.1	20.6	127.0
	7	1.88	11.4	48.3	20.3	126.9
	8	1.91	10.6	48.9	20.4	128.2
	9	1.91	11.7	47.5	21.3	126.0
AC30 Ultimate Compaction Unaged	1	2.00	5.5	52.7	14.7	138.1
	2	1.94	4.6	53.2	13.9	138.7
	3	1.94	4.0	53.7	13.9	138.9
	4	1.97	4.4	53.4	13.7	138.5
	5	1.94	4.7	53.4	13.9	139.0
	6	1.94	4.3	53.4	13.9	139.0
	7	1.97	5.4	52.7	14.7	138.1
	8	1.94	4.0	54.0	14.3	138.9
	9	2.00	4.0	54.5	13.8	139.1
AC30 Ultimate Compaction STOA	1	1.94	5.4	52.3	14.5	139.2
	2	1.94	4.4	53.5	13.8	139.8
	3	1.94	4.8	52.8	14.1	139.6
	4	2.00	4.6	53.2	14.0	139.7
	5	1.94	4.0	53.2	13.8	139.9
	6	1.94	4.3	53.2	13.9	139.8
	7	1.94	5.3	52.3	14.5	139.2
	8	1.94	4.8	52.7	14.2	139.5
	9	1.94	5.1	52.5	14.3	139.4
AC30 Ultimate Compaction LTOA	1	1.94	4.8	52.7	14.3	139.5
	2	1.94	5.1	51.7	14.9	139.4
	3	1.94	4.8	52.8	14.1	139.6
	4	1.94	4.8	52.6	14.5	139.7
	5	1.94	4.5	53.2	14.0	139.9
	6	1.94	4.3	53.8	13.8	139.8
	7	1.94	5.2	51.8	15.2	139.4
	8	1.97	4.8	52.8	14.5	139.6
	9	1.94	4.9	52.3	14.9	139.5

Table A.9 Height, %Air Voids, Gyratory Shear, %VMA, and Bulk Density of the GTM Specimens (Continued)

Mixture	ID #	Height (in.)	Air Void (%)	Gyratory Shear (psi)	%VMA	Bulk Density (psi)
AC30+GTR Initial Compaction Unaged	1	1.94	6.9	52.3	16.1	133.9
	2	2.03	6.6	51.9	15.8	134.7
	3	1.94	6.9	52.1	16.0	134.3
	4	1.94	7.0	52.0	16.2	132.9
	5	1.94	7.0	52.1	16.1	133.6
	6	1.94	6.6	52.0	16.1	133.3
	7	1.94	6.8	51.8	15.5	133.4
	8	1.94	6.7	51.9	15.8	133.3
	9	1.94	6.7	51.9	15.7	133.4
AC30+GTR Initial Compaction STOA	1	1.94	8.0	49.5	16.0	133.6
	2	2.00	8.8	48.8	17.1	133.0
	3	2.00	8.4	49.2	16.6	133.3
	4	1.94	7.8	49.8	16.8	133.2
	5	1.97	8.1	49.5	16.7	133.2
	6	1.94	8.0	49.6	16.8	133.2
	7	2.00	7.5	48.9	20.1	128.4
	8	1.94	7.0	49.8	16.1	133.8
	9	1.97	7.6	49.3	16.7	133.2
AC30+GTR Initial Compaction LTOA	1	1.98	7.3	49.6	16.4	133.5
	2	1.97	7.0	49.6	16.2	133.6
	3	1.97	8.2	49.1	16.9	133.0
	4	1.97	7.6	49.4	16.6	133.3
	5	1.97	7.9	49.2	16.7	133.2
	6	1.98	8.2	49.0	17.0	133.0
	7	1.97	8.1	49.1	16.9	133.1
	8	1.98	8.2	48.9	16.9	132.8
	9	1.97	7.6	50.8	16.0	133.9
AC30+GTR Ultimate Compaction Unaged	1	1.91	5.5	52.7	14.7	138.1
	2	1.91	4.5	52.9	14.1	138.9
	3	2.00	4.5	52.8	14.2	138.6
	4	1.88	4.0	54.1	13.7	139.0
	5	1.94	4.7	53.3	14.2	138.6
	6	2.00	4.8	52.4	14.6	138.2
	7	1.94	5.4	52.7	14.7	138.1
	8	1.94	4.2	53.9	14.1	138.8
	9	1.94	4.5	53.3	14.2	138.7
AC30+GTR Ultimate Compaction STOA	1	2.00	5.2	52.3	14.5	139.2
	2	1.94	5.0	52.7	14.2	139.2
	3	1.94	4.7	53.0	13.8	139.2
	4	2.00	4.8	52.8	14.0	139.2
	5	1.94	5.0	52.8	14.1	138.8
	6	1.94	4.9	52.8	14.0	139.0
	7	1.94	5.0	52.3	14.2	138.7
	8	1.94	4.7	53.0	14.1	138.9
	9	1.94	4.9	52.7	14.2	138.8
AC30+GTR Ultimate Compaction LTOA	1	1.91	4.8	52.7	14.3	139.5
	2	1.88	4.7	53.6	13.7	139.6
	3	1.91	4.9	52.7	14.0	139.0
	4	1.88	4.8	52.6	14.5	139.7
	5	1.94	4.8	52.9	13.8	139.2
	6	1.94	4.8	52.8	13.7	139.3
	7	1.94	5.2	52.6	14.3	139.4
	8	1.94	5.0	52.7	14.0	139.4
	9	1.94	5.0	52.4	41.3	138.7

Table A.9 Height, %Air Voids, Gyratory Shear, %VMA, and Bulk Density of the GTM Specimens (Continued)

Mixture	ID #	Height (in.)	Air Void (%)	Gyratory Shear (psi)	%VMA	Bulk Density (psi)
AC10+SBR Initial Compaction Unaged	1	1.94	7.2	52.0	16.9	133.3
	2	1.94	7.0	52.3	16.2	133.6
	3	1.94	7.1	52.2	16.6	133.5
	4	1.91	6.7	52.5	16.5	133.8
	5	1.94	6.5	52.3	16.5	133.6
	6	1.94	6.3	53.0	16.0	134.1
	7	1.94	7.2	52.1	16.8	133.2
	8	1.94	6.5	52.7	16.0	134.1
	9	1.94	6.9	52.4	16.4	133.7
AC10+SBR Initial Compaction STOA	1	1.88	7.0	52.4	15.0	136.3
	2	1.91	6.9	52.7	14.8	136.6
	3	1.94	7.0	52.6	14.9	136.5
	4	1.91	7.1	52.2	15.3	136.0
	5	2.00	7.0	52.4	15.1	136.2
	6	1.94	7.3	52.0	15.2	136.1
	7	1.94	7.2	52.2	15.2	136.2
	8	1.94	6.8	52.5	14.6	136.8
	9	2.00	7.0	52.3	14.9	136.5
AC10+SBR Initial Compaction LTOA	1	2.00	6.6	53.0	14.2	136.8
	2	1.97	6.8	52.7	14.5	136.6
	3	1.94	6.7	52.8	14.4	136.7
	4	1.94	6.7	52.8	14.5	136.7
	5	2.00	7.2	52.0	14.9	136.2
	6	2.00	6.6	52.8	14.4	136.7
	7	1.94	6.9	52.4	14.7	136.5
	8	1.94	6.8	52.6	14.5	136.6
	9	1.94	7.2	52.2	15.0	135.8
AC10+SBR Ultimate Compaction Unaged	1	1.94	3.5	54.0	13.5	138.5
	2	1.94	3.8	53.8	13.9	138.0
	3	1.94	3.7	53.9	13.9	138.3
	4	1.94	3.5	54.2	13.3	138.6
	5	2.00	3.6	53.8	13.7	138.4
	6	2.03	3.8	53.3	14.2	138.3
	7	2.00	3.9	52.7	14.7	138.1
	8	2.00	3.4	54.6	13.0	138.5
	9	1.94	3.6	53.4	13.8	138.3
AC10+SBR Ultimate Compaction STOA	1	1.94	3.6	53.8	13.7	138.4
	2	1.94	3.8	53.7	13.2	139.2
	3	1.84	3.7	53.8	13.5	138.8
	4	1.94	3.6	54.3	12.8	139.5
	5	1.94	3.7	53.2	13.8	139.9
	6	1.91	3.7	53.8	13.3	139.7
	7	1.88	3.9	53.5	13.6	139.8
	8	1.88	3.8	53.6	13.4	139.8
	9	1.88	3.7	54.0	13.0	139.4
AC10+SBR Ultimate Compaction LTOA	1	1.97	3.7	53.8	13.1	139.1
	2	1.98	3.7	53.9	13.1	139.3
	3	1.97	3.5	54.9	12.8	139.8
	4	1.97	3.6	54.4	12.9	139.5
	5	1.94	3.6	54.7	12.9	139.7
	6	1.95	3.8	53.7	13.0	139.2
	7	1.97	3.7	54.2	12.9	139.4
	8	1.95	3.6	54.5	12.9	139.8
	9	1.97	4.2	53.5	13.3	139.0

Table B.1 Results of Instantaneous and Total Resilient Modulus

Mixture ID	AGING	AIR VOIDS %		Temp.	Instantaneous Resilient Modulus (x GPa)			Instantaneous Poisson's Ratio		
		Actual	Average	(°C)	Cycle 1	Cycle 2	Cycle 3	Cycle 1	Cycle 2	Cycle 3
AC30 Initial Compaction	Unaged (A)	8.5	8.4	0	11.82	11.45	11.30	0.19	0.19	0.22
		8.4		-10	12.08	12.21	12.02	0.22	0.21	0.22
		8.3		-20	16.77	17.43	16.97	0.20	0.20	0.19
	STOA (B)	11	11.3	0	8.52	8.42	8.69	0.19	0.20	0.18
		11.3		-10	14.41	14.76	14.31	0.28	0.27	0.29
		11.6		-20	13.10	12.93	13.41	0.23	0.24	0.22
	LTOA (C)	11.4	11.3	0	11.11	10.14	11.26	0.17	0.23	0.16
		11.3		-10	13.02	13.13	12.94	0.25	0.23	0.24
		11.2		-20	12.48	13.41	13.66	0.25	0.19	0.20
AC30 Ultimate Compaction	Unaged (A)	4.5	4.53	0	10.72	10.71	10.75	0.17	0.16	0.16
		4.5		-10	8.84	8.86	8.93	0.14	0.15	0.14
		4.6		-20	11.42	11.58	11.04	0.23	0.22	0.25
	STOA (B)	5.1	4.77	0	15.37	15.41	14.77	0.26	0.29	0.31
		4.8		-10	12.95	12.77	12.82	0.18	0.19	0.19
		4.5		-20	23.00	22.06	21.41	0.29	0.32	0.35
	LTOA (C)	4.5	4.7	0	13.33	13.41	13.40	0.21	0.21	0.19
		4.7		-10	21.51	22.07	21.09	0.35	0.35	0.37
		4.9		-20	17.42	17.62	18.00	0.24	0.23	0.22
AC30+GTR Initial Compaction	Unaged (A)	7	6.8	0	7.41	7.28	7.33	0.22	0.22	0.22
		6.8		-10	9.18	9.07	9.03	0.27	0.27	0.27
		6.6		-20	13.38	13.75	13.59	0.19	0.18	0.18
	STOA (B)	7.4	7.6	0	8.41	8.32	8.80	0.16	0.17	0.13
		7.6		-10	10.74	10.73	11.11	0.16	0.17	0.14
		7.8		-20	10.59	11.13	10.99	0.26	0.22	0.23
	LTOA (C)	7.7	7.8	0	12.14	12.08	11.98	0.21	0.22	0.22
		7.8		-10	14.15	14.21	14.26	0.28	0.28	0.28
		7.9		-20	16.84	17.00	16.70	0.26	0.24	0.25
AC30+GTR Ultimate Compaction	Unaged (A)	4.7	4.6	0	11.53	11.41	11.30	0.26	0.27	0.26
		4.6		-10	13.87	13.60	14.00	0.23	0.23	0.21
		4.5		-20	21.62	22.55	22.14	0.47	0.41	0.42
	STOA (B)	4.8	4.9	0	12.33	12.45	12.40	0.24	0.23	0.22
		4.9		-10	14.41	14.76	14.31	0.28	0.27	0.29
		5		-20	16.55	16.23	16.35	0.24	0.26	0.26
	LTOA (C)	4.7	4.9	0	12.20	12.11	12.03	0.28	0.28	0.28
		4.9		-10	15.27	15.40	15.55	0.26	0.27	0.26
		5.1		-20	14.40	14.77	14.28	0.17	0.15	0.17
AC10+SBR Initial Compaction	Unaged (A)	6.7	6.8	0	10.34	10.35	10.17	0.22	0.22	0.23
		6.8		-10	13.59	13.86	13.56	0.23	0.21	0.23
		6.9		-20	16.33	15.95	16.03	0.25	0.26	0.26
	STOA (B)	7.2	7	0	12.32	12.39	12.43	0.32	0.34	0.32
		7		-10	17.22	17.49	17.23	0.30	0.29	0.32
		6.8		-20	19.93	20.22	20.06	0.27	0.26	0.25
	LTOA (C)	6.8	7	0	11.87	11.76	11.85	0.26	0.26	0.26
		7		-10	16.54	17.04	16.54	0.26	0.24	0.26
		7.2		-20	17.79	17.86	17.67	0.24	0.24	0.26
AC10+SBR Ultimate Compaction	Unaged (A)	3.5	3.6	0	12.78	12.89	12.41	0.23	0.23	0.25
		3.6		-10	16.17	15.85	15.94	0.27	0.28	0.28
		3.7		-20	18.74	18.98	18.83	0.28	0.27	0.28
	STOA (B)	3.8	3.7	0	12.09	11.94	11.66	0.21	0.21	0.23
		3.7		-10	16.29	16.26	16.17	0.26	0.25	0.26
		3.6		-20	22.38	22.56	22.10	0.33	0.31	0.33
	LTOA (C)	3.6	3.73	0	14.71	14.20	14.86	0.27	0.32	0.27
		3.7		-10	18.32	18.38	18.01	0.25	0.26	0.27
		3.9		-20	19.25	18.99	19.33	0.21	0.22	0.21

Table B.1 Results of Instantaneous and Total Resilient Modulus (Continued)

Mixture ID	AGING	AIR VOIDS %		Temp.	Total Resilient Modulus (x GPa)			Total Poisson's Ratio		
		Actual	Average	(°C)	Cycle 1	Cycle 2	Cycle 3	Cycle 1	Cycle 2	Cycle 3
AC30 Initial Compaction	Unaged (A)	8.5	8.4	0	11.57	11.25	11.33	0.20	0.22	0.22
		8.4		-10	11.95	11.91	11.72	0.21	0.21	0.22
		8.3		-20	16.51	17.54	16.27	0.20	0.17	0.21
	STOA (B)	11	11.3	0	8.44	8.40	8.35	0.20	0.20	0.20
		11.3		-10	14.39	14.28	13.79	0.24	0.27	0.31
		11.6		-20	12.93	12.91	13.39	0.24	0.24	0.22
	LTOA (C)	11.4	11.3	0	9.76	11.17	10.35	0.19	0.13	0.16
		11.3		-10	12.73	13.36	12.10	0.24	0.17	0.28
		11.2		-20	13.33	12.49	12.60	0.15	0.19	0.20
AC30 Ultimate Compaction	Unaged (A)	4.5	4.53	0	10.54	10.18	10.66	0.17	0.20	0.15
		4.5		-10	8.64	8.61	8.74	0.14	0.15	0.14
		4.6		-20	11.36	11.43	11.00	0.24	0.23	0.25
	STOA (B)	5.1	4.77	0	14.95	14.90	14.30	0.26	0.27	0.30
		4.8		-10	12.84	12.58	12.80	0.19	0.21	0.20
		4.5		-20	22.11	22.19	21.93	0.34	0.33	0.34
	LTOA (C)	4.5	4.7	0	13.12	13.20	13.21	0.23	0.22	0.20
		4.7		-10	21.13	21.62	20.51	0.35	0.34	0.37
		4.9		-20	17.76	17.58	17.61	0.22	0.24	0.24
AC30+GTR Initial Compaction	Unaged (A)	7	6.8	0	7.02	6.91	6.98	0.21	0.22	0.21
		6.8		-10	8.83	8.82	8.74	0.27	0.27	0.27
		6.6		-20	13.64	13.14	12.79	0.14	0.18	0.18
	STOA (B)	7.4	7.6	0	8.35	8.22	8.09	0.15	0.17	0.17
		7.6		-10	10.89	11.18	11.61	0.23	0.21	0.17
		7.8		-20	11.03	10.45	10.19	0.18	0.22	0.24
	LTOA (C)	7.7	7.8	0	11.78	11.71	11.69	0.21	0.22	0.22
		7.8		-10	14.07	14.02	14.14	0.28	0.29	0.28
		7.9		-20	16.66	16.96	16.56	0.26	0.24	0.26
AC30+GTR Ultimate Compaction	Unaged (A)	4.7	4.6	0	11.08	10.98	10.76	0.25	0.25	0.25
		4.6		-10	13.51	13.56	13.64	0.23	0.22	0.22
		4.5		-20	21.70	22.05	21.58	0.43	0.42	0.42
	STOA (B)	4.8	4.9	0	12.34	11.89	12.15	0.24	0.26	0.23
		4.9		-10	14.39	14.28	13.79	0.24	0.27	0.31
		5		-20	16.27	15.73	16.67	0.24	0.28	0.24
	LTOA (C)	4.7	4.9	0	11.85	11.88	11.88	0.28	0.28	0.28
		4.9		-10	15.05	15.00	15.21	0.26	0.27	0.26
		5.1		-20	14.15	14.25	14.69	0.18	0.17	0.15
AC10+SBR Initial Compaction	Unaged (A)	6.7	6.8	0	9.88	9.91	9.82	0.22	0.21	0.22
		6.8		-10	13.48	13.56	13.06	0.22	0.21	0.24
		6.9		-20	15.47	16.34	16.27	0.29	0.25	0.26
	STOA (B)	7.2	7	0	11.88	11.97	12.01	0.32	0.33	0.32
		7		-10	16.89	16.85	16.66	0.28	0.29	0.31
		6.8		-20	19.78	20.02	20.05	0.27	0.26	0.26
	LTOA (C)	6.8	7	0	11.37	11.37	11.39	0.26	0.26	0.25
		7		-10	16.32	16.53	16.33	0.26	0.25	0.26
		7.2		-20	17.45	17.58	17.52	0.24	0.25	0.26
AC10+SBR Ultimate Compaction	Unaged (A)	3.5	3.6	0	12.55	12.56	12.27	0.25	0.25	0.27
		3.6		-10	16.75	16.85	16.92	0.37	0.35	0.34
		3.7		-20	19.00	18.61	18.46	0.26	0.28	0.29
	STOA (B)	3.8	3.7	0	11.53	11.68	11.23	0.22	0.21	0.23
		3.7		-10	16.08	15.81	16.00	0.26	0.26	0.25
		3.6		-20	22.08	22.20	21.80	0.33	0.31	0.34
	LTOA (C)	3.6	3.73	0	14.19	14.23	14.35	0.29	0.29	0.28
		3.7		-10	18.13	18.05	17.86	0.26	0.26	0.28
		3.9		-20	18.99	19.00	19.32	0.22	0.22	0.21

Table B.2 Results of Indirect Tensile Creep and Strength Test

Mixture ID	Loading Time(sec)	Creep Compliance (1/psi) at -20°C	at -10°C	at -0°C	Tensile Strength at -10°C (psi)
	1	4.36E-07	7.79E-07	6.24E-07	
	2	4.6E-07	8.43E-07	8.19E-07	
	5	4.62E-07	9.33E-07	1E-06	
	10	5.05E-07	9.9E-07	1.18E-06	
	20	5.62E-07	1.15E-06	1.48E-06	
	50	5.69E-07	1.33E-06	1.85E-06	
AC30	100	6.33E-07	1.46E-06	2E-06	258.6
Unaged	200	6.69E-07	1.74E-06	2.65E-06	426.6
Initial	500	7.93E-07	2.11E-06	3.84E-06	378.6
Compaction	550	8.05E-07	2.18E-06	4.03E-06	
	600	8.05E-07	2.25E-06	4.21E-06	
	650	8.15E-07	2.28E-06	4.34E-06	
	700	8.12E-07	2.37E-06	4.61E-06	
	750	8.25E-07	2.4E-06	4.87E-06	
	800	8.37E-07	2.45E-06	4.97E-06	
	850	8.35E-07	2.49E-06	5.07E-06	
	900	8.46E-07	2.56E-06	5.29E-06	
	950	8.58E-07	2.62E-06	5.5E-06	
	1000	8.85E-07	2.62E-06	5.65E-06	
Poisson's Ratio		0.25	0.19	0.16	
	1	6.94E-07	9.39E-07	7.65E-07	
	2	7.05E-07	1.07E-06	8.94E-07	
	5	7.65E-07	1.17E-06	1E-06	
	10	8.07E-07	1.25E-06	1.16E-06	
	20	8.66E-07	1.45E-06	1.36E-06	
	50	9.43E-07	1.77E-06	1.75E-06	
AC30	100	1.03E-06	1.99E-06	2.18E-06	327.6
Unaged	200	1.16E-06	2.44E-06	2.92E-06	197.2
Ultimate	500	1.41E-06	3.37E-06	4.33E-06	367.7
Compaction	550	1.43E-06	3.51E-06	4.5E-06	
	600	1.47E-06	3.61E-06	4.62E-06	
	650	1.51E-06	3.69E-06	4.81E-06	
	700	1.55E-06	3.81E-06	5E-06	
	750	1.58E-06	3.89E-06	5.17E-06	
	800	1.6E-06	4E-06	5.27E-06	
	850	1.63E-06	4.09E-06	5.39E-06	
	900	1.66E-06	4.19E-06	5.51E-06	
	950	1.69E-06	4.28E-06	5.62E-06	
	1000	1.7E-06	4.4E-06	5.7E-06	
Poisson's Ratio		0.29	0.14	0.16	

Table B.2 Results of Indirect Tensile Creep and Strength Test (Continued)

Mixture ID	Loading Time(sec)	Creep Compliance (1/psi) at -20°C	at -10°C	at -0°C	Tensile Strength at -10°C (psi)
	1	6.26E-07	7.83E-07	1.08E-06	
	2	6.22E-07	8.03E-07	1.13E-06	
	5	6.34E-07	8.64E-07	1.35E-06	
	10	6.51E-07	9.3E-07	1.28E-06	
	20	7.07E-07	9.93E-07	1.67E-06	
	50	7.59E-07	1.24E-06	2.15E-06	
AC30	100	8.13E-07	1.26E-06	2.42E-06	334.6
STOA	200	9.07E-07	1.44E-06	3.03E-06	259.4
Initial	500	1.09E-06	1.75E-06	4.25E-06	240.5
Compaction	550	1.1E-06	1.82E-06	4.41E-06	
	600	1.13E-06	1.88E-06	4.6E-06	
	650	1.16E-06	1.93E-06	4.75E-06	
	700	1.18E-06	1.98E-06	4.9E-06	
	750	1.19E-06	2.05E-06	5.04E-06	
	800	1.22E-06	2.09E-06	5.2E-06	
	850	1.26E-06	2.15E-06	5.36E-06	
	900	1.27E-06	2.2E-06	5.55E-06	
	950	1.29E-06	2.24E-06	5.69E-06	
	1000	1.31E-06	2.25E-06	5.84E-06	
Poisson's Ratio		0.29	0.24	0.21	
	1	2.83E-07	4.95E-07	6.3E-07	
	2	3.01E-07	5.28E-07	6.95E-07	
	5	3.36E-07	6.36E-07	8.52E-07	
	10	3.68E-07	8.11E-07	9.5E-07	
	20	3.78E-07	7.57E-07	1.12E-06	
	50	3.89E-07	9.05E-07	1.47E-06	
AC30	100	3.98E-07	1.11E-06	1.93E-06	237.6
STOA	200	4.22E-07	1.33E-06	2.46E-06	494.4
Ultimate	500	5.03E-07	1.8E-06	3.61E-06	607.5
Compaction	550	5.05E-07	1.87E-06	3.81E-06	
	600	5.18E-07	1.95E-06	4.01E-06	
	650	5.25E-07	2.01E-06	4.18E-06	
	700	5.47E-07	2.05E-06	4.35E-06	
	750	5.39E-07	2.12E-06	4.48E-06	
	800	5.57E-07	2.17E-06	4.65E-06	
	850	5.56E-07	2.22E-06	4.81E-06	
	900	5.57E-07	2.25E-06	4.95E-06	
	950	5.57E-07	2.28E-06	5.09E-06	
	1000	5.66E-07	2.33E-06	5.22E-06	
Poisson's Ratio		0.5	0.3	0.33	

Table B.2 Results of Indirect Tensile Creep and Strength Test (Continued)

Mixture ID	Loading Time(sec)	Creep Compliance (1/psi) at -20°C	at -10°C	at -0°C	Tensile Strength at -10°C (psi)
	1	4.98E-07	5.86E-07	5.27E-07	
	2	5.33E-07	6.18E-07	7.14E-07	
	5	5.59E-07	6.56E-07	8.31E-07	
	10	5.93E-07	7.28E-07	9.77E-07	
	20	6.29E-07	7.94E-07	1E-06	
	50	6.78E-07	9.61E-07	1.22E-06	
AC30	100	7.22E-07	1.1E-06	1.55E-06	358.4
LTOA	200	8.16E-07	1.25E-06	1.85E-06	254
Initial	500	9.73E-07	1.68E-06	2.5E-06	272.4
Compaction	550	1.01E-06	1.72E-06	2.7E-06	
	600	1.03E-06	1.78E-06	2.89E-06	
	650	1.06E-06	1.83E-06	2.99E-06	
	700	1.08E-06	1.9E-06	3.11E-06	
	750	1.11E-06	1.94E-06	3.2E-06	
	800	1.14E-06	1.99E-06	3.3E-06	
	850	1.16E-06	2.02E-06	3.4E-06	
	900	1.2E-06	2.08E-06	3.5E-06	
	950	1.23E-06	2.12E-06	3.54E-06	
	1000	1.24E-06	2.15E-06	3.68E-06	
Poisson's Ratio		0.31	0.29	0.24	
	1	4.16E-07	4.24E-07	8.07E-07	
	2	4.32E-07	4.5E-07	8.25E-07	
	5	4.48E-07	5.06E-07	8.68E-07	
	10	4.76E-07	5.41E-07	9.17E-07	
	20	4.72E-07	5.53E-07	9.9E-07	
	50	4.92E-07	6.01E-07	1.26E-06	
AC30	100	5.47E-07	6.18E-07	1.5E-06	527.6
LTOA	200	6.03E-07	7.08E-07	1.85E-06	591.8
Ultimate	500	7.2E-07	8.32E-07	2.37E-06	475.2
Compaction	550	7.33E-07	8.54E-07	2.47E-06	
	600	7.34E-07	8.65E-07	2.57E-06	
	650	7.45E-07	8.77E-07	2.65E-06	
	700	7.74E-07	8.92E-07	2.68E-06	
	750	7.77E-07	9.06E-07	2.75E-06	
	800	7.76E-07	9.06E-07	2.8E-06	
	850	7.97E-07	9.24E-07	2.88E-06	
	900	8.17E-07	9.37E-07	2.92E-06	
	950	8.36E-07	9.49E-07	2.97E-06	
	1000	8.38E-07	9.52E-07	3.06E-06	
Poisson's Ratio		0.26	0.32	0.12	

Table B.2 Results of Indirect Tensile Creep and Strength Test (Continued)

Mixture ID	Loading Time(sec)	Creep Compliance (1/psi) at -20°C	at -10°C	at -0°C	Tensile Strength at -10°C (psi)
	1	5.51E-07	1.13E-06	1.36E-06	
	2	6.1E-07	1.24E-06	1.58E-06	
	5	6.35E-07	1.39E-06	1.89E-06	
	10	6.55E-07	1.57E-06	2.14E-06	
	20	7.41E-07	1.76E-06	2.47E-06	
	50	8.31E-07	2.15E-06	3.28E-06	
AC30+GTR	100	8.8E-07	2.51E-06	4.15E-06	274.5
Unaged	200	1.03E-06	2.93E-06	5.57E-06	276.2
Initial	500	1.33E-06	4.18E-06	7.41E-06	302.4
Compaction	550	1.37E-06	4.37E-06	7.88E-06	
	600	1.41E-06	4.57E-06	8.26E-06	
	650	1.41E-06	4.74E-06	8.57E-06	
	700	1.44E-06	4.94E-06	8.97E-06	
	750	1.48E-06	5.11E-06	9.25E-06	
	800	1.51E-06	5.32E-06	9.54E-06	
	850	1.55E-06	5.51E-06	9.79E-06	
	900	1.58E-06	5.69E-06	1.01E-05	
	950	1.6E-06	5.87E-06	1.03E-05	
	1000	1.64E-06	6.06E-06	1.06E-05	
Poisson's Ratio		0.25	0.23	0.21	
	1	2.68E-07	6.76E-07	9.94E-07	
	2	3.16E-07	7.4E-07	1.07E-06	
	5	3.38E-07	7.86E-07	1.16E-06	
	10	3.52E-07	8.61E-07	1.35E-06	
	20	3.8E-07	8.94E-07	1.53E-06	
	50	4.21E-07	1.02E-06	1.8E-06	
AC30+GTR	100	4.45E-07	1.11E-06	2.2E-06	455.1
Unaged	200	5.02E-07	1.34E-06	2.75E-06	460
Ultimate	500	6E-07	1.65E-06	3.59E-06	434.9
Compaction	550	6.1E-07	1.7E-06	3.74E-06	
	600	6.17E-07	1.73E-06	3.85E-06	
	650	6.22E-07	1.77E-06	4.03E-06	
	700	6.31E-07	1.81E-06	4.17E-06	
	750	6.37E-07	1.86E-06	4.28E-06	
	800	6.49E-07	1.91E-06	4.38E-06	
	850	6.6E-07	1.94E-06	4.53E-06	
	900	6.67E-07	1.97E-06	4.63E-06	
	950	6.75E-07	1.99E-06	4.73E-06	
	1000	6.85E-07	2.02E-06	4.82E-06	
Poisson's Ratio		0.5	0.2	0.22	

Table B.2 Results of Indirect Tensile Creep and Strength Test (Continued)

Mixture ID	Loading Time(sec)	Creep Compliance (1/psi) at -20°C	at -10°C	at -0°C	Tensile Strength at -10°C (psi)
	1	7.77E-07	8.3E-07	1.24E-06	
	2	8.31E-07	8.76E-07	1.52E-06	
	5	8.69E-07	9.63E-07	1.61E-06	
	10	9.36E-07	1.04E-06	1.97E-06	
	20	9.87E-07	1.11E-06	2.21E-06	
	50	1.15E-06	1.34E-06	2.63E-06	
AC30+GTR	100	1.26E-06	1.73E-06	3.22E-06	336.2
STOA	200	1.45E-06	2.14E-06	4.07E-06	415.5
Initial	500	1.89E-06	2.98E-06	5.85E-06	387.9
Compaction	550	1.96E-06	3.11E-06	6.15E-06	
	600	2.01E-06	3.22E-06	6.45E-06	
	650	2.07E-06	3.31E-06	6.64E-06	
	700	2.11E-06	3.45E-06	6.85E-06	
	750	2.17E-06	3.57E-06	7.12E-06	
	800	2.23E-06	3.66E-06	7.33E-06	
	850	2.28E-06	3.73E-06	7.53E-06	
	900	2.33E-06	3.82E-06	7.73E-06	
	950	2.38E-06	3.94E-06	7.93E-06	
	1000	2.47E-06	4.05E-06	8.13E-06	
Poisson's Ratio		0.23	0.19	0.12	
	1	4.67E-07	7.24E-07	7.35E-07	
	2	4.86E-07	7.35E-07	8.36E-07	
	5	5.1E-07	7.74E-07	7.18E-07	
	10	5.24E-07	8.55E-07	1.07E-06	
	20	5.81E-07	8.63E-07	1.1E-06	
	50	6.4E-07	1.02E-06	1.42E-06	
AC30+GTR	100	6.62E-07	9.9E-07	1.75E-06	467.4
STOA	200	6.83E-07	1.09E-06	2.15E-06	375.8
Ultimate	500	7.53E-07	1.3E-06	2.78E-06	372.6
Compaction	550	7.61E-07	1.31E-06	2.9E-06	
	600	7.65E-07	1.34E-06	2.98E-06	
	650	8.01E-07	1.39E-06	3.13E-06	
	700	7.98E-07	1.41E-06	3.2E-06	
	750	7.98E-07	1.44E-06	3.28E-06	
	800	8.27E-07	1.44E-06	3.3E-06	
	850	8.35E-07	1.48E-06	3.34E-06	
	900	8.39E-07	1.48E-06	3.4E-06	
	950	8.44E-07	1.47E-06	3.47E-06	
	1000	8.59E-07	1.45E-06	3.47E-06	
Poisson's Ratio		0.31	0.17	0.18	

Table B.2 Results of Indirect Tensile Creep and Strength Test (Continued)

Mixture ID	Loading Time(sec)	Creep Compliance (1/psi) at -20°C	at -10°C	at -0°C	Tensile Strength at -10°C (psi)
	1	4.58E-07	5.88E-07	4.8E-07	
	2	4.91E-07	6.25E-07	6.32E-07	
	5	4.97E-07	6.62E-07	6.28E-07	
	10	5.27E-07	7.14E-07	8.03E-07	
	20	5.53E-07	7.74E-07	8.12E-07	
	50	6.02E-07	8.49E-07	1.08E-06	
AC30+GTR	100	6.38E-07	9.7E-07	1.27E-06	454.9
LTOA	200	7.24E-07	1.17E-06	1.58E-06	364
Initial	500	8.2E-07	1.45E-06	2.1E-06	359.8
Compaction	550	8.39E-07	1.51E-06	2.15E-06	
	600	8.49E-07	1.56E-06	2.22E-06	
	650	8.69E-07	1.62E-06	2.28E-06	
	700	8.81E-07	1.65E-06	2.31E-06	
	750	9.08E-07	1.71E-06	2.34E-06	
	800	9.29E-07	1.76E-06	2.36E-06	
	850	9.42E-07	1.86E-06	2.36E-06	
	900	9.55E-07	1.9E-06	2.4E-06	
	950	9.66E-07	1.97E-06	2.44E-06	
	1000	9.63E-07	2.02E-06	2.45E-06	
Poisson's Ratio		0.32	0.33	0.44	
	1	4.78E-07	5.49E-07	7.69E-07	
	2	4.75E-07	5.61E-07	8.45E-07	
	5	5.09E-07	6.34E-07	9.77E-07	
	10	5.38E-07	6.25E-07	1.11E-06	
	20	5.82E-07	6.9E-07	1.11E-06	
	50	5.96E-07	7.95E-07	1.48E-06	
AC30+GTR	100	6.4E-07	8.89E-07	1.69E-06	391.3
LTOA	200	7.04E-07	1.01E-06	1.99E-06	355.1
Ultimate	500	8.12E-07	1.31E-06	2.76E-06	380.2
Compaction	550	8.28E-07	1.34E-06	2.8E-06	
	600	8.47E-07	1.37E-06	2.83E-06	
	650	8.61E-07	1.41E-06	2.9E-06	
	700	8.64E-07	1.45E-06	3E-06	
	750	8.81E-07	1.5E-06	3.14E-06	
	800	8.99E-07	1.51E-06	3.21E-06	
	850	9E-07	1.56E-06	3.24E-06	
	900	9.14E-07	1.6E-06	3.34E-06	
	950	9.27E-07	1.63E-06	3.43E-06	
	1000	9.49E-07	1.68E-06	3.49E-06	
Poisson's Ratio		0.26	0.32	0.25	

Table B.2 Results of Indirect Tensile Creep and Strength Test (Continued)

Mixture ID	Loading Time(sec)	Creep Compliance (1/psi) at -20°C	at -10°C	at -0°C	Tensile Strength at -10°C (psi)
	1	4.46E-07	6.36E-07	1.01E-06	
	2	4.58E-07	6.9E-07	1.1E-06	
	5	4.98E-07	8.16E-07	1.33E-06	
	10	5.19E-07	8.67E-07	1.58E-06	
	20	5.87E-07	9.31E-07	1.81E-06	
	50	6.39E-07	1.24E-06	2.28E-06	
AC10+SBR	100	6.8E-07	1.46E-06	2.87E-06	387.6
Unaged	200	7.44E-07	1.86E-06	3.71E-06	440.1
Initial	500	8.85E-07	2.66E-06	5.27E-06	460.6
Compaction	550	9.06E-07	2.78E-06	5.51E-06	
	600	9.22E-07	2.89E-06	5.7E-06	
	650	9.44E-07	3.04E-06	5.94E-06	
	700	9.55E-07	3.14E-06	6.19E-06	
	750	9.73E-07	3.27E-06	6.39E-06	
	800	9.91E-07	3.4E-06	6.6E-06	
	850	1E-06	3.5E-06	6.79E-06	
	900	1.02E-06	3.63E-06	6.97E-06	
	950	1.03E-06	3.73E-06	7.12E-06	
	1000	1.05E-06	3.81E-06	7.32E-06	
Poisson's Ratio		0.4	0.25	0.21	
	1	4.18E-07	5.74E-07	7.6E-07	
	2	4.33E-07	6.62E-07	8.76E-07	
	5	4.59E-07	7.1E-07	9.71E-07	
	10	4.87E-07	7.64E-07	1.15E-06	
	20	5.06E-07	9.73E-07	1.36E-06	
	50	5.72E-07	1.13E-06	1.72E-06	
AC10+SBR	100	6.23E-07	1.31E-06	2.05E-06	410.8
Unaged	200	6.87E-07	1.66E-06	2.58E-06	536.5
Ultimate	500	8.88E-07	2.28E-06	3.76E-06	567.9
Compaction	550	9.02E-07	2.38E-06	3.92E-06	
	600	9.24E-07	2.54E-06	4.08E-06	
	650	9.51E-07	2.5E-06	4.18E-06	
	700	9.69E-07	2.57E-06	4.32E-06	
	750	1E-06	2.65E-06	4.43E-06	
	800	1.02E-06	2.7E-06	4.55E-06	
	850	1.04E-06	2.78E-06	4.69E-06	
	900	1.06E-06	2.86E-06	4.84E-06	
	950	1.08E-06	2.95E-06	4.99E-06	
	1000	1.1E-06	3.01E-06	5.16E-06	
Poisson's Ratio		0.32	0.35	0.33	

Table B.2 Results of Indirect Tensile Creep and Strength Test (Continued)

Mixture ID	Loading Time(sec)	Creep Compliance (1/psi) at -20°C	at -10°C	at -0°C	Tensile Strength at -10°C (psi)
	1	3.59E-07	5.48E-07	6.51E-07	
	2	3.87E-07	5.65E-07	7.71E-07	
	5	4.02E-07	6.47E-07	9.69E-07	
	10	4.33E-07	7.07E-07	1.18E-06	
	20	4.29E-07	7.33E-07	1.49E-06	
	50	4.94E-07	8.25E-07	1.97E-06	
AC10+SBR	100	5.36E-07	8.93E-07	2.64E-06	507.9
STOA	200	6.1E-07	1.11E-06	3.53E-06	555.4
Initial	500	7.34E-07	1.42E-06	5.35E-06	539.5
Compaction	550	7.49E-07	1.45E-06	5.61E-06	
	600	7.63E-07	1.48E-06	5.87E-06	
	650	7.79E-07	1.52E-06	6.08E-06	
	700	8E-07	1.57E-06	6.28E-06	
	750	8.07E-07	1.6E-06	6.55E-06	
	800	8.27E-07	1.63E-06	6.77E-06	
	850	8.35E-07	1.67E-06	6.91E-06	
	900	8.5E-07	1.69E-06	7.15E-06	
	950	8.66E-07	1.72E-06	7.39E-06	
	1000	8.81E-07	1.76E-06	7.65E-06	
Poisson's Ratio		0.33	0.33	0.22	
	1	2.83E-07	5.83E-07	8.69E-07	
	2	3.01E-07	6.12E-07	9.43E-07	
	5	3.38E-07	7.2E-07	1.18E-06	
	10	3.56E-07	7.59E-07	1.19E-06	
	20	3.77E-07	8.45E-07	1.52E-06	
	50	4.31E-07	9.4E-07	1.86E-06	
AC10+SBR	100	4.49E-07	1.12E-06	2.26E-06	577.9
STOA	200	4.92E-07	1.34E-06	2.83E-06	578.7
Ultimate	500	5.84E-07	1.77E-06	4.14E-06	571.1
Compaction	550	5.99E-07	1.83E-06	4.4E-06	
	600	6.1E-07	1.9E-06	4.57E-06	
	650	6.25E-07	1.94E-06	4.75E-06	
	700	6.31E-07	2E-06	4.88E-06	
	750	6.34E-07	2.06E-06	5.04E-06	
	800	6.44E-07	2.1E-06	5.23E-06	
	850	6.47E-07	2.14E-06	5.34E-06	
	900	6.55E-07	2.17E-06	5.5E-06	
	950	6.63E-07	2.21E-06	5.66E-06	
	1000	6.65E-07	2.26E-06	5.8E-06	
Poisson's Ratio		0.5	0.25	0.22	

Table B.2 Results of Indirect Tensile Creep and Strength Test (Continued)

Mixture ID	Loading Time(sec)	Creep Compliance (1/psi) at -20°C	at -10°C	at -0°C	Tensile Strength at -10°C (psi)
	1	4.2E-07	5.07E-07	6.92E-07	
	2	4.38E-07	5.25E-07	7.67E-07	
	5	4.92E-07	6E-07	9.46E-07	
	10	5.23E-07	6.67E-07	1.1E-06	
	20	5.6E-07	7.41E-07	1.3E-06	
	50	6.27E-07	8.6E-07	1.54E-06	
AC10+SBR	100	6.68E-07	1.03E-06	1.83E-06	495.1
LTOA	200	7.59E-07	1.25E-06	2.19E-06	492.2
Initial	500	9.28E-07	1.57E-06	2.94E-06	581.4
Compaction	550	9.36E-07	1.63E-06	3.05E-06	
	600	9.62E-07	1.67E-06	3.22E-06	
	650	9.88E-07	1.72E-06	3.3E-06	
	700	1.01E-06	1.77E-06	3.39E-06	
	750	1.03E-06	1.81E-06	3.48E-06	
	800	1.05E-06	1.87E-06	3.62E-06	
	850	1.07E-06	1.9E-06	3.7E-06	
	900	1.09E-06	1.94E-06	3.83E-06	
	950	1.1E-06	1.98E-06	3.86E-06	
	1000	1.11E-06	2.07E-06	3.87E-06	
Poisson's Ratio		0.26	0.3	0.38	
	1	4E-07	4.44E-07	6.17E-07	
	2	4.25E-07	4.86E-07	6.09E-07	
	5	4.45E-07	5.34E-07	7.66E-07	
	10	4.62E-07	5.62E-07	8E-07	
	20	5.15E-07	5.97E-07	9.07E-07	
	50	5.24E-07	7.21E-07	1.07E-06	
AC10+SBR	100	5.92E-07	7.77E-07	1.27E-06	580.5
LTOA	200	6.17E-07	8.76E-07	1.41E-06	589.6
Ultimate	500	7.1E-07	1.07E-06	1.8E-06	647.1
Compaction	550	7.26E-07	1.1E-06	1.88E-06	
	600	7.41E-07	1.15E-06	1.93E-06	
	650	7.62E-07	1.18E-06	1.99E-06	
	700	7.75E-07	1.21E-06	1.99E-06	
	750	7.9E-07	1.23E-06	2.06E-06	
	800	8.06E-07	1.27E-06	2.12E-06	
	850	8.17E-07	1.29E-06	2.14E-06	
	900	8.29E-07	1.3E-06	2.18E-06	
	950	8.42E-07	1.32E-06	2.24E-06	
	1000	8.75E-07	1.35E-06	2.33E-06	
Poisson's Ratio		0.25	0.29	0.41	

REFERENCES

1. Goodrich, J.L., "Asphalt and Polymer Modified Asphalt Properties Related to the Performance of Concrete Mixes," Journal of the Association of Asphalt Paving Technologists, Vol. 57, 1988, pp.116-175.

2. Roberts, F.L., P.S. Kandhal, E.R. Brown, D.Y. Lee, and T.W. Kennedy, "Hot Mix Asphalt Materials, Mixture Design, and Construction," NAPA Education Foundation, Langham, MD, 1991.

3. "Background of SHRP Asphalt Binder Test Methods - Lecture Notes," National Asphalt Training Center, Demonstration Project 101, Asphalt Institute Research Center, Lexington ,KY, September 1993, pp.1-35.

4. Anderson, D.A., D.W. Christensen, and H. Bahia, "Physical Properties of Asphalt Cement and the Development of Performance-Related Specifications, "Journal of the Association of Asphalt Paving Technologists, Vol. 60, 1991, pp.437-475.

5. Upshow, P.B., "Evaluation of New SHRP Performance-Related Tests for Asphalt Binders Used in Florida," Master thesis, University of Florida, 1994.

6. Anderson, D.A., and T.W. Kennedy,"Development of SHRP Binder Specification," Journal of the Association of Asphalt Paving Technologists, Vol. 62, 1993, pp.481-507.

7. Chiu, C.T., "Investigation on Laboratory Asphalt Aging Processes for Development of an Effective Procedure to Characterize Asphalt Durability," Ph.D. Dissertation, University of Florida, 1994.

8. "Background of SHRP Asphalt Binder Test Methods," National Asphalt Training Center, Demonstration Project 101, Asphalt Institute Research Center, Lexington, KY, September 1993, pp.1-14.

9. Majidzadeh, K. and H.E. Schweyer, "Non-Newtonian Behavior of Asphalt Cements," Journal of the Association of Asphalt Paving Technologists, Vol. 34, 1965, pp.20-44.

10. Puzinauskas, V.P., "Properties of Asphalt Cements," Journal of the Association of Asphalt Paving Technologists, Vol. 48, 1979, pp.646-710.

11. McLeod, N.W., "A 4-Year Survey of Low Temperature Transverse Pavement Cracking on the three Ontario Roads," Journal of the Association of Asphalt Paving Technologists, Vol. 41, 1971, pp.424.

12. McLeod, N.W., "Relationship of Paving Asphalt Temperature Susceptibility as Measured by PVN to Paving Asphalt Specifications, Asphalt Paving Mixture Design and Asphalt Pavement Performance," Journal of the Association of Asphalt Paving Technologists, Vol. 58, 1989, pp.504-539.

13 Davis, R.L., "Relationship Between the Rheological Properties of Asphalt and the Rheological Properties of Mixtures and Pavements," Asphalt Rheology: Relationship to Mixture, ASTM STP 941, 1987, pp.28-50.

14. Kandhal, P.S., Sandvig, L.D., Kkoehler, W.C. and M.E. Wenger, "Asphalt Viscosity - Related Properties of In-Service Pavements in Pennsylvania," ASTM, Special Technical Publication No.532, 1973.

15. Kennedy, T.W. and E.T. Harrigan, "The SHRP Asphalt Research Program Product," Journal of the Association of Asphalt Paving Technologists, Vol. 59, 1990, pp.610-620.

16. "Standard Specification For Performance Graded Asphalt Binder," AASHTO Designation: MP1 - Edition 1A, American Association of State Highway and Transportation Officials Provisional Standard, August 1993.

17. Kennedy, T.W. Moulthrop, J. S. and G. A. Huber, "Development of SHRP Mixture Specification and Design and Analysis System," Journal of the Association of Asphalt Paving Technologists, Vol. 62, 1993, pp.508-528.

18. Anderson, D.A., and D.W. Christensen, "Interpretation of Dynamic Mechanical Test Data for Paving Grade Asphalt Cements," Journal of the Association of Asphalt Paving Technologists, Vol. 61, 1992, pp.67-116.

19. AbWahab, Y., D. Sosnovske, C. A. Bell, and P. Ryus, "Evaluation of Asphalt-Aggregate Mixture Aging by Dynamic Mechanical Analysis," A paper presented at the 72nd Annual Meeting of Transportation Research Board, Washington, D. C., January, 1993.

20. Lenoble, C., and N. Nahas, "Dynamic Rheology and Hot-Mix Performance of Polymer Modified Asphalts," Journal of the Association of Asphalt Paving Technologists, Vol. 63, 1994.

21. Roque, R., and Ruth, B.E., "Mechanism and Modeling of Surface Cracking in Asphalt Pavement," Journal of the Association of Asphalt Paving Technologists, Vol. 59, 1990, pp.396-421.

22. Guan, L., Ruth, B.E. and R. Roque, "A Computerized Mechanistic System for Evaluation and Rehabilitation of Flexible Pavements," Journal of the Association of Asphalt Paving Technologists, Vol. 60, 1991, pp.364-402.

23. Guan, L., "A Mechanistic Analysis and Design System for Evaluation and Rehabilitation of Flexible Pavements," Ph.D. Dissertation, University of Florida, 1990.

24. Page, G.C., Murthy, K.H., Ruth, B.E. and R. Roque, "Asphalt Binder Hardening - Causes and Effects," Journal of the Association of Asphalt Paving Technologists, Vol. 54, 1985, pp.140-161.

25. Chari, C.T., "Evaluation of Age Hardening on the Characteristics of Asphalts and Mixtures," Ph.D. Dissertation, Department of Civil Engineering, University of Florida, 1988.

26. "Standard Practice for Accelerated Aging of Asphalt Binder Using a Pressurized Aging Vessel (PAV)," AASHTO Designation: PP1 - Edition 1A, American Association of State Highway and Transportation Officials Provisional Standard, August 1993.

27. Tia, M. and B.E. Ruth, "Basic Rheology and Rheological Concepts Established by H.E. Schweyer," Asphalt Rheology: Relationship to Mixture, ASTM STP 941, O.E. Briscoe, Ed., American Society for Testing and Materials, Philadelphia, PA, 1987, pp.118-145.

28. King, G., and H. King, "Influence of Asphalt Grade and Polymer Concentration on the Low Temperature Performance of Polymer Modified Asphalt," Journal of the Association of Asphalt Paving Technologists, Vol. 62, 1993, pp.1-22.

29. Thenoux, G., Lees, G. and Bell, C.A., "Laboratory Investigation of the Fraass Brittle Test," Journal of the Association of Asphalt Paving Technologists, Vol. 54, 1985, pp.529-550.

30. "Standard Test Method for Determining the Rheological Properties of Asphalt Binder Using a Dynamic Shear Rheometer (DSR)," AASHTO Designation: TP5 - Edition 1A, American Association of State Highway and Transportation Officials Provisional Standard, August 1993.

31. "Standard Test Method for Determining the Flexural Creep Stiffness of Asphalt Binder Using the Bending Beam Rheometer (BBR)," AASHTO Designation: TP1 - Edition 1A, American Association of State Highway and Transportation Officials Provisional Standard, August 1993.

32. "Standard Test Method for Determining the Fracture Properties of Asphalt Binder in Direct Tension (DT)," AASHTO Designation: TP3 - Edition 1A, American Association of State Highway and Transportation Officials Provisional Standard, August 1993.

33. Goodrich, J.L., "Asphalt Binder Rheology, Asphalt Concrete Rheology and Asphalt Concrete Mix Properties," Journal of the Association of Asphalt Paving Technologists, Vol. 60, 1991, pp.80-120.

34. Roque, R. and W. G. Buttlar, "The Development of a Measurement and Analysis System to Accurately Determine Asphalt Concrete Properties Using the Indirect Tensile Mode," Journal of the Association of Asphalt Paving Technologists, Vol. 61, 1992, pp.304-332.

35. Buttlar, W. G. and R. Roque,"Experimental Development and Evaluation of the New SHRP Measurement and Analysis System for Indirect Tensile Testing at Low Temperatures, " Transportation Research Record, No. 1454, pp.163-171, 1994.

36. Buttlar, W. G, "Relationships Between Asphalt Binder and Mixture Stiffness at Low Temperatures for the Control of Thermal Cracking Pavement Performance," Ph.D. Dissertation, The Pennsylvania State University, University Park, PA, 1996.

37. "Test Method for Determining the Creep Compliance and Strength of Hot Mix Asphalt (HMA) Using the Indirect Tensile Test Device," AASHTO Designation: TP9-94 Edition 1B, American Association of State Highway and Transportation Officials Provisional Standard, March 1995.

38. "Standard Test Method for Quantitative Extraction of Bitumen from Bituminous Paving Mixtures," ASTM D2172-81, Annual Book of ASTM Standards, Vol. 04.03, 1990.

39. "Standard Test Method for Recovery of Asphalt from Solution by Abson Method," ASTM D1856-79, Annual Book of ASTM Standards, Vol. 04.03, 1990.

40. "Standard Test Method for Recovery of Asphalt from Solution by Using the Rotavapor Apparatus," Florida Department of Transportation, Draft 9, January 24, 1992.

41. Montgomery, D.C., Design and Analysis of Experiments, 2nd Edition, John Wiley and Sons, New York, 1984.

42. Reese, R. and J. Goodrich, "California Desert Test Road-A Step Closer to Performance-based Specification," Journal of the Association of Asphalt Paving Technologists, Vol. 62, 1993.

43. Reese, R., "Development of a Physical Property Specification for Asphalt-Rubber Binder," Journal of the Association of Asphalt Paving Technologists, Vol. 63, 1994.

44. Tayebali, A., Deacon, J., Coplantz, J. and C. Monismith "Modeling Fatigue Response of Asphalt-Aggregates Mixtures," Journal of the Association of Asphalt Paving Technologists, Vol. 62, 1993.

45. Pell, P. S., and K. E. Cooper "The Effect of Testing and Mix Variables on the Fatigue Performance of Bituminous Materials," Journal of the Association of Asphalt Paving Technologists, Vol. 44, 1975, pp.1-37.

46. Bahia, H. U. and D. A. Anderson,"The SHRP Binder Rheological Parameters: Why are They Required and How do They Compare to Conventional Properties," Transportation Research Board, 1995, Washington, D. C.

47. Francken, L., "Die Rheologie von Bitumen und Bitumenhaltigen Bindemitteln," Bitumen, Vol. 57, pp. 154-164, April, 1993.

BIOGRAPHICAL SKETCH

Ming-Gin Lee was born on October 14, 1960, in Taoyan, Taiwan, where he attended elementary and secondary schools. He attended high school in Taipei, Taiwan, and received his high school diploma in June 1979. In June 1984, he received a Bachelor of Science degree in civil engineering from Tamkang University, Tamsui, Taiwan. After two years of military service, he worked for the Sanitation Bureau as an environmental sanitary inspector in Taipei. He attended the graduate school at National Central University and started his graduate career in the field of civil engineering materials. He received his Master of Science degree in civil engineering in June 1989 and worked as a lecturer at Nanya Junior College, Chung-Li, Taiwan. He came to the Department of Civil Engineering at the University of Florida for his Ph.D. study in August 1992.

I certify that I have read this study and that in my opinion it conforms to acceptable standards of scholarly presentation and is fully adequate, in scope and quality, as a dissertation for the degree of Doctor of Philosophy.

Mang Tia

Mang Tia, Chairman
Professor of Civil Engineering

I certify that I have read this study and that in my opinion it conforms to acceptable standards of scholarly presentation and is fully adequate, in scope and quality, as a dissertation for the degree of Doctor of Philosophy.

Byron E. Ruth

Byron E. Ruth, Cochairman
Professor of Civil Engineering

I certify that I have read this study and that in my opinion it conforms to acceptable standards of scholarly presentation and is fully adequate, in scope and quality, as a dissertation for the degree of Doctor of Philosophy.

Reynaldo Roque

Reynaldo Roque
Associate Professor of Civil Engineering

I certify that I have read this study and that in my opinion it conforms to acceptable standards of scholarly presentation and is fully adequate, in scope and quality, as a dissertation for the degree of Doctor of Philosophy.

David Bloomquist
Associate Professor of Civil Engineering

I certify that I have read this study and that in my opinion it conforms to acceptable standards of scholarly presentation and is fully adequate, in scope and quality, as a dissertation for the degree of Doctor of Philosophy.

Mark C. K. Yang
Professor of Statistics

This dissertation was submitted to the Graduate Faculty of the College of Engineering and to the Graduate School and was accepted as partial fulfillment of the requirements for the degree of Doctor of Philosophy.

August, 1996

Winfred M. Phillips
Dean, College of Engineering

Karen A. Holbrook
Dean, Graduate School